ISOPRENOID SYNTHESIS: NEW ROLES FOR IRON SULFUR CLUSTERS

Except where reference is made to the work of others, the work described in this dissertation is my own work or was done in collaboration with my advisory committee. This dissertation does not include proprietary or classified information.

_____

Dolapo A. Adedeji

Certificate of Approval:

_____	_____
Douglas C. Goodwin Associate Professor Chemistry and Biochemistry	Evert C. Duin, Chair Assistant Professor Chemistry and Biochemistry
_____	_____
Holly R. Ellis Associate Professor Chemistry and Biochemistry	Edward J. Parish Professor Chemistry and Biochemistry

_____

Joe F. Pittman
Interim Dean
Graduate School

ISOPRENOID SYNTHESIS: NEW ROLES FOR IRON SULFUR CLUSTERS

Dolapo A. Adedeji

A Dissertation

Submitted to

the Graduate Faculty of

Auburn University

in Partial Fulfillment of the

Requirements for the

Degree of

Doctor of Philosophy

Auburn, Alabama
August 4, 2007

ISOPRENOID SYNTHESIS: NEW ROLES FOR IRON SULFUR CLUSTERS

Dolapo A. Adedeji

_____
Signature of Author

_____
Date of Graduation

DISSERTATION ABSTRACT

ISOPRENOID SYNTHESIS: NEW ROLES FOR IRON SULFUR CLUSTERS

Dolapo A. Adedeji

Doctor of Philosophy, August 4, 2007
(B.S., University of Agriculture, Nigeria, 1999)

173 Typed Pages

Directed by Evert C. Duin

Spectroscopic investigations of the GcpE and LytB enzymes involved in the last two steps of the DOXP pathway for isoprene synthesis have been described. YfgB, one of the accessory proteins has also been characterized.

The LytB enzyme converts (E)-4-hydroxy-3-methyl-but-2-enyl diphosphate (HMBPP) to isopentenyl diphosphate (IPP) and dimethylallyl diphosphate (DMAPP) in the last step of the DOXP pathway for isoprenoid synthesis. EPR measurements on the LytB enzyme showed that the purified enzyme contains mixture of $[3Fe\text{-}4S]^{+1}$ and $[4Fe\text{-}4S]^{+1}$ clusters after reduction with dithionite solution. We propose that the LytB enzyme is also a 4Fe cluster containing enzyme. The formation of 3Fe clusters in the active site is due to instability of the 4Fe cluster.

The GcpE enzyme converts 2-C-methyl-D-erythritol-2,4-cyclodiphosphate (MEcPP) to (E)-4-hydroxy-3-methyl-but-2-enyl diphosphate (HMBPP) in the second to the last step of the DOXP pathway. Purification of the enzyme under exclusion of molecular oxygen yielded a protein that solely contained a [4Fe-4S] cluster. An unusual

paramagnetic species that resembles the signal of a HiPIP-type 4Fe cluster is detected under turnover conditions in the presence of substrate and the artificial reductant dithionite. The EPR signal is similar to that found in ferredoxin:thioredoxin reductase. Since it was shown for the latter enzyme that the 4Fe cluster is directly involved in the binding of substrate, we propose that the 4Fe cluster in GcpE has a similar function. Pre-steady-state experiments showed that the HiPIP-like signal represents a true reaction intermediate. Further characterization of the HiPIP-like signal by Electron nuclear double resonance (ENDOR) spectroscopy revealed the presence of a weak ^{31}P superhyperfine coupling due to the phosphate groups present in the substrate MEcPP. This would further confirm the binding of the substrate to the cluster during the reaction mechanism. However, due to the presence of other EPR-active species this is not a solid conclusion.

The YfgB enzyme, one of the accessory proteins of DOXP pathway, belongs to the radical SAM family enzyme. The YfgB enzyme contains a well defined CxxxCxxC motif that is common to all radical SAM enzymes. Reconstitution of the cluster in YfgB resulted in the presence of a $[4Fe\text{-}4S]^{2+/1+}$ cluster. The presence of only one 4Fe cluster would be in line with the role of activating enzyme as in pyruvate formate-lyase activating enzyme (PFL-AE) and anaerobic ribonucleotide reductase activating enzyme (ARR-AE).

ACKNOWLEDGEMENTS

I give praise and thanks to the Lord for the gift of life, grace, good health and the opportunity to take part in this study.

I highly acknowledge and appreciate the guidance and support of my advisor, Dr. Evert Duin, for his wisdom, patience and persistence throughout the period of my graduate study at Auburn University.

Valuable contributions and helpful discussions of my committee members, Professors Goodwin, Ellis and Parish are acknowledged with gratitude. Also, the contributions of professor Stephen Kempf of Biological sciences department are appreciated.

I am also indebted to my colleagues in my group, Weiya Xu, Na Yang and Mi Wang for their help and support during the course of this work.

I also appreciate the financial support from the department of Chemistry and Biochemistry at Auburn University.

Overall, I am really thankful and grateful for my husband, Dr. Adetayo Victor Adedeji for his support, encouragement and assistance during my study. I truly appreciate my two sons, Jethro and Enoch for their love, support, understanding and endurance during my study.

Style manual or journal used: Journal of Biochemistry (together with the style known as “auphd”). Bibliography follows the style used in Biochemistry journal.

Computer software used: Microsoft word, Origin 7, CorelDraw, Chem Window and Reference manager 10.

TABLE OF CONTENTS

LIST OF FIGURES

LIST OF TABLES

CHAPTER 1

GENERAL INTRODUCTION AND ANALYTICAL TECHNIQUES

1.1 General Introduction

1.1.1 Background and Significance

Isoprenoids are essential biomolecules present in all organisms. They form the largest group of natural products and thousands have been isolated from microorganisms, plants and animals, where they serve vital functions. They are involved in membrane structure (sterols, hopanoids), redox reactions (ubiquinone, plastoquinone, menaquinone, phylloquinone), in light harvesting and photo protection (carotenoids and chlorophylls). They are involved in the regulation of growth and development (steroid hormones, cytokinins, gibberellins, abscisic acids) and have various functions as secondary metabolites in plants, including the protection against herbivores and pathogens, and attracting pollinators and seed-dispersing animals (*1-3*).

Despite their various functions, all isoprenoids are derived from the five-carbon building blocks isopentenyl diphosphate (IPP) and its isomer dimethylallyl diphosphate (DMAPP) (*4-6*). Two pathways are known for the synthesis of IPP and DMAPP, that are distributed differently in different organisms.

In the mevalonate pathway, IPP is synthesized from acetyl-CoA (Figure 1-1) and then isomerized to DMAPP. This pathway is found in mammals, fungi, archeabacteria, certain eubacteria and in the plants' cytoplasm. This pathway has been studied

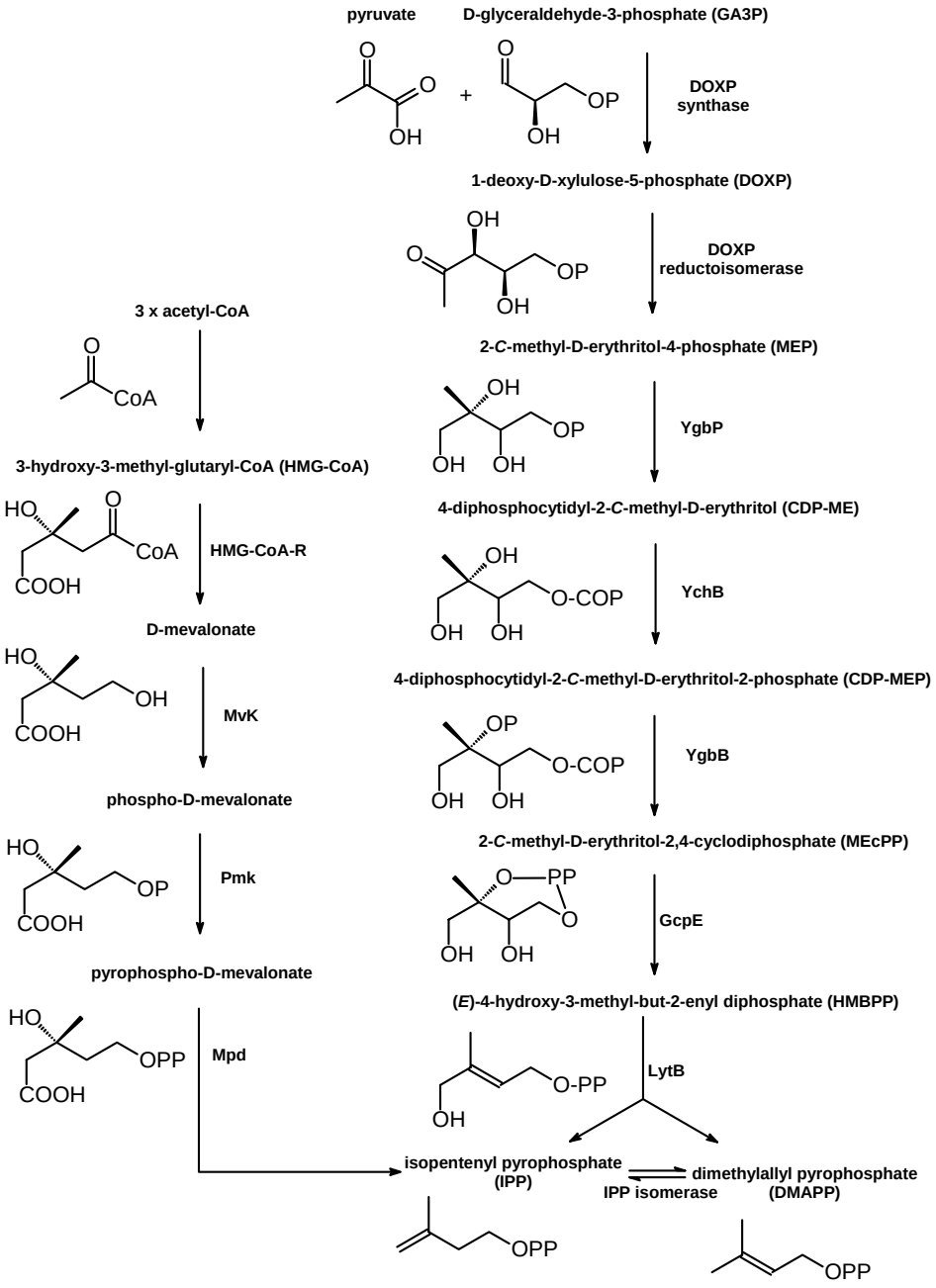

Figure 1-1: The Mevalonate (left) and the DOXP (right) pathways of Isoprenoid biosynthesis. Most of the enzymes are named after their respective genes. For simplicity, the phosphate groups are represented by the letter "P'.

extensively in the 1950s and has resulted in the discovery of a large number of natural products (*4,7,8*).

The second pathway is the non-mevalonate pathway (Figure 1-1) also known as the deoxy-D-xylulose-5-phosphate (DOXP) pathway. Using ^{13}C-labelling experiments, the groups of Rohmer and Arigoni independently observed that the labeling patterns for hopanoid precursors in certain bacteria, for menaquinone by *Escherichia coli* and for glinkgolides by *Ginkgo biloba* seedlings was not compatible with a mevalonate pathway and this led to the reassigning of a large number of isoprenoids whose origin were said to be mevalonate to a non-mevalonate origin (*9-13*) .

The non-mevalonate pathway is present in most eubacteria, in several pathogenic organisms and in the plants' chloroplasts (*14*). This pathway is initiated by the condensation of pyruvate and D-glyceraldehyde-3-phosphate by DOXP synthase to form 1-deoxy-D-xylulose-5-phosphate (DOXP) which is then converted to 2-C-methyl-D-erythritol-4-phosphate (MEP) by DOXP reductoisomerase as shown in figure 1-1. The first five enzymes involved in this pathway have been characterized and are well understood (*15-18*). The reaction mechanism of the enzymes involved in the last two steps 1-hydroxy-2-methyl-2-(E)-butenyl-4-diphosphate synthase (GcpE) and (E)-4-hydroxyl-3-methylbut-2-enyl diphosphate reductase (LytB) yielding IPP and DMAPP are not well understood. Here, we show that both enzymes are iron-sulfur cluster containing proteins.

The rapidly increasing resistance developed by many pathogenic organisms to most of the currently available drugs is posing a serious health concern. The situation has led to an increase in multi-drug resistant pathogens (*19,20*).

Among these pathogens is the *Mycobacterium tuberculosis* that causes tuberculosis and is responsible for more than one-quarter of adult deaths in the world.

Plasmodium falciparum, a protozoan parasite, which causes malaria, is a major threat to human health in most developing countries causing 1.5 to 2.7 million deaths among children and pregnant women annually (*21*). Although the mechanism of antibiotics has been investigated, little has been achieved with regard to the implementation of preventive measures. There is a need for the development of new drugs for the treatment of bacterial infections and malaria; and this should exploit target mechanisms that are different from commercial drugs that are currently available. Therefore, it is important to fully understand the operation of the metabolic pathways that exist in these pathogenic organisms so as to find the appropriate target that can be used in the development of drugs against them (*22*,*23*).

The 1-deoxy-D-xylulose-5-phosphate (DOXP) (Figure 1-1) pathway is one of such metabolic processes that is used in various pathogenic organisms for isoprene biosynthesis (*19*). This is a new and unique target for the development of anti-infective drugs. Since the DOXP pathway is not utilized by mammalian cells, specific compounds that inhibit this pathway should kill the respective pathogens, with little toxicity to humans (*10*).

It has been shown that Fosmidomycin is an effective and safe anti-malarial drug in the treatment of patients having uncomplicated *Plasmodium falciparum* infections. However, recrudescent infections occurred in some patients after termination of the treatment which restricted its use as a single therapeutic agent (*24*). Fosmidomycin in

combination with clindamycin (*25*) has proven clinically to be effective in the treatment of malaria parasites with an overall cure rate of 95%.

Fosmidomycin, (3-(N-formyl-N-hydroxyamino) propylphosphonic acid) also known as FR31564 and its derivative FR90098 are two compounds that have been shown so far to inhibit DOXP reductoisomerase, an enzyme involved in the DOXP pathway. The structures of Fosmidomycin and its derivative are shown in figure 1-2. Fosmidomycin is a natural antibiotic from *Streptomyces lavendulae* that shows a potent antibacterial activity against most Gram-negative and some Gram-positive bacteria (*26*,*27*)

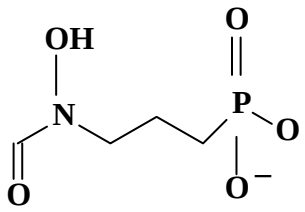

Fosmidomycin

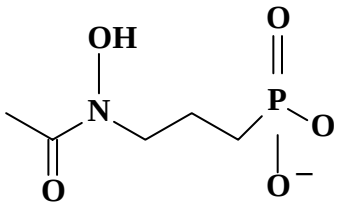

FR90098

Figure 1-2: Structure of Fosmidomycin and its derivative (*28*).

The second reason to target this pathway is the possible broad application of the anti-infective drugs that can be developed that would eventually save more human lives from diseases since the alternative pathway is found in a variety of pathogenic organisms.

Table 1-1: List of microorganisms that utilize the DOXP pathway and the diseases they cause (*19*)

Microorganisms	Examples of diseases
Gram – negative cocci	
Neisseria menningitidis	Menningtis
N. gonnorrhoea	Gonorrhoea
Gram positive non – spore forming rods	
Corynebacterium diphteriae	Diphteria
Listeria monocytogenes	Listeriosis
Gram positive spore forming rods	
Bacillus anthracis	Anthrax
Clostridium histolyticum	Gas gangrene
C. difficle	Colitits
C. botulinum	Botulism
C. tetani	Tetanus
Gram negative rods	
E. coli	Urinary tract infection
Salmonella typhi	Typhus
Yersinia enterocolitica	Enterocolitis
Y. pestis	Plague
Y. peudotuberculosis	Gastroenteritis
Psedomonas sp.	Wound infections, sepsis
Haemophilus inflenzae	Pneumonia, meningitis

Gram negative / spiral shaped bacteria	
Vibrio cholerae	Cholera
Haemophilus pylori	Gastritis Type B
Campylobacter jejuni	Enterocolitis
Acid fast rods	
M. tuberculosis	Tuberculosis
M. bovis	Tuberculosis
M. leprae	Leprosy
M. ovium-intracellulare	Pulmonary Tuberculosis

1.1.2 Iron Sulfur Clusters

Proteins containing iron-sulfur clusters comprise a huge class with a wide range of biological functions. Iron-sulfur clusters contain one or more iron ions covalently bound to sulfide ions. These form a core structure or cluster that is linked to the polypeptide chain by thiolate side chains of cysteine residues. They are found in all known living organisms ranging from anaerobic, aerobic, photosynthetic bacteria to fungi, algae, plants and mammals (*29*,*30*).

Classification of iron-sulfur proteins

Iron-sulfur proteins have been classified into two basic groups in accordance with the International Union of Biochemistry (IUB) (*31*).

1. **Simple Fe-S proteins:** They contain iron sulfur clusters only, without any other prosthetic groups. These include rubredoxins and ferredoxins which function only in electron transfer and other proteins in which the iron-sulfur cluster(s) are involved in catalysis like hydrogenases, endonuclease III and aconitase (*32*,*33*).
2. **Complex iron sulfur proteins:** They have other prosthetic groups in addition to the iron sulfur clusters and usually have enzymatic activity. These include iron-sulfur proteins containing flavin, molybdopterin and siroheme (*32*)

Structures of [Fe-S] Clusters

To understand the properties of Fe-S clusters, we can think of the more complex clusters as an assembly of the simplest cluster, the [2Fe-2S] cluster. The cubane [4Fe-4S] can be formed from two [2Fe-2S] cluster units; the [3Fe-4S] can be assembled from [4Fe-4S] cluster unit with a loss of one Fe atom; the [8Fe-7S] cluster can also be assembled by cluster fusion of two units of [4Fe-4S] cluster. Based on the various spectroscopic techniques that have been applied together with many biochemical studies, five basic structures of Fe-S clusters have been established. Figure 1-3 gives an overview of the standard type iron-sulfur clusters as found in different proteins.

The standard types are the single iron, [2Fe-2S], Rieske [2Fe-2S-His], [3Fe-4S] and [4Fe-4S] clusters (*34*). They are called standard types because they were first isolated and characterized from ferredoxins. Figure 1-4 shows the EPR spectra of the standard type iron-sulfur clusters that have been detected in ferredoxins.

For the [4Fe-4S] cluster three oxidation states are possible. *In vivo* these clusters show only 2+/1+ transition in standard 4Fe clusters, or 2+/3+ transition in high-potential

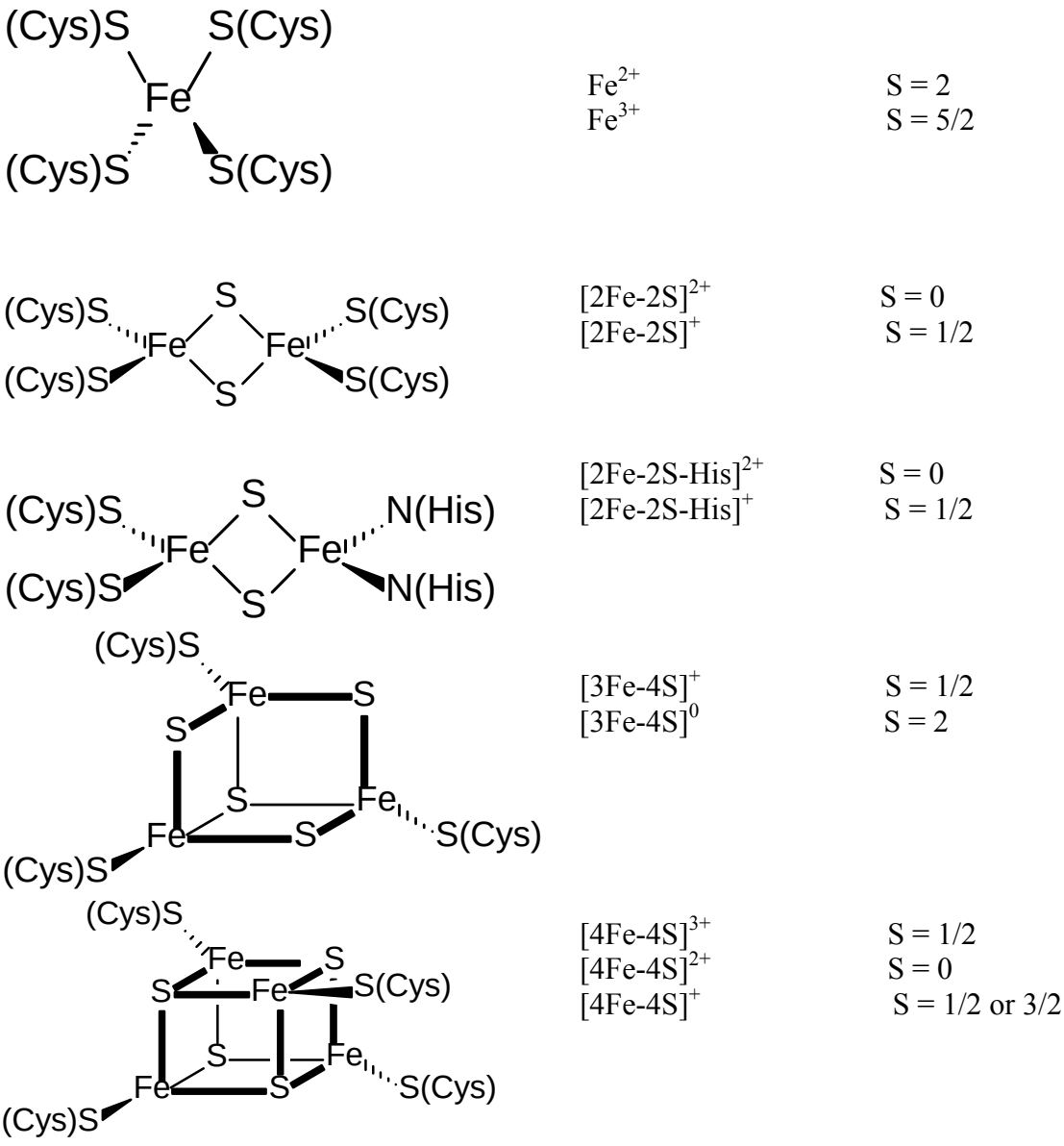

Figure 1-3: Structures, core oxidation states and spin states of some structurally characterized [Fe-S] clusters in biology (*35*). From top to bottom: A single iron, a [2Fe-2S] cluster, Rieske [2Fe-2S-2-His] cluster, a [3Fe-4S] cluster and a [4Fe-4S] cluster.

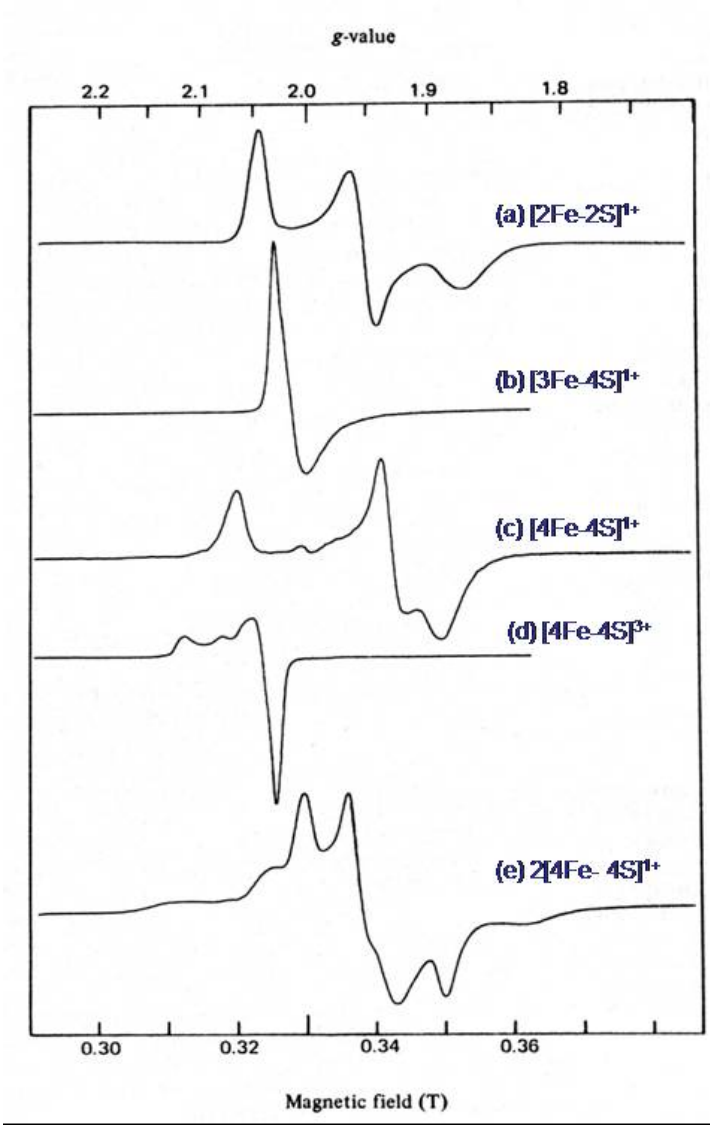

Figure 1-4: EPR spectra of Fe-S clusters in ferredoxins isolated from:

(a) *Mastigocladus laminosus*, (b) *Desulfovibrio gigas,* (c) *Bacillus stearothermophillus,*

(d) *Chromatium vinosum* high-potential iron-sulfur protein and (e) *Clostridium*

pasteurianum. Spectra were recorded between 10 K and 20 K.

(Used with permission from ref (*36*). Copyright Portland Press/The Biochemical

Society)

iron-sulfur proteins (HiPIPs). For [3Fe-4S] cluster, transitions from 1+/0 or 0/1+ are possible (Figure 1-5).

The remarkable structures of Fe-S clusters form the basis for their various functions (*37*,*38*).

Properties of iron-sulfur clusters

Fe-S clusters have the ability for conversion and inter-conversion in the free form and protein-bound form, which supports the fact that they are modular structures (*37*). An example is found in synthetic complexes in which [2Fe-2S] clusters is converted to [4Fe-4S] clusters that is, $2[2Fe\text{-}2S]^{1+} \rightarrow [4Fe\text{-}4S]^{2+}$ (*39*). In *Desulfovibrio gigas* ferrodoxin II and aconitase (*40*), there is inter-conversion between $[3Fe\text{-}4Fe]^{1+}$ and $[4Fe\text{-}4S]^{2+}$ structures (*41*) as depicted in figure 1-5.

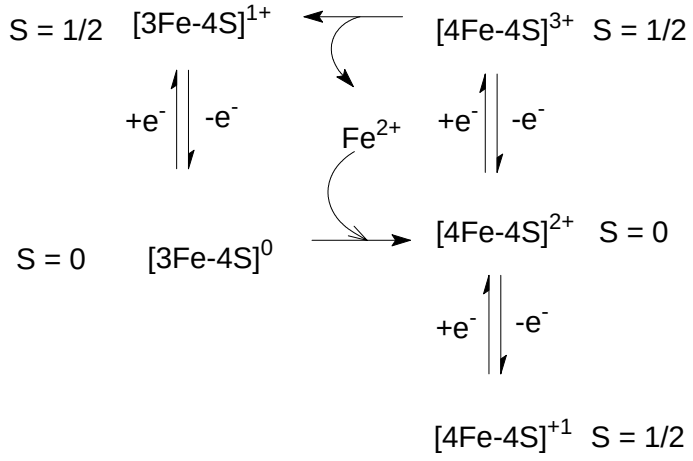

Figure 1-5: Relationship between various cluster forms as seen in the enzyme aconitase (*41*).

Moreover, Fe-S clusters have the tendency to undergo ligand exchange processes without cluster conversion (*37*). This was observed in *Azotobacter vinelandii* ferredoxin which contains two types of Fe-S clusters, [3Fe-4S] and [4Fe-4S], both of which are

cuboidal. The enzyme contains 107 residues in which eight are cysteine (cys) residues, seven of these cysteines bind the two Fe-S clusters present. Mutation of Cys 20, a ligand to the [4Fe-4S] to Alanine resulted in the binding of Cys 24 to this [4Fe-4S] cluster; Cys 24 is a free residue in the native protein. Even when Cys 20 was mutated into a serine residue was the thiolate from Cys 24 preferred over the oxygen from Ser 20 (*42*).

Spin States

The spin state of the different types of clusters can be explained using the spin coupling model (*43-45*). First the iron ions in the cluster are considered separately. They can either have a +3 (d^5) or a +2 (d^6) oxidation state. In both cases they have a high spin configuration: S = 5/2 for Fe^{3+} and S = 2 for Fe^{2+} (*46*). A $[2Fe\text{-}2S]^{2+/1+}$ cluster shows S = 0 in the oxidized state and S = ½ in the reduced state. This could be explained based on Mössbauer spectroscopy data (*47*); one doublet could be detected due to two Fe^{3+} ions for the oxidized state and two doublet with the same intensity due to one Fe^{3+} and one Fe^{2+} for the reduced state. The total spin of S = ½ for the reduced cluster resulted from the antiferromagnetic coupling of high spin Fe^{2+} (S = 2) and high spin Fe^{3+} (S = 5/2) ions. In the oxidized form, two S = 5/2 ferric ions couple to the diamagnetic S = 0 spin state (*48*).

The $[3Fe\text{-}4S]^{1+/0}$ cluster form has a spin state S = ½ in the oxidized state and in the reduced state, a spin S = 2. It was shown by Mössbauer that a mixed valence Fe^{2+} - Fe^{3+} dimer exist in a reduced state, the spin S = 5/2 ferric and S = 2 ferrous ions couple ferromagnetically leading to a S = 9/2 spin state. Antiferromagnetic coupling of S = 9/2

with the S = 5/2 of the third ferric ion lead to S = 2 spin state. In the oxidized cluster, two S = 5/2 spins are coupled to an intermediate spin S = 2 (or 3) which is then coupled to the third spin S = 5/2 yielding the S = ½ spin state (*49*).

For the $[4Fe\text{-}4S]^{2+/1+}$ and $[4Fe\text{-}4S]^{3+/2+}$ clusters, three different coupled pairs were used in determining their spin states (*48*); (Fe^{3+} - Fe^{3+}) with S = 5, (Fe^{2+} - Fe^{3+}) with S = 9/2 and (Fe^{2+} - Fe^{2+}) with S = 4. For $[4Fe\text{-}4S]^{3+}$, (Fe^{3+} - Fe^{3+}) coupled to (Fe^{2+} - Fe^{3+}) to give S = ½ spin state. For $[4Fe\text{-}4S]^{2+}$, (Fe^{2+} - Fe^{3+}) coupled to (Fe^{2+} - Fe^{3+}) gives S = 0 spin state. For $[4Fe\text{-}4S]^{1+}$, (Fe^{2+} - Fe^{3+}) coupled to (Fe^{2+} - Fe^{2+}) gives S = ½ or 3/2 spin state.

Functions of biological iron sulfur clusters

1. **Electron Transfer**

Iron sulfur clusters function as electron carriers in biological systems; this is due to their ability to delocalize electron density over iron and sulfur. They are involved in various biological processes such as nitrogen fixation and photosynthesis (*50*). Fe-S clusters have varying redox potentials depending on the cluster type. The more prevalent type of $[2Fe\text{-}2S]^{2+/+}$ clusters that are coordinated to the protein by four Cys residues encompass a wide range of redox potentials, ranging from -450 mV to +100 mV versus the normal hydrogen electrode (NHE) (*35,51-53*). Figure 1-6 shows an overview of the redox potential range vs NHE of various forms of iron-sulfur clusters.

The Rieske type $[2Fe\text{-}2S]^{2+/+}$ have higher redox potentials in the range of -150 mV to +300 mV due to the presence of two histidyl-N ligands at the reducible Fe site (*54-57*).

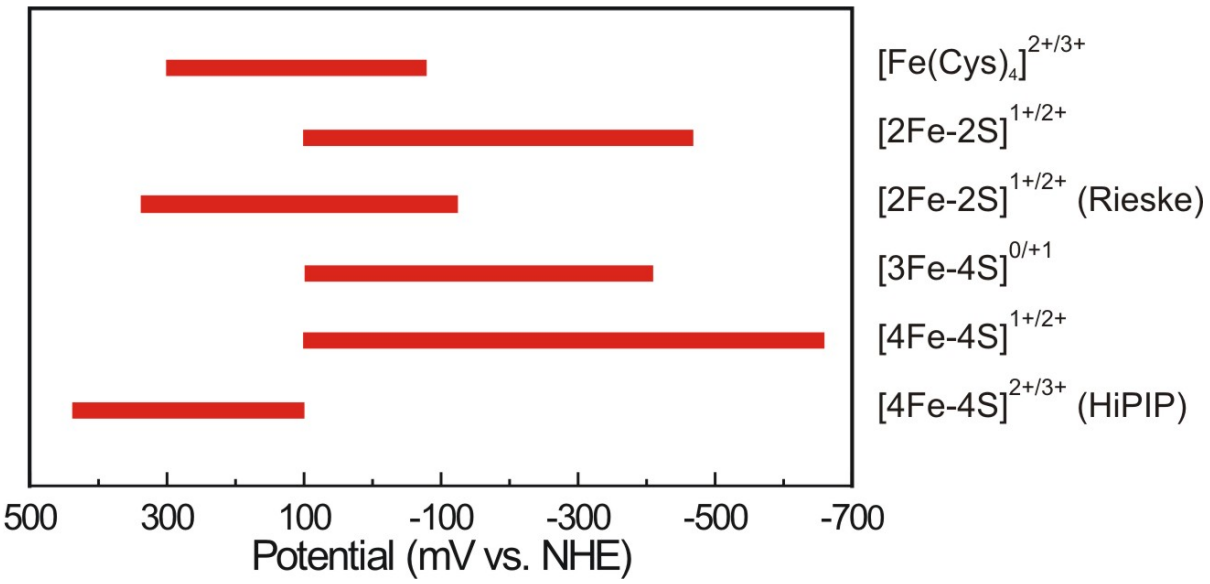

Figure 1-6: The redox potential range (mV vs. NHE) of various forms of iron-sulfur clusters (*35*).

Cuboidal $[3Fe\text{-}4S]^{+/0}$ clusters have redox potentials that fall in the range from -420 mV to +100 mV vs N.H.E. Ferredoxin-like cuboidal [4Fe-4S] clusters have potentials between -650 mV and +100 mV vs N.H.E (*35,58,59*). The high potential iron proteins (HiPIPs) have midpoint potentials at around +350 mV, this was observed in photosynthetic bacterial (*60*).

A large range of redox potentials may be observed for each cluster type due to the protein environment, which might include the nature of the cluster ligands and the hydrophobicity and charge of residues in the environment of the cluster (*32,35*).

2. **Substrate binding and catalysis**

Iron sulfur clusters can serve as the substrate binding sites in redox and non-redox enzymes (*61*). The first example of this is a group of hydratases and dehydratases. The iron-sulfur cluster that is present in the active site is coordinated to the protein by only three cysteine-sulfur ligands. This creates a unique 'uncoordinated' Fe on the cluster that can bind the substrate during turnover (*62*). An example is the mitochondrial aconitase enzyme in which the unique Fe binds the substrate citrate (*63*).

Another example is the 4Fe cluster in the radical SAM family that has a unique iron site that is involved in the binding of S-adenosyl–methionine (SAM) via the amino and carboxylate groups of the methionine fragment to facilitate reductive cleavage and generation of the 5'-deoxyadenosyl radical in the radical (*64*). Examples of the radical SAM superfamily enzymes are anaerobic ribonucleotide reductase (*65*), biotin synthase (*66*), pyruvate formate lyase (*67*) in which most of the reactions occur by free radical mechanisms (*68*).

3. **Regulatory and sensing function**

The ability of the Fe-S clusters to assume different oxidation states and the fact that they are oxygen sensitive makes them useful in sensing and signaling reactions (*69,70*) .

An example is the SoxR/SoxS system of *E.coli*. SoxR is a transcriptional activator that triggers the response to the O^-_2 radical in *E.coli*. SoxR contains a 2Fe cluster. SoxR is inactive in the +1 oxidation state. In the presence of di-oxygen, the [2Fe-2S] becomes oxidized to the +2 state which activates SoxR and thereby stimulates transcriptional expression of SoxS, which is responsible for activating the transcription of numerous enzymes in the oxidative stress response (*71-73*).

The FNR (fumarate and nitrate reduction) active protein dimer dissociate into inactive monomers ($[2Fe\text{-}2S]^{2+}$) in the presence of oxygen. This controls gene expression in both aerobic and anaerobic pathways of *E.coli* (*73*).

Cytoplasmic aconitase (or iron regulatory protein – IRP) functions as a sensor for Fe ions. Low Fe concentrations result in the loss of 4Fe cluster that is present in the protein. The loss of the cluster results in activation of the protein which bind to specific RNA structures called iron responsive elements (IREs). IREs are RNA stem loop structures which occur in the untranslated regions of certain messenger RNAs. The most studied IREs are those of ferritin mRNA and transferring receptor mRNA which are regulated by the assembly of [4Fe-4S] on IRP (*63*).

Both GcpE and LytB contain a [4Fe-4S] cluster in their active sites that seems to be directly involved in substrate binding. Therefore, we will give an overview of three types of Fe-S proteins that have an active-site cluster involved in substrate binding - the

class of hydrolases, the class of radical SAM proteins and the smaller group containing ferredoxin:thioredoxin reductase (FTR) and heterodisulfide reductase (HDR).

Class of hydrolases enzyme

The most famous protein in the class of hydrolases is the enzyme aconitase (*74*). Aconitase catalyzes the conversion of citrate to isocitrate via the intermediate cis-aconitate in the Kreb's cycle (*75*). The reaction is shown in figure 1-7.

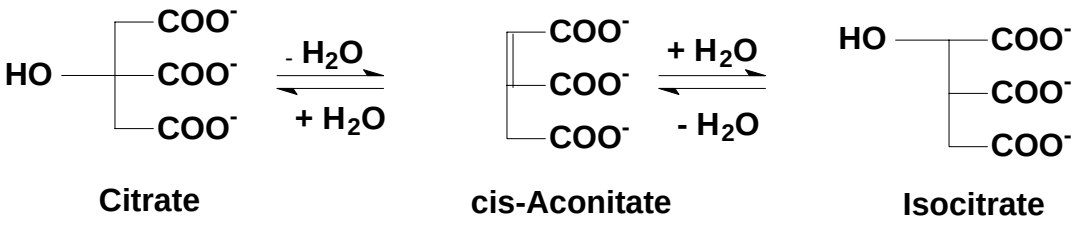

Figure 1-7: Reaction catalysed by enzyme aconitase

Early work on aconitase showed that it was unstable. It was found later that the activity of aconitase can be recovered by the addition of a ferrous ion. This led to the discovery that aconitase was an iron-sulfur protein (*76*). Aconitase as-purified contained $[3Fe\text{-}4S]^{+1}$ clusters (*77*), this is the oxidized form of the protein and it is inactive.

The presence of the 3Fe cluster in aconitase arises because the fourth iron in the cluster is not coordinated to a cysteine thiolate group, but was coordinated to OH/H_2O. Only three cysteine residues are conserved in the active site of aconitase. The iron can easily be removed during isolation to give the 3Fe cluster. The application of spectroscopy (Mössbauer spectroscopy in combination with electron paramagnetic resonance) with chemical methods in the study of aconitase established the conversion of a $[3Fe\text{-}4S]^{0}$ cluster to a $[4Fe\text{-}4S]^{2+}$ form (*78*) as shown in figure 1-5 above.

Furthermore, the studies showed that the iron added during the reaction was returned to the same site where it was removed during isolation. This means it was site specific, thus leading to the investigation of the function of the cluster in the catalytic mechanism of the enzyme aconitase (*79*). The diamagnetic $[4Fe\text{-}4S]^{2+}$ cluster which is the native form of the active enzyme can be reduced to the $[4Fe\text{-}4S]^{1+}$ form which is detectable in EPR with the enzyme still retaining its activity (about 30%) (*80*). In the absence and presence of the substrate with the reduced $[4Fe\text{-}4S]^{1+}$ form, the EPR spectra were different thus indicating that there is a direct interaction between the substrate and the cluster.

The use of Mössbauer and ^{1}H, ^{2}H, ^{17}O-ENDOR demonstrated that the hydroxyl of the fourth Fe is converted to a water molecule upon the binding of the substrate to the cluster. This led to a change in the coordination number (*81*,*82*). The non-ligated iron atom (Fe_a) serves as a Lewis acid in catalyzing abstraction of the hydroxyl and a proton from adjacent carbons. Figure 1-8 shows the ENDOR representation of the $[4Fe\text{-}4S]^{+}$ cluster of aconitase enzyme-substrate complex.

Reaction mechanism of aconitase enzyme

Aconitase catalyzes four stereospecific reactions (since the enzymatic reaction is reversible); the dehydration of citrate or isocitrate to cis-aconitate and the rehydration of cis-aconitate to isocitrate and citrate. Aconitase contains a $[4Fe\text{-}4S]^{+2}$ cluster with a hydroxyl bound to the unique iron (Fe4) in its substrate-free form. Upon binding of the substrate, the hydroxyl group bound to Fe4 is protonated and the coordination number of Fe4 increases from four to six (Figure 1-9 A) (*83*).

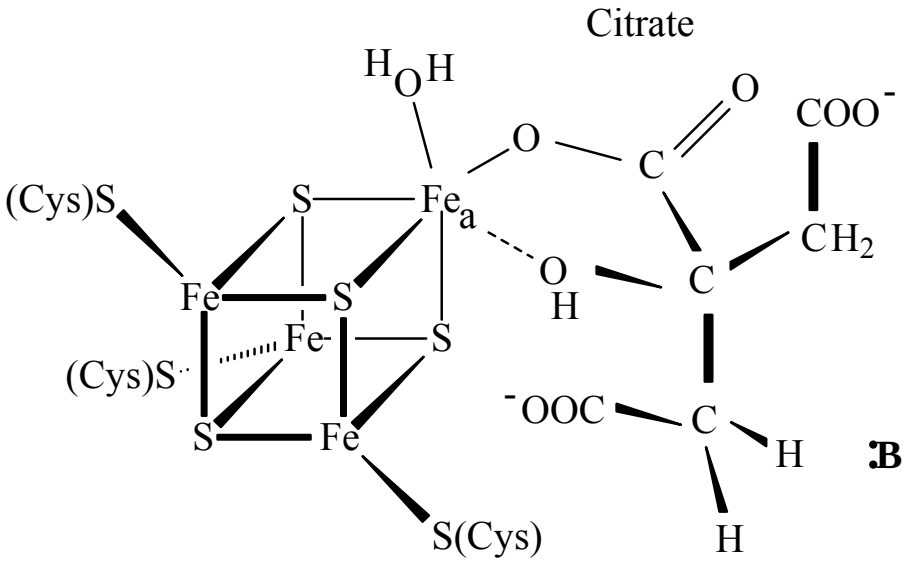

Figure 1-8: ENDOR-derived structure of the $[4Fe\text{-}4S]^{+}$ cluster of the aconitase enzyme-substrate complex (*83*)

The proton donated to form H_2O is derived from His 101. The proton could also be donated by His 167. The binding of the substrate to the cluster leads to a conformational change that reorients the cluster to also maintain the position of the hydroxyl/H_2O molecule on Fe4 (*83*,*84*)

The amino acid residue that is involved in the abstraction of a proton from the Cβ atom of citrate and isocitrate is Ser 642 shown as "B" (Figure 1-9 B). After abstraction of a proton from the Cβ of the isocitrate, there is formation of a carbanion intermediate (Figure 1-9 B). Collapse of the carbanion intermediate with concomitant protonation of the substrate hydroxyl by His 101 cleaves the carbon-oxygen bonds to yield the products – cis-aconitate and water (*83*,*85*).

Class of ferredoxin:thioredoxin reductase (FTR) and heterodisulfide reductase (HDR).

The FTR enzyme is involved in the reduction of a disulfide on the substrate thioredoxin, in two one-electron steps by using reduced [2Fe-2S] ferredoxin as the electron donor. The enzyme contains an active-site disulfide and a $[4Fe\text{-}4S]^{2+}$ cluster as the prosthetic group. The function of the $[4Fe\text{-}4S]^{2+}$ is to mediate transfer of an electron to the active-site disulfide and stabilizing the cystenyl radical intermediate resulting from one-electron reduction of the active-site disulfide (*86*).

The basis for assigning this role comes from various spectroscopic studies of N-ethylmaleimide-modified FTR (NEM-FTR) from spinach. NEM causes the alkylation of one of the disulfide cysteines resulting in the formation of a paramagnetic species (g_{xyz} = 1.98, 2.00, 2.11). This is interpreted as a $[4Fe\text{-}4S]^{3+}$ cluster. The $[4Fe\text{-}4S]^{3+}$ observed

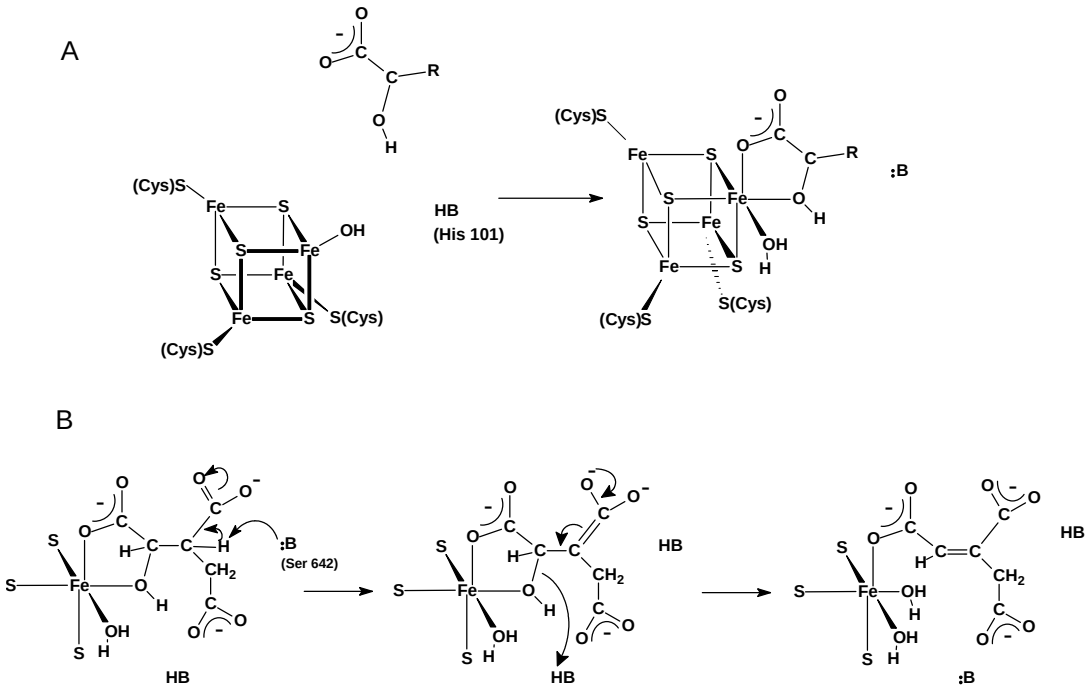

Figure 1-9: (A) Schematic representation of the transition from substrate free aconitase to the substrate bound form. (B) Reaction of isocitrate to cis-aconitate assuming deprotonation when substrate binds and Fe-OH_2 is formed. Formation of the an intermediate and collapse of this intermediate forms the product (*83*).

has different properties from the $[4Fe\text{-}4S]^{3+}$ cluster in high potential iron-sulfur proteins (*87,88*) which can be reduced in a one-electron step to a diamagnetic state (Figure 1-10).

The cluster properties observed in NEM-FTR were attributed to the association of one of the cysteine residues of the active site disulfide to the cluster. EPR studies on FTR reduced with benzyl viologens showed the same EPR signal as seen in NEM-FTR ($[4Fe\text{-}4S]^{3+}$ cluster) under turnover conditions. This indicates that the latter species is a stable analog of a one-electron reduced intermediate (*88*).

A mechanism involving a one-electron reduced intermediate that incorporates the thiol-disulfide interchange reaction established for NAD(P)H-dependent flavin containing disulfide oxidoreductases (*89*) was proposed to rationalize the redox and spectroscopic properties of FTR and NEM-FTR as shown in figure 1-10.
The initial electron from the reduced Fd is used to cleave the active-site disulfide leading to the formation of an interchange thiol that is then free to attack and cleave the substrate disulfide with the formation of a heterodisulfide. Subsequent one electron reduction leads to cleavage of the heterodisulfide that then effects complete reduction of thioredoxin disulfide with restoration of the FTR active-site disulfide (*88*).

HDR catalyzes the reversible reduction of heterodisulfide (CoM-S-S-CoB) to the thiol coenzymes, coenzyme M (CoM-SH) and coenzyme B (CoB-SH). The heterodisulfide functions as the terminal electron acceptor of an energy conserving electron transport chain that is known as the disulfide respiration process.

Variable temperature magnetic circular dichroism (VTMCD) and EPR studies of HDR revealed the presence of a novel type of $[4Fe\text{-}4S]^{3+}$ cluster which is readily formed

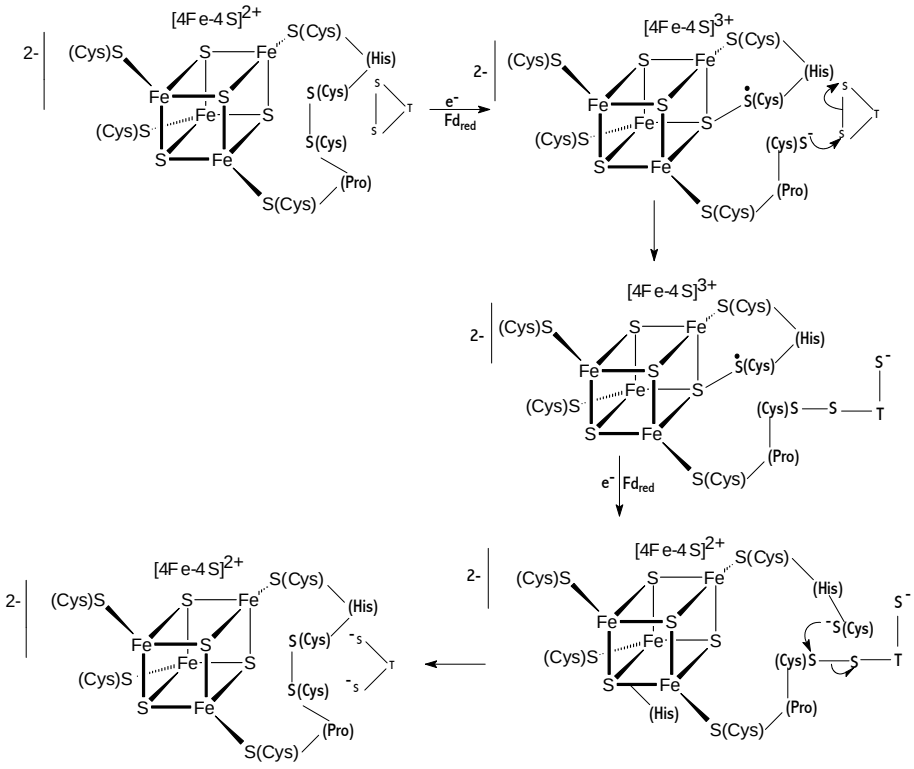

Figure 1-10: Proposed mechanism of FTR. The substrate thioredoxin is represented by T (*88*).

under oxidizing conditions with duroquinone and on addition of thiols such as CoB-SH, CoM-SH to give CoB-HDR and CoM-HDR respectively with electronic and redox properties similar to those of the $[4Fe\text{-}4S]^{3+}$ cluster that was characterized in NEM-FTR (*88*,*90*).

Two different mechanisms (Figures 1-11 and 1-12) were proposed for the reversible heterodisulfide/dithiol cleavage reaction that is catalyzed by HDR in two one-electron steps. This is based on the fact that the redox potentials favor the reductive reaction (E_m = -30 mV and -185 mV for CoB-HDR and CoM-HDR respectively). The first one electron reduction of the $[4Fe\text{-}4S]^{2+}$ only occurs in the presence of a substrate to give $[4Fe\text{- }4S]^{1+}$ that is proposed as a transient intermediate that quickly reacts to cleave the heterodisulfide. Since disulfides are generally cleaved by nucleophilic substitution reactions, it was proposed that a cluster ligating cysteine (Figure 1-11) or a cluster sulfur (Figure 1-12) becomes electron rich on reduction to initiate the nucleophilic attack on the heterodisulfide (*90*).

In the mechanism shown in figure 1-11, the nucleophilic attack results in the formation of CoB-SH and a transient intermediate with a weakly coordinated CoM-S-S-Cys heterodisulfide that is cleaved by accepting two electrons from the cluster to give a $[4Fe\text{-}4S]^{3+}$ cluster with Cys-S^- and CoM-S^- thiolates attached to one Fe atom. Nucleophilic attack in mechanism shown in figure 1-12 results in the formation of CoB-SH and a $[4Fe\text{-}4S]^{3+}$ with CoM-S^- attached to a cluster sulfur. In both mechanisms a second one electron reduces $[4Fe\text{-}4S]^{3+}$ cluster back to its resting state$[4Fe\text{-}4S]^{2+}$ with concomitant dissociation and protonation of CoM-S^- (*90*).

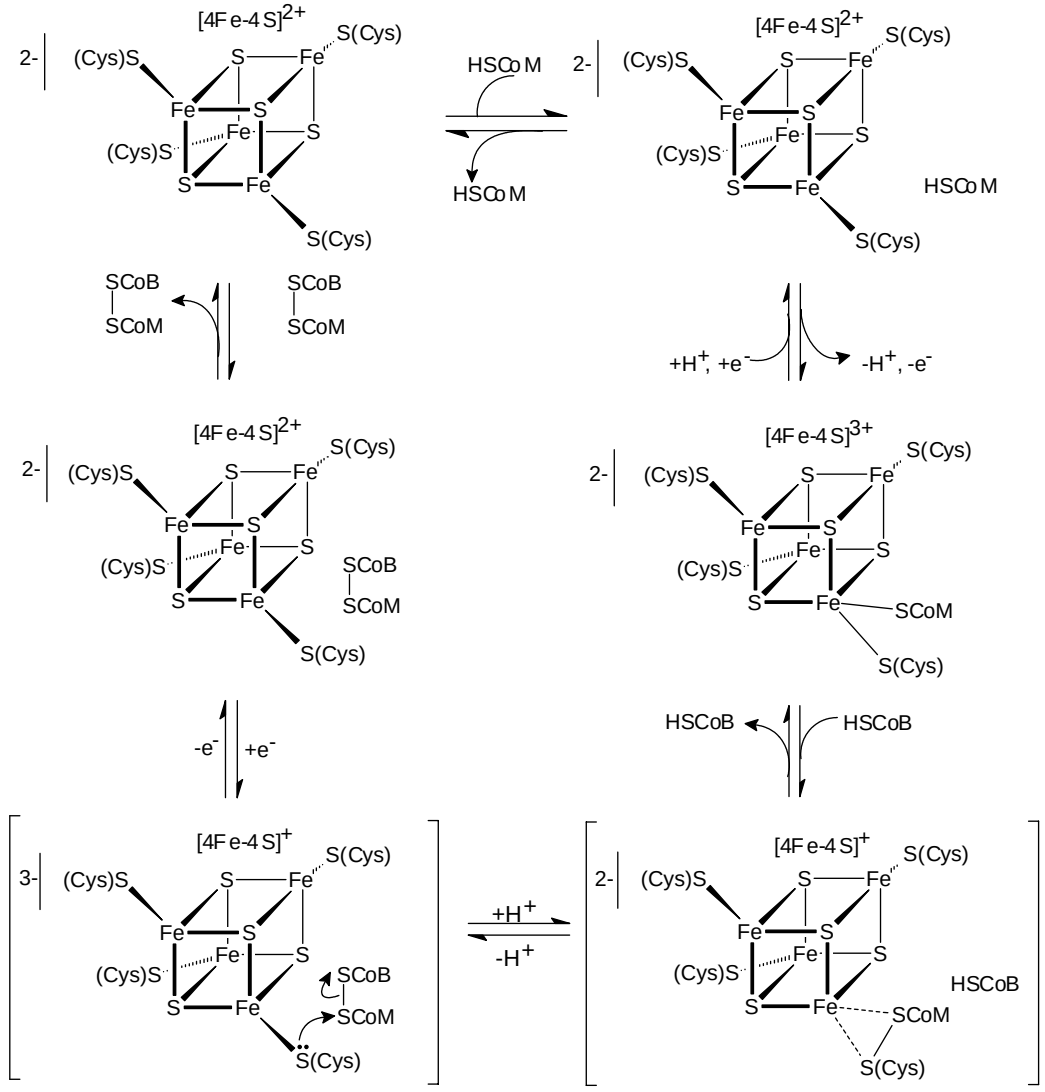

Figure 1-11: The proposed active site mechanism for the reversible heterodisulfide/dithiol reaction catalyzed by HDR where a cluster ligating cysteine becomes electron rich. The reaction intermediates are shown in parenthesis. The oxidation state of the [4Fe-4S] cores is indicated above each of the cubane clusters (*90*).

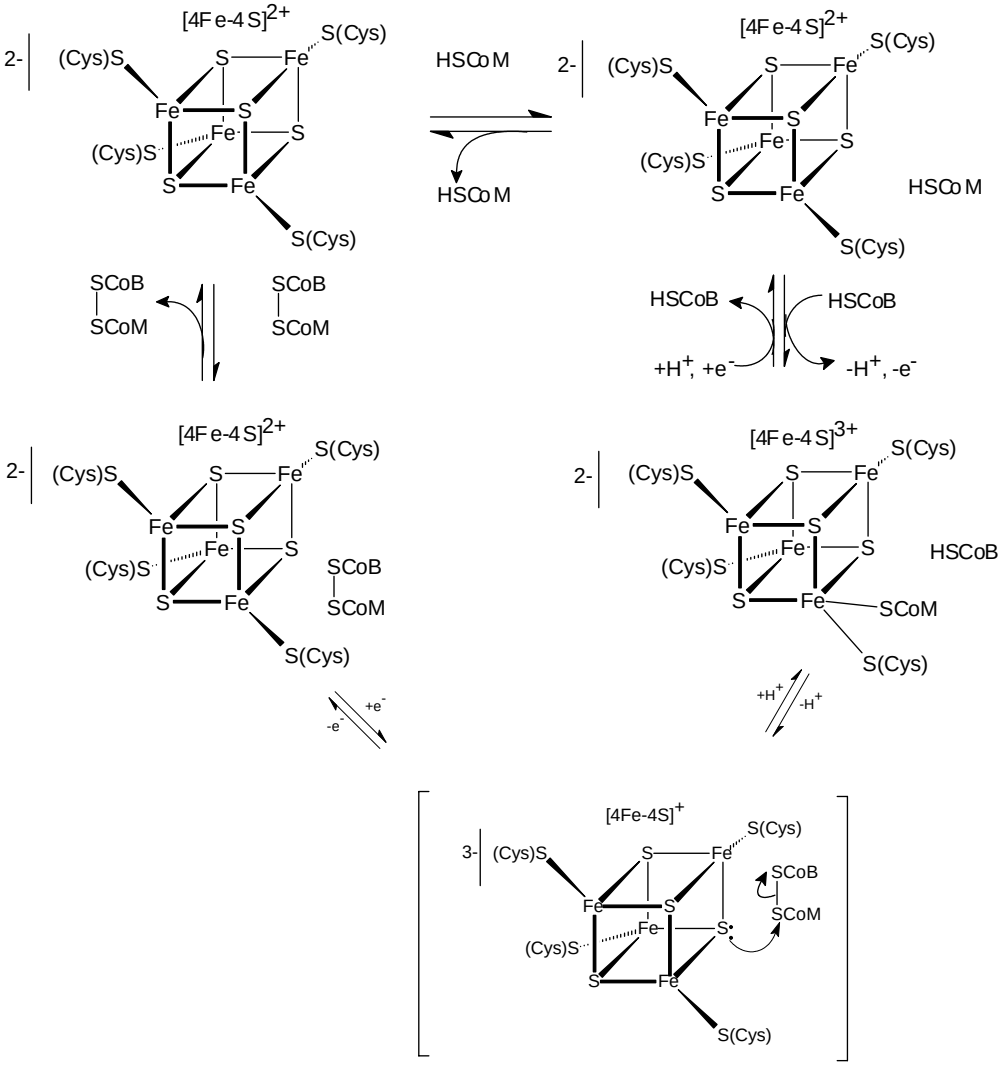

Figure 1-12: The proposed active site mechanism for the reversible heterodisulfide/dithiol reaction catalyzed by HDR where a cluster sulfur becomes electron rich. The reaction intermediates are shown in parenthesis. The oxidation state of the [4Fe-4S] cores is indicated above each of the cubane clusters (*90*).

Class of radical SAM enzymes

Enzyme catalysis involving both stable and transient organic radicals is emerging as a major mechanistic tool in diverse biological systems. The ability to observe radicals using spectroscopy gives convincing evidence that radicals participate in some enzymatic reactions. Enzymes that utilize radical chemistry are able to catalyze difficult chemical reactions that are challenging and unusual, but are not easy to work with because of their high reactivity and sensitivity to oxygen (*91*).

Radical SAM proteins use SAM to create a low potential radical on an amino acid residue in the protein that can be used to catalyze radical-type reactions either by actual protein or by acceptor proteins. Most radical enzymes are able to generate their own organic radicals while many depend on activating enzymes (activases) to provide the organic radical that they store as stable glycyl, cystenyl, tyrosinyl or tryptophanyl radicals for repeated catalytic turnovers (*92-94*).

Radical SAM enzymes belong to a protein family that has over 600 members and are present in plants, bacterial and mammals. They function in various biosynthetic pathways and catalyze a variety of reactions that include unusual methylations, sulfur insertion, isomerization, ring formation, anaerobic oxidation and protein radical formation. They also function in biodegradation pathways and in the synthesis of antibiotics, herbicides, DNA precursors and vitamins (*95*). Examples of the radical SAM enzymes include lysine 2,3-aminomutase (LAM), lipoate synthase (LipA), Biotin synthase (BioB), spore photoproduct lyase (SPP lyase); activating enzymes of anaerobic ribonucleotide reductase (aRNR-AE), pyruvate formate lyase (PFL-AE) and benzyl succinate synthase (BssDrAE) (*96,97*). HemN (oxygen-independent

Coproporphyrinogen lll oxidase), MiaB, a tRNA-methylthiotransferase, and the B_{12}-independent glycerol dehydrates activating enzyme are some that are discovered recently (*98-100*).

Although they have diverse functions, all radical SAM enzymes contain a [4Fe-4S] cluster that is ligated by three cystenyl residues. The [4Fe-4S] clusters of radical SAM enzymes are not very stable. They can easily break down to [3Fe-4S] or [2Fe-2S] clusters. They all share a conserved defining "CxxxCxxC" motif (where C is the amino acid cysteine and "x" is any amino acid) that is demonstrated to be responsible for the binding of the [4Fe-4S] cluster. This cluster is used in the reductive cleavage of SAM to generate a 5'deoxyadenosyl radical (*92,101,102*).

Radical SAM enzymes require the presence of S-adenosyl-L-methionine (Adomet or SAM), functioning as a co-substrate/cofactor, to be near the [4Fe-4S] cluster to perform carbon based radical chemistry through which electron can be transferred from the [4Fe-4S] to SAM. The non-cyteine ligated Fe atom has been shown by spectroscopic studies to be coordinated by both the amino group and a carboxylate oxygen of SAM as shown in figure 1-13 (*103,104*).

Reaction Steps of Radical SAM Enzymes

The initial step in all radical SAM enzymes is the reduction of the $[4Fe\text{-}4S]^{+2}$ clusters from the +2 oxidation state to the active +1 oxidation state (Figure 1-14). This is usually done by an external electron donor like dithionite. Reduced flavodoxin has been used for some radical SAM enzymes in *E.coli* (*105-108*) and adrenodoxin in plant biotin synthase (BioB) (*109-111*). The next step involves the transfer of an electron from the

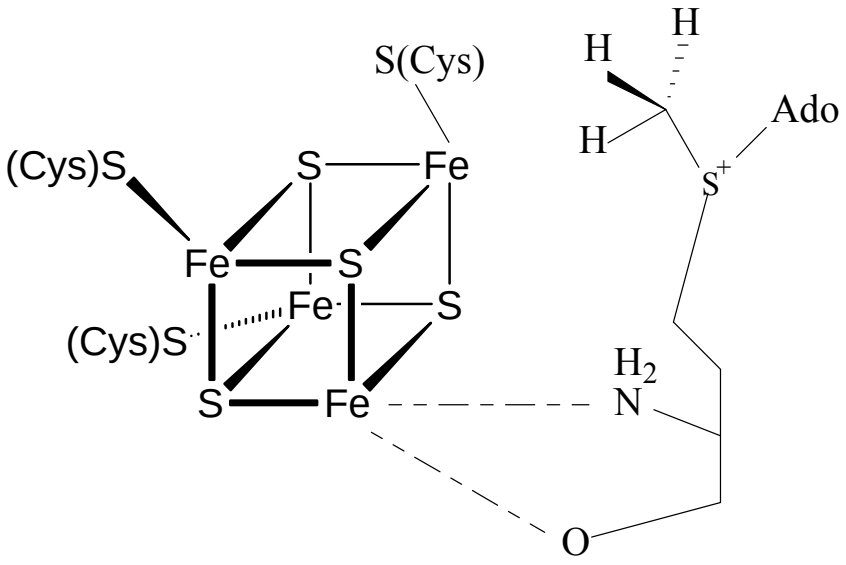

Figure 1-13: Derived Structures of the [4Fe-4S] cluster and SAM showing the coordination of the non-cysteine ligated Fe and SAM (*92*).

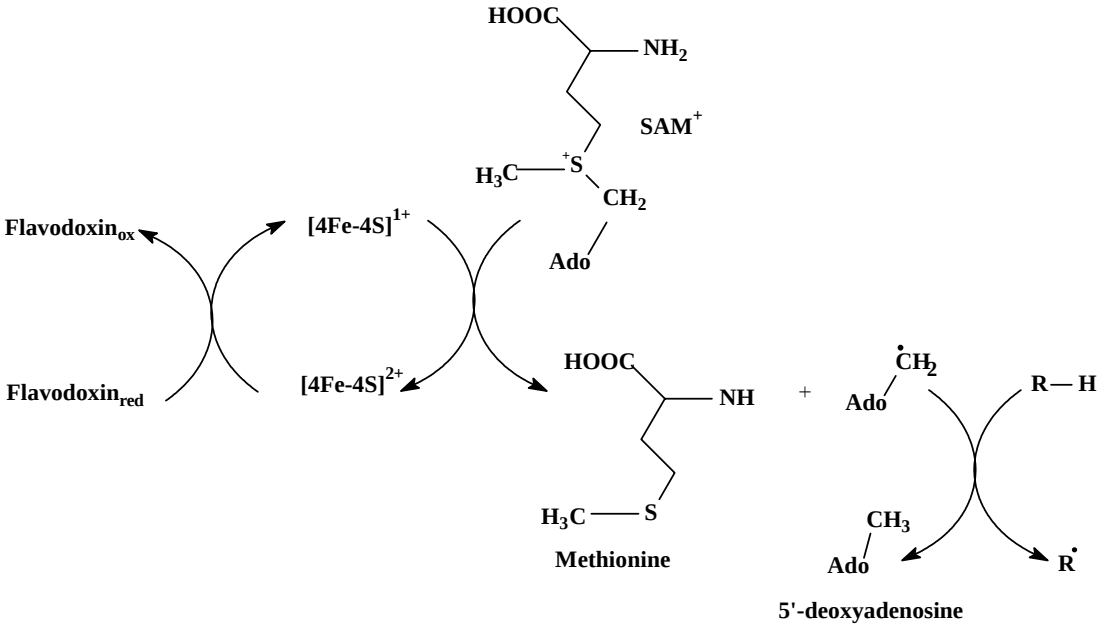

Figure 1-14: Reaction steps common to all radical SAM enzymes (*95*)

reduced [4Fe-4S] cluster ($[4Fe\text{-}4S]^{+1}$) to the sulfonium atom of SAM resulting in the break down of SAM into methionine and the 5'-deoxyadenosyl radical that cannot be observed because of its high reactivity (*111*).

Two mechanisms have been proposed for the reductive cleavage of SAM (*112,113*). Both mechanisms are dependent on the non-cystenyl Fe of the iron-sulfur cluster being coordinated through the carboxylate and the amino groups of SAM. ^{15}N and ^{17}O ENDOR spectroscopy proved SAM is directly ligated to the iron sulfur cluster in BioB, PFL activase and LAM as shown in figure 1-15a (*104,112*).

Selenium XAS showed that selenium is ligated to the unique iron in the [4Fe-4S] cluster upon reductive cleavage when Se-adenosylselenomethionine is employed as the coenzyme for LAM (*96,114*). This evidence suggests that the sulfur of methionine is liganded to iron when an electron is transferred to generate the 5'-deoxyadenosyl radical and methionine. This mechanism is supported by the active structures of LAM, HemN and MoaA (*98,115*). Another mechanism proposed is the ligation of the methionine sulfur to a sulfide of the [4Fe-4S] cluster upon reductive cleavage. This mechanism (Figure 1-15b) is proposed for PFL activase and BioB (*113*), but there is no currently available structural evidence that might support this mechanism for a glycyl radical activase.

The 5'-deoxyadenosyl radical generated abstracts a hydrogen atom from either an organic substrate to give a substrate radical (example is LAM) or a protein yielding a stable glycyl radical which can be observed directly by electron paramagnetic resonance (EPR) (*95,116*).

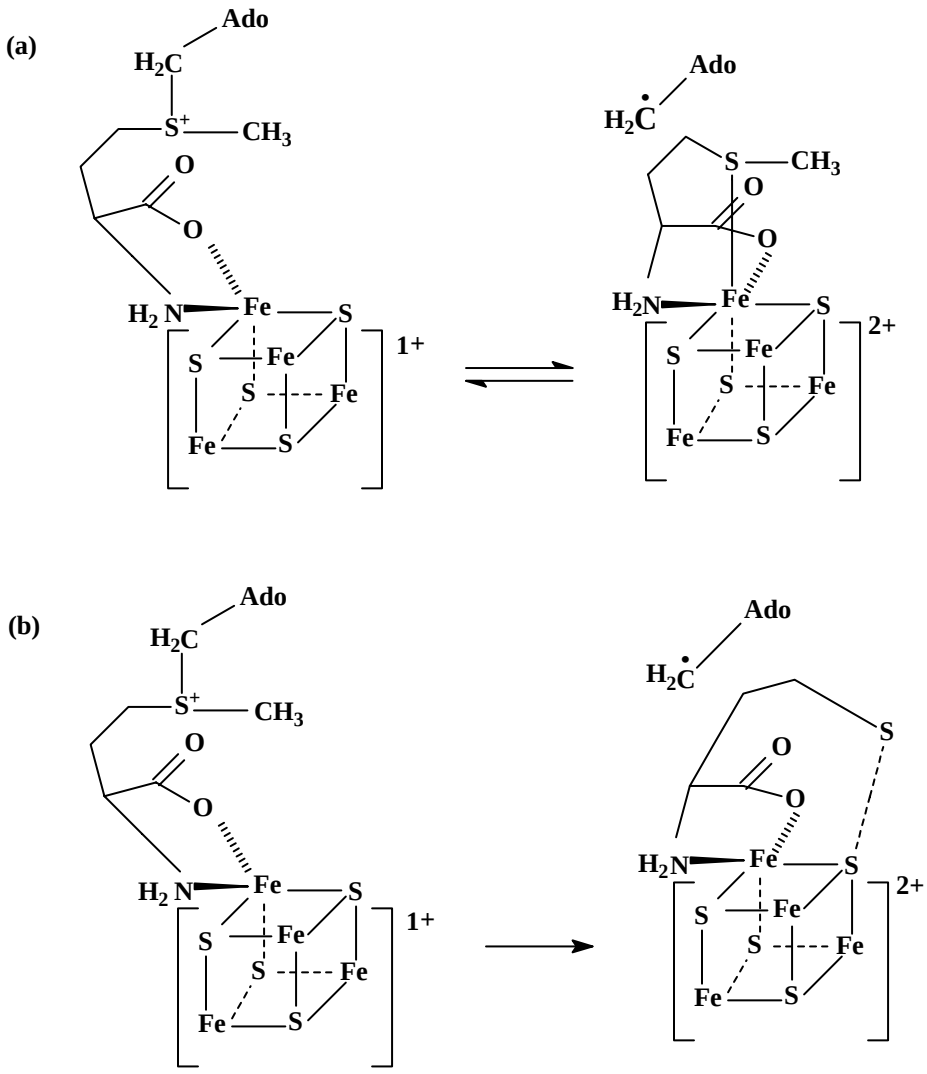

Figure1-15: Mechanisms for the reductive cleavage of SAM. (a) The reversible cleavage with ligation of sulfur in methionine to the unique iron. (b) Irreversible cleavage with interaction of sulfur in methionine with a sulfide in the [4Fe-4S] cluster.

The last step which can be different for different radical SAM enzymes involves either restoration of SAM in that the product radical re-abstracts a hydrogen atom from 5'deoxyadenosine (SAM acts as a cofactor) or SAM is consumed and functions as a co-substrate. However, in some cases, the stable protein radicals are regenerated at the end of the reaction cycle and are used over and over.

1.2 SPECTROSCOPIC TECHNIQUES

1.2.1 Electron Paramagnetic Resonance (EPR) spectroscopy

Introduction and Background

EPR is a technique that involves the absorption of energy from a microwave electromagnetic field by a system containing unpaired electron spins when placed in a strong magnetic field (*116*). It involves reorientation of the magnetic moment of an electron as induced by the magnetic field. According to the Pauli exclusion principle, only electrons that are unpaired can reorient their spins, so this technique is limited to such systems.

EPR has been successfully applied to biological systems for studying metal centers, since the technique can provide information concerning the redox state of the metal, the g-values, ground state spin hyperfine and zero-field splitting (*117*).

An EPR spectrometer is composed of the main console, magnetic power supply and the microwave bridge. The main console consists of the oscilloscope, detector, computer field modulation unit that set the center field and sweep the range of the applied DC magnetic field. A diagram of a continuous-wave EPR is shown in figure 1-16.

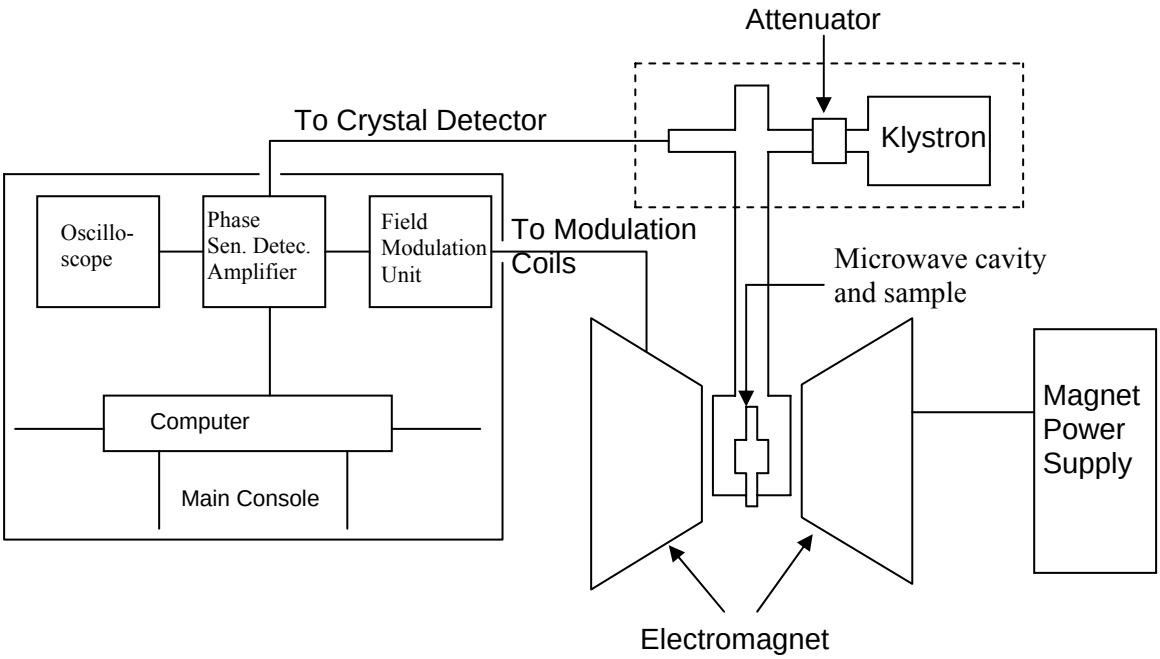

Figure 1-16: Schematic representation of a continuous–wave EPR spectrometer

The magnetic power supply is a current controlled magnetic field source that produces strong magnetic field lines along two adjustable pole pieces spaced apart to allow for the placement of the sample within the field. The maximum field of the magnet depends on its size, the maximum operating current and the positioning of the pole pieces.

The microwave bridge consists of microwave cavity and sample. The sample is inserted into the microwave cavity. At Auburn University the microwave cavity is either a high sensitivity perpendicular-mode or a dual-mode. The cavities can be fitted with either a liquid nitrogen finger dewar for measurement at 77 K or with a variable temperature helium flow cryostat for measurement in the 3.8 – 300 K range.

Magnetic resonance relies on the behavior of particles that possess both a magnetic moment and angular momentum. The angular momentum or the spin of an electron is given by a spin vector, S, which can have the value $\pm \hbar / 2$ and can take the values ±1/2 (spin quantum number) in any direction specified by the experiment. The magnetic moment of an electron (μ) is related to the angular momentum by the equation (*118*),

$$\mu = \frac{-g\beta S}{\hbar} \qquad (eq.1\text{-}1)$$

(the minus sign indicates that the spin and the magnetic moment are in opposite directions) where, S is the angular momentum or spin of an electron, β is the Bohr magneton, and g is a dimensionless factor, for a free electron, the value is 2.0032 (g_e).

Thus if an electron is placed in a magnetic field, the electron magnetic moment will align itself so that the angular momentum (spin) will be in opposite direction to the field. The energy of such a moment in a field is

$$\mathcal{H} = -\vec{\mu} \cdot \vec{H}_o \qquad (eq.1\text{-}2)$$

If the direction of magnetic field is H_o,

$$\mathcal{H} = -\vec{\mu} \cdot \vec{H}_o = \frac{g \beta S H_o}{\hbar} \qquad (eq.1\text{-}3)$$

The Zeeman energy of the electron has the value $\frac{-g \beta H_o}{\hbar}$ and $\frac{+g \beta H_o}{\hbar}$.

The minimum energy state is that in which the spin angular momentum vector ($-\hbar/2$) is aligned opposite to the magnetic moment vector ($g\beta/2$). The ground spin state of an electron in a magnetic field is -1/2; the excited spin state is +1/2 (*116,119*).

In principle, the EPR experiment involves the excitation of an electron from the ground state to an excited state, that is, the realignment of both the angular momentum and magnetic moment vectors in the applied magnetic field, H_o. The difference between these two states or the energy splitting is,

$$\Delta E = h\nu = g\beta H_o \qquad (eq.1\text{-}4)$$

where E is the energy, h is the Planck's constant and ν is the frequency of the electromagnetic radiation from the spectrometer (~ 9 GHz at X-band).

The energy difference between the spin states depends upon the value of H_o, which is usually represented by a splitting diagram (Figure 1-17). Equation 1-4 defines the "resonance" condition – which is the combination of electromagnetic radiation ($h\nu$), magnetic field (H_o) and orbital behavior of the electron (the g-value). Under these

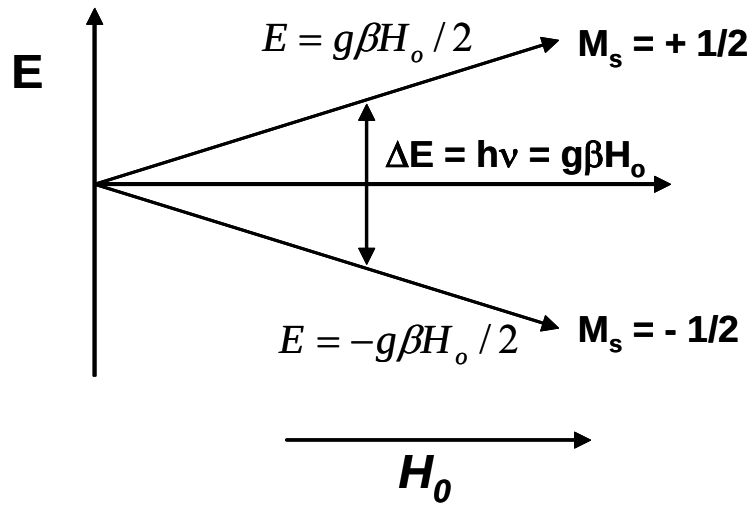

Figure 1-17: Representation of the energy level diagram for a free electron as a function of an applied magnetic field, H (*117*).

conditions, the sample will absorb microwave energy. In essence, the EPR experiment involves the application of a constant microwave frequency ν, while an applied magnetic field, H_o, is swept, the only condition being that $h\nu/H_o = g\beta$. A spin flip then results when the resonance condition is met. The selection rules governing this condition within a magnetic field applied perpendicular to the microwave energy is $\Delta Ms = \pm 1$ (*117*). EPR spectra are usually obtained by a procedure similar to continuous wave method; in which the absorption of energy from a continuous electromagnetic field satisfies the relationship, $h\nu = g\beta H_o$ (resonance condition) (*117*). The energy interval available from the incident electromagnetic radiation is fixed at ($h\nu = \Delta E$), a spectrum is generated by steadily changing the difference between ground and excited spin states of the electron spin systems by changing the magnetic field, thus making the difference equal to hν for each system. In going from lower to higher values of H_o, one brings the system into resonance that have steadily decreasing g values; that is, as H_o increases, the value of g necessary to satisfy $h\nu = g\beta H_o$ decreases.

To allow for the necessary signal amplification, the d.c absorption is converted to an a.c one by modulating the external magnetic field, H_o, at a fixed frequency with a secondary field H_m. The detector is driven at the same frequency and is therefore sensitive only to input which varies with the frequency of modulation; essentially the d.c noise is ignored. The result of this modulation is that the "absorption" is displayed in the first derivative or dispersion mode which indicates that the absorption difference between $H_o \pm H_m$ represents the instantaneous slope of the absorption curve at H_o. As H_o is swept through the absorption envelope, the change in slope per increment in H_o is measured and a first derivative is generated (Figure 1-18) (*120-122*).

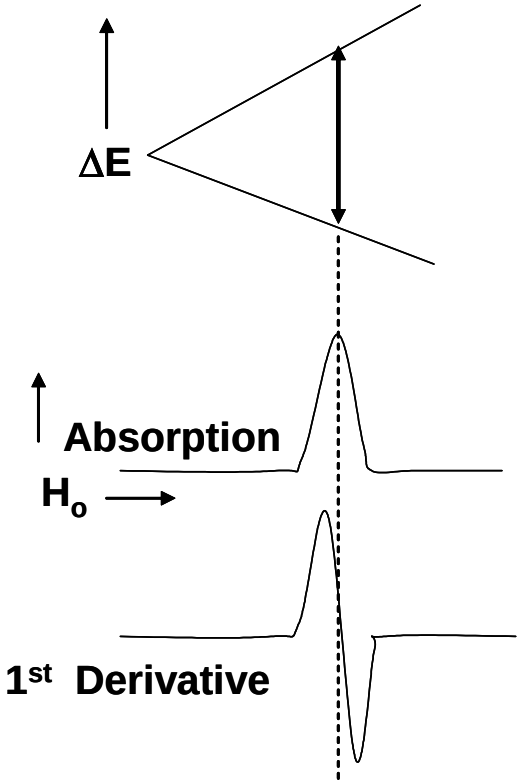

Figure 1-18: Schematic representation of EPR experiment (*121*)

In making an EPR measurement, the temperature to use needs to be considered. Physiological processes usually occur in an aqueous environment and at temperatures above about 273K, at these temperatures water is liquid which is difficult for EPR measurements. The type of paramagnetic species may dictate the choice of the temperature, often EPR are too broad to measure at physiological temperatures, due to rapid spin relaxation rates which cause broadening of the EPR signals. This can be observed if the paramagnetic species has $S > ½$ or has significant g anisotropy and so most transition metal ions and high spin species require cryogenic temperatures for EPR studies (*122*).

Temperature is also important in EPR measurements with regard to the Boltzman population of the various spin states. The intensity of an EPR signal is directly proportional to the population difference between the two levels in resonance, and this population difference is inversely proportional to the temperature. The population difference is small at room temperature, but is much larger at liquid helium temperature for measurements at X-band frequency, for metalloproteins in which the EPR spectral extend over a magnetic field range, the gain in sensitivity at cryogenic temperatures is an important factor in detecting EPR signals (*123*).

Quantitative analyses EPR signals can be of interest in EPR measurements. This involves comparing the doubly integrated area of the EPR signal that is of importance to that of a concentration standard, most commonly used standards are copper (II) sulfate, potassium peroxylamine disulfonate ($K_2NO(SO_3)_2$), copper permanganate and TEMPO (2,2,6,6-tetramethyl-1-piperindinoxy) (*117*). It is crucial that both the sample and the standard EPR spectra are recorded under non-saturating conditions (*124*).

Under non-saturating conditions, the EPR signal intensity is directly proportional to the concentration of the spins provided the spectra are recorded under the same conditions (i.e. temperature, sample volume, magnetic field modulation frequency and amplitude, and microwave power), thus, the ratio of the doubly integrated areas of the standard and sample will be equal to the ratio of their concentrations.

For biological systems, the sample may contain more than one paramagnetic center. This is usually observed for proteins that are involved in electron transfer. Spectral simulation of different EPR signal components is of important use. A set of parameters that are obtained can be verified by spectrum simulation and comparison with the experimental spectrum (*125*). Integration of the simulated spectrum can be helpful in identifying overlapped or hidden signals. In addition, it is possible to calculate the total doubly integrated area of single species by measuring the area of a resolved peak at a single turning in the first derivative such as $g = g_z$ provided that all the g values are known (*126*). This method has been helpful and widely used for quantitative EPR measurements in biological systems.

g- value

The most important information in an EPR spectrum is the g-value. The g- value for a free electron in space is 2.0023 and this is the ideal value. The value of g can be calculated from the numerical expression below assuming ν to be in units of GHz and H_o expressed as gauss.

$$g = h\nu/\beta H_o \quad \text{or} \quad g = \frac{(714.5)\nu}{H_o} \qquad (eq.1\text{-}5)$$

The above expression is valid for a molecule in one orientation in a magnetic field. For a free unpaired electron, the Zeeman splitting constant is

$$g_e = 2.00232$$

although the orbital angular momentum and interactions with other spins (other electrons or nuclei) can cause the g- value of 2.0 to vary according to

$$g = g_e + \Delta g \qquad (eq.1\text{-}6)$$

Most metal complexes in biological systems have g-values that deviate from the ideal value. This is due to the fact that when an electron rotates around a nucleus, the electron experiences another magnetic field (H_1) due to the movement of the nucleus around the electron (from it's point of view) in addition to the applied magnetic field, (H_o). The orbital angular momentum together with the spin angular momentum now have an effect on the magnetic moment of the electron and thus the nature of the additional field (H_1) depends on the orbital in which the electron resides causing the g-value to stray from the ideal value.

Lowered symmetry caused the ground state orbital angular momentum to be quenched for metal ions in biological systems; however, spin-coupling provides an effective mechanism for mixing excited states with orbital angular momentum into the ground states. The efficiency of this coupling varies from system to system, so spin orbit coupling is an important component of the g value that makes characterization of the paramagnetic center possible; at the same time, this coupling must have directionality, it must be anisotropic (*118,127*).

The spin-orbital Hamiltonian is given by:

$$H_{s.o.} = \beta(B \bullet g \bullet S) \qquad (eq.1\text{-}7)$$

where g is a 3x3 tensor, B is the row vector, and S is a column vector.

Biological samples are typically measured as solutions of frozen liquid in which the molecules are randomly oriented with respect to the applied magnetic field. Three possible groups of g-anisotropy in a simple S = ½ EPR signal and their first derivative line shapes are shown in figure 1-19. The first group is the isotropic resonance in which $g_x = g_y = g_z$ (for a cubic). The second group is called the axial system in which $g_x = g_y \neq g_z$. In this group g_z is denoted as $g_{//}$ (g: parallel) and $g_x = g_y = g_{\perp}$; $g_{\perp}$ (g: perpendicular) and may be either greater or less than $g_{//}$ as shown in the figure 1-18. The third group is called the anisotropy (rhombic) in which all the g values are unequal ($g_x \neq g_y \neq g_z$) (*118,128*).

Zero-field splitting (ZFS) can occur in complex systems that involve two or more unpaired electrons as a result of spin-orbit coupling between the ground states and the excited states resulting in the difference in energies of the spin sub-states (Ms).

The Kramer's systems are those with an odd number of unpaired electrons and should, in principle, always exhibit an EPR signal even on large ZFS due to degeneracy within the ± Ms Levels. For a S = 5/2 with no ZFS as depicted in figure 1-20, transitions occur at the same magnetic field and frequency for all ΔMs ± 1. Introduction of weak ZFS results in the same transition but at a slightly different magnetic fields a shown in figure 1-21A. When the axial ZFS is greater than the quanta of microwave energy, only the Ms ± 1 doublet transition is allowed as depicted in figure 1-21B.

When both axial and rhombic ZFS are present, the description above becomes more detailed and the spin Hamiltonian becomes:

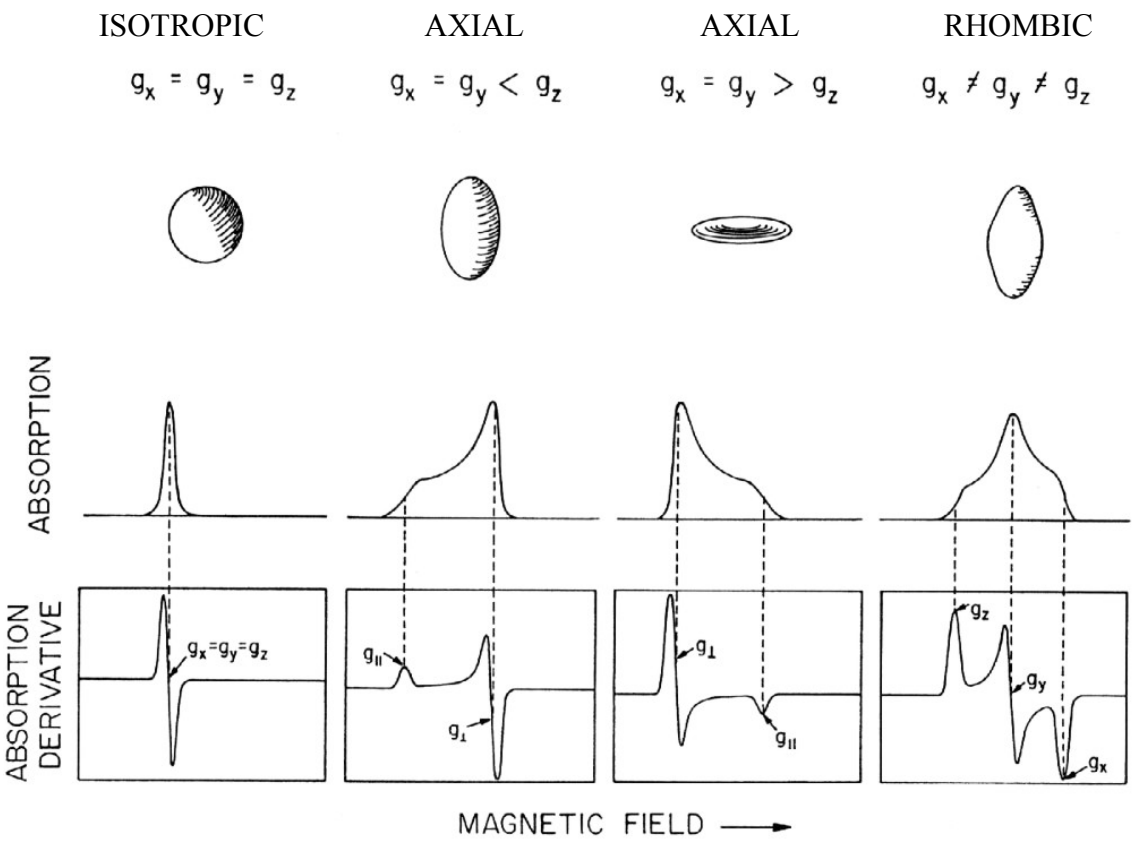

Figure 1-19: Idealized powder EPR spectra of isotropic, axial and rhombic S = 1/2ystem. Taken with permission from (*118*). (Copyright University Science Books)

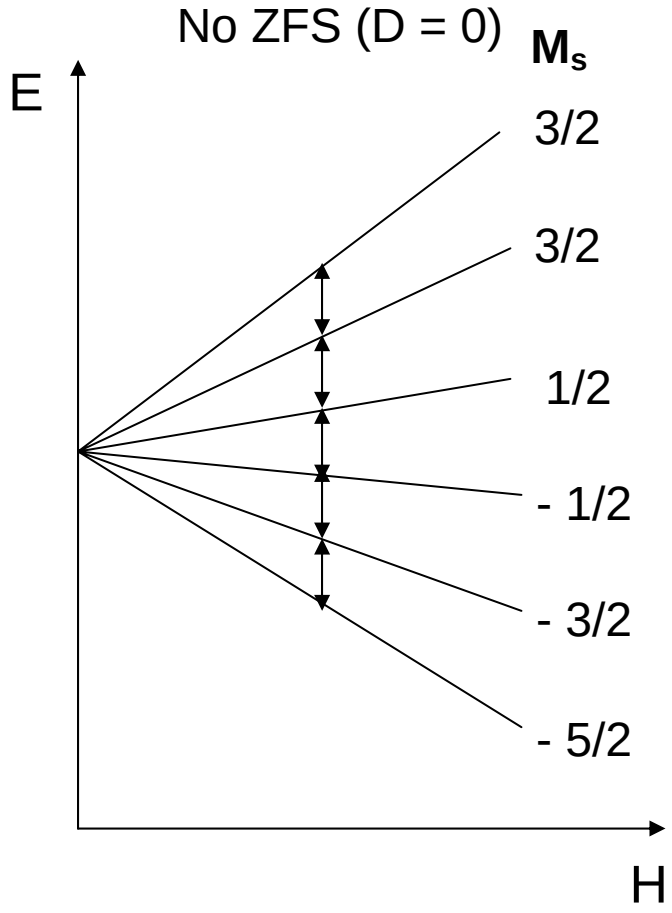

Figure 1-20: The energy level diagram for a d^5 high spin system (S = 5/2) in the absence of zero-field splitting (D = 0) (*117*)

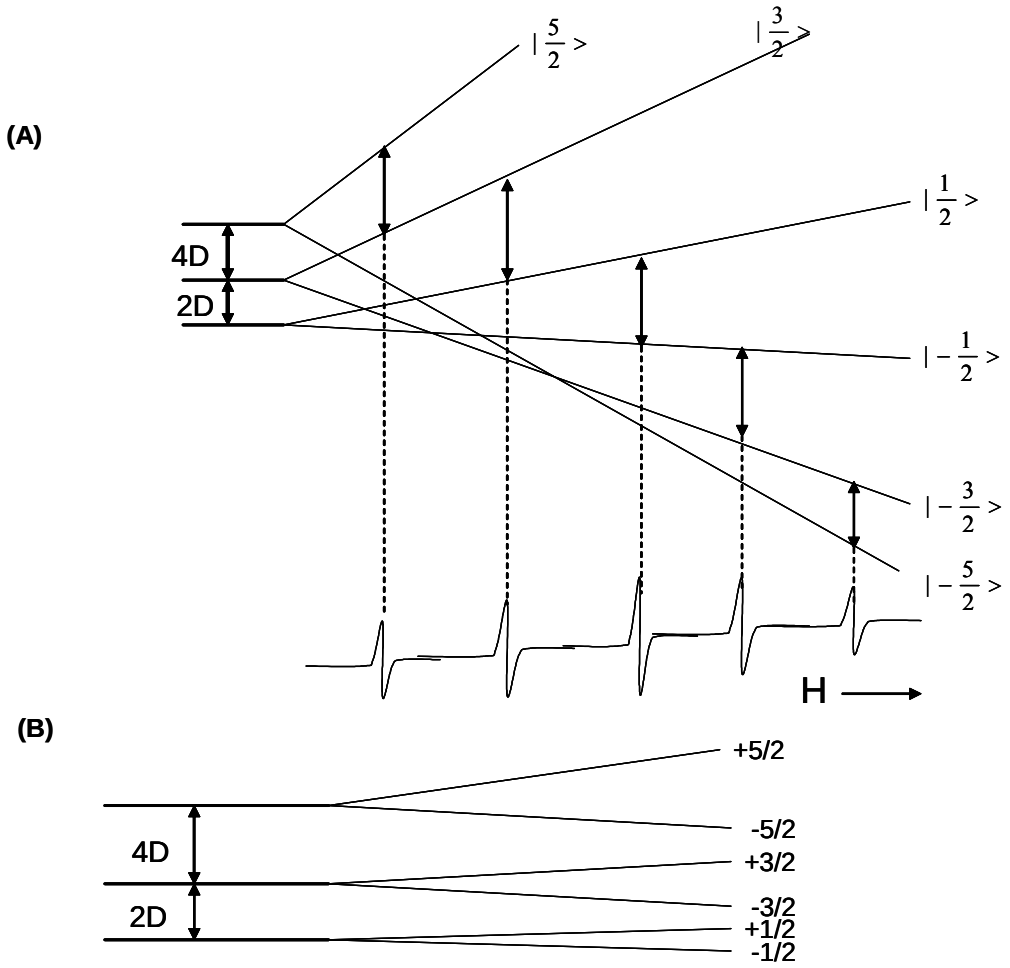

Figure 1-21: The energy level diagram and spectrum of a d^5 high-spin ion in both a weak (A) and strong (B) tetrahedral magnetic field applied parallel to the tetragonal axis (*121*).

$$\mathcal{H} = D\left[S_z^2 - \frac{S(S+1)}{3}\right] + E\left(S_x^2 - S_y^2\right) + g_e \beta B \bullet S \qquad (eq.1\text{-}8)$$

where D and E are the axial and rhombic ZFS parameters respectively. Rhombic distortion serves to mix the Ms level so that transitions within each level become possible. Effective g-values can be predicted as a function of E/D for each doublet, based on the above equation and assuming the free electron value (i.e., $g_e = 2$). The resulting plots are called "rhombograms" depicted in figure 1-22 (*129*), that are helpful for the interpretation of EPR spectral for systems with S > ½. The intensity of the transitions from the individual doublets depend on the Boltzman population and both the transition probability and the ZFS. For a pure axial system, E = 0 and |D| > 0. In a rhombic system, E/D = 0.33, E > 0, and D can either be negative or positive.

Non- Kramer's systems, those with even number of unpaired electrons, generally usually have a large ZFS as opposed to Kramer's systems. For a S = 2 system in which D < 0 for a typical reduced $[3Fe\text{-}4Fe]^0$ cluster as shown in figure 1-23, the two lowest levels of the S = 2 (Ms ± 2) are split by an energy defined by $\Delta = 3E^2/D$. The energy levels of the lowest doublet can be separated by an amount that is much more than 0.3 cm^{-1} (provided by most X-band spectrometers) depending on the degree of rhombicity in the ZFS. This transition is not usually observed by EPR spectroscopy (*130*).

Changing the orientation of the microwave magnetic field from the perpendicular applied magnetic field to the parallel magnetic field changes the EPR selection rule to ΔMs = 0. Due to the mixing of field-induced mixing of zero-field components, ΔMs = 2 and ΔMs = 4 transitions are now possible, but the transitions from Kramer's systems are formally forbidden.

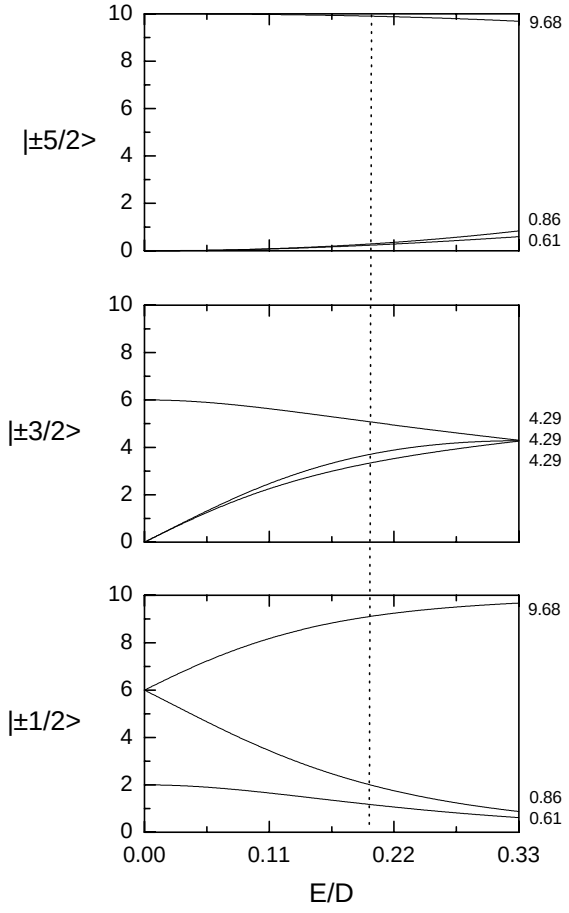

Figure 1-22: Rhombogram plot for a S = 5/2 as function of the ratio of rhombic and axial zero-field splitting parameters (E/D). The upper panel represents the $M_s = \pm 5/2$ doublet; the middle panel represents $M_s = \pm 3/2$ doublet and the lower panel represents the $M_s = \pm ½$ doublet (*121*).

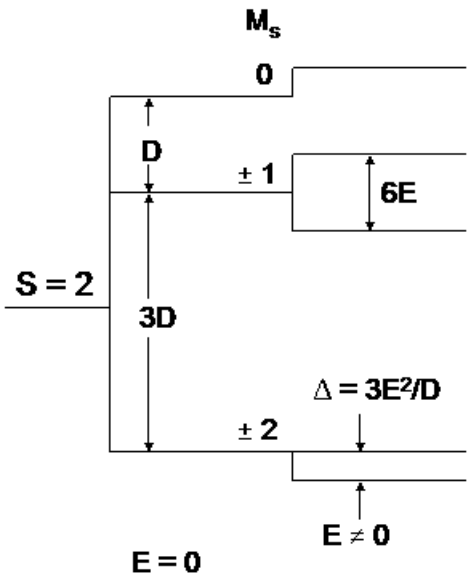

Figure 1-23: Graphical representation of the zero-field splitting of the S = 2 of a ground state of a reduced $[3Fe\text{-}4S]^0$ cluster (*131*).

Hyperfine Splitting

The interactions of the unpaired electrons of a paramagnetic center with a nearby nucleus give rise to hyperfine interactions. These interactions can result from the electron interacting with its own nucleus (simply called hyperfine interaction) or interaction of the electron with a nucleus that belongs to a different part of the molecule, most commonly the ligand to the metal, this type of interaction is known as superhyperfine interaction.

The electron-nuclear interactions result in splitting of the EPR spectrum, thus adding another term to the energy expression of the EPR transition as thus,

$$E = h\nu = M_s g\beta H_0 + AhM_I M_s \qquad (eq.\ 1\text{-}9)$$

where A is the hyperfine coupling constant, M_I is the nuclei spin.

The hyperfine coupling constants can be calculated from splittings in the EPR spectrum. For most metalloproteins, these splittings cannot be resolved and the importance of the chemical information which they carry cannot be known. Electron nuclear double resonance (ENDOR) spectroscopy retrieves this information, thus making ENDOR to be of great use in the study of metalloproteins (*132*).

1.2.2 Electron Nuclear Double Resonance (ENDOR) of Metalloproteins

ENDOR is an important spectroscopic technique that helps in the understanding of the functions of metal ions in biological systems. Its application is growing unabated since new biological systems are being explored and enzymic intermediates become the central point of research. Information about the structure, composition and bonding at

the active site of biological systems is important, leading to the identification of enzymic mechanisms (*133*).

ENDOR experiments have been performed on a number of biological systems to determine the active site structure. This involves the use of bonding and geometric information to know the hyperfine interaction tensor (A), [for hyperfine coupled nuclei (I = 1/2)] together with the quadrupole interaction tensor (I>1/2).

In metalloenzymes, identification of the spin center that gives rise to the EPR signal has been investigated by using continuous wave (CW) ENDOR, in combination with isotopic labeling since few metals have isotopes in their natural abundance that have nuclear spin greater than 0 (I > 0). ENDOR from ^{57}Fe (I = 1/2) and ^{95}Mo (I = 5/2) have been used to determine the contribution of these nuclei to the electron spin S = 1/2 and S = 3/2 clusters of carbon monoxide dehydrogenase (CODH) (*134*) and nitrogenase (*135*) respectively.

Proton ENDOR is being used to probe the origin of EPR signals of most organic based radicals by the use of isotopic labeling of amino acids. Proton ENDOR has been used to identify the tyrosyl radicals in photosystem II and in ribonucleotide reductase and a tryptophan in cytochrome-c-peroxidases (CcP) (*136*,*137*). Hydrogen bonding to the clusters in Fe-S is important since this interaction can also modulate the cluster function. Isotopic substitution of ^{2}D gives insight to probe the hydrogen bonding to metal clusters (*138*).

Metal ligands of metalloproteins have been identified by the use of ENDOR by obtaining information from ENDOR signals of ^{14}N (I = 1), ^{1}H (I = 1/2) in native samples which is then confirmed by isotopic labeling with ^{15}N (I = 1/2) and ^{2}D (I = 1). ENDOR

study of the Rieske [2Fe-2S] center of phthalate dioxygenase (CDO) (*139*) from *Pseudomonas cepacia* confirmed that the two imidazole nitrogens from histidine are coordinated to the [2Fe-2S] cluster. This makes it different from the ferredoxin-type [2Fe-2S] center that is ligated by cysteine residues.

Furthermore, ENDOR has been used in the characterization of the iron sulfur cluster in aconitase enzyme (*83,140*) both in the substrate free [E] and substrate bound states [ES].

1.2.3 RESONANCE RAMAN SPECTROSCOPY

Raman spectroscopy is a scattering technique and a form of vibrational spectroscopy. Vibrational spectra are observed experimentally as infrared or raman spectra (*141*). Raman scattering effect occurs by the interaction of the incident light with the electrons in the molecule. The energy of the incident light is not enough to excite the molecule to a higher electronic level. This results in changing the molecule from its initial vibrational state to a different vibrational state (*142*) . Raman spectra give insight into the vibrational motions of atoms in molecules. Since these vibrations are sensitive to chemical changes, the vibrational spectrum can be used in monitoring molecular chemistry.

A Raman spectrum is the dispersion of scattered light from a sample that is illuminated by a monochromatic light source. This scattering results from the interaction of the electric vector of an electromagnetic wave with the electrons of a compound leading to the scattering of the incident light.

Raman scattering uses excitation at a given frequency (ν_0), such that most of the scattered light has the same frequency i.e., it does not involve a change in the energy content of the incident and the scattered light. This is known as Rayleigh scattering (Figure 1- 24b) and it is elastic.

When the scattered light has a lower energy than the incident light, and thus has a lower frequency (higher wavelength), this effect is called Stokes Raman scattering (Figure1-24a). Anti-stokes Raman scattering occurs when the scattered light is of higher energy than the incident light i.e, the scattered light has a higher frequency (shorter wavelength) (Figure 1-24c). These two forms of Raman scattering are known as inelastic scattering (*143,144*). In Raman scattering, the Raman shift ($\Delta\nu = \nu_1 - \nu_2$), relates to the energy of the vibrational transition which gives information about the molecular structure.

Resonance Raman of Metalloproteins

Resonance Raman spectroscopy (RR) is used in the study of metal centers of metalloproteins. The RR technique is a form of Raman spectroscopy in which the wavelength of the incident light beam lies under an electronic absorption of the sample. It makes use of the monochromatic laser light that is tuned to the same frequency as an allowed electronic transition of the chromophore (Figure 1-25). Thus, only the normal modes which are vibronically active in the electronic transition will have their raman intensities increased (*141*). This results in the observation of a resonance enhancement in the scattering intensity of only the bands that are coupled to electronic transition. This

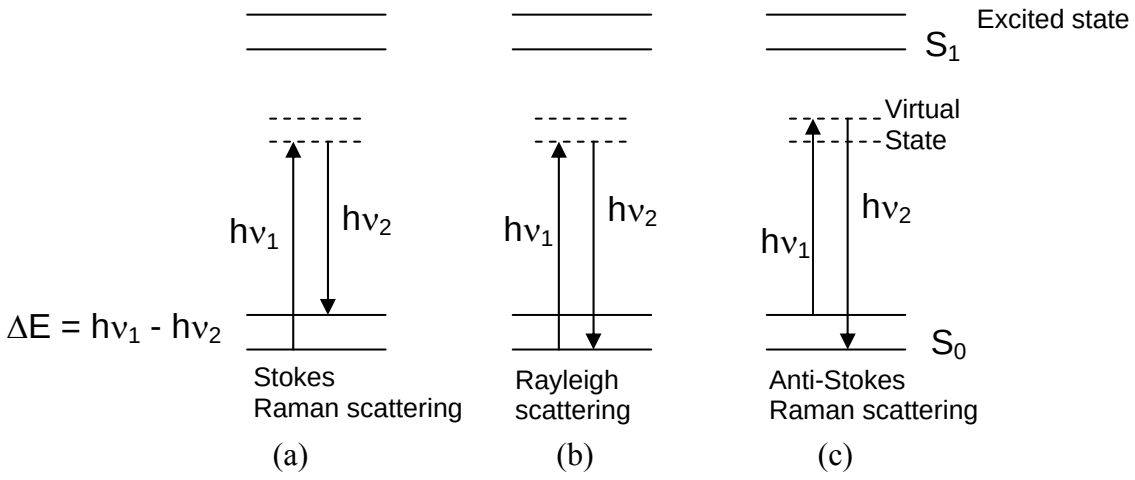

Figure 1-24: Schematic diagram showing the relationship between (a) Stokes Raman scattering (b) Rayleigh scattering and (c) Anti-Stokes Raman scattering (*141*).

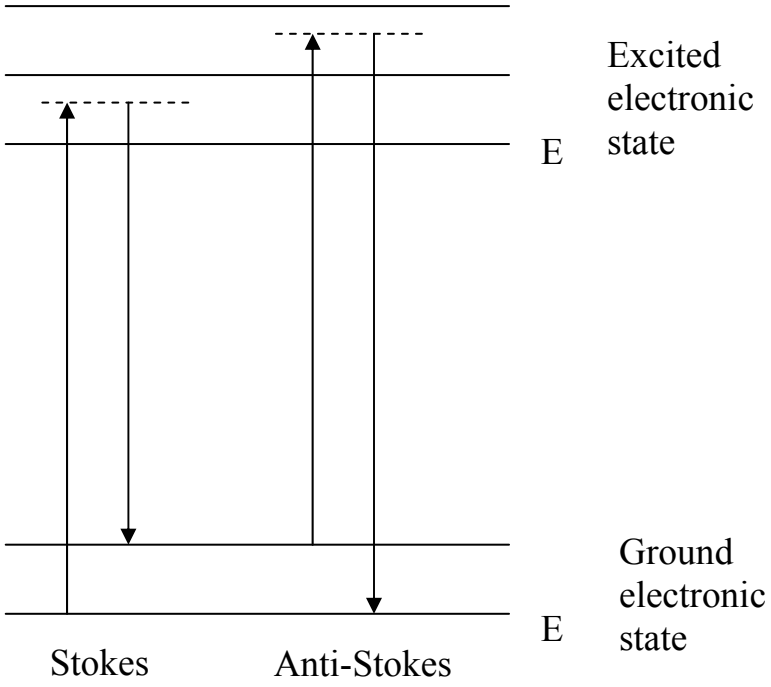

Figure 1-25: Schematic diagram of a Resonance Raman scattering. The dashed lines represent the virtual excited states (*141*).

then minimizes the interference from the sample environment such as amino acid vibrations and hence selectively identifies the chromophoric centers of interest.

The enhancement depends on the energy and intensity of electronic transitions and on their coupling to the vibrational modes that are involved in the chromophore. Resonance Raman can be of importance in monitoring the structural changes of a chromophore, in particular metal centers, that are modulated by its environment, since most of these metal centers of the chromophores are located at the active sites that is responsible for the function of the metalloprotein. The frequencies and intensities of the RR bands are sensitive to the nature of the chemical bonding and the molecular configuration of the atoms participating in the vibrations and thus provide structural and mechanistic information about chromophoric metalloproteins (*145*).

In metalloproteins, metal d-d transitions are ineffective in resonance enhancement because they are too weak. Metal to ligand charge transfer (MLCT) transitions are possible when the metal is bound to π acid ligands, as is the case for compounds such as CO, NO, O_2 and porphyrin. Ligand to metal charge transfer (LMCT) are possible for any metal, but only the more reducible ones like Fe (III) and Cu (II) have LMCT in the visible regions.

In Fe-S clusters, most of the transitions in the visible region are due to S → Fe (III) charge transfer, the amount of ferric character determines the degree of resonance enhancement gain. Therefore, the greater the resonance enhancement, the more Fe (III) character present in the cluster (*146-148*). Table 1-2 shows the different types of clusters in the reduced and oxidized state and the ferric character associated with each of them.

Resonance Raman spectroscopy has also provided signatures of the cluster type in

Fe-S protein. The frequency and intensity of Fe-S vibrational mode allows a distinction between [2Fe-2S], [3Fe-4S] and [4Fe-4S] clusters (*146*). Figure 1-25 shows the overview of RR spectra for some standard type Fe-S clusters.

Table 1-2: Resonance enhancement of different Fe-S clusters (*149*)

Cluster type	Formal Oxidation State	Resonance Enhancement
$[2Fe\text{-}2S]^{2+}$	2Fe (III)	Strong
$[2Fe\text{-}2S]^{1+}$	1Fe (III), 1Fe (II)	Medium
$[3Fe\text{-}4S]^{1+}$	3Fe (III)	Strong
$[3Fe\text{-}4S]^{0}$	2Fe (III), 1Fe (II)	Medium
$[4Fe\text{-}4S]^{3+}$	3Fe (III), 1Fe (II)	Medium
$[4Fe\text{-}4S]^{2+}$	2Fe (III), 2Fe (II)	Medium
$[4Fe\text{-}4S]^{1+}$	1Fe (III), 3Fe (II)	Very weak

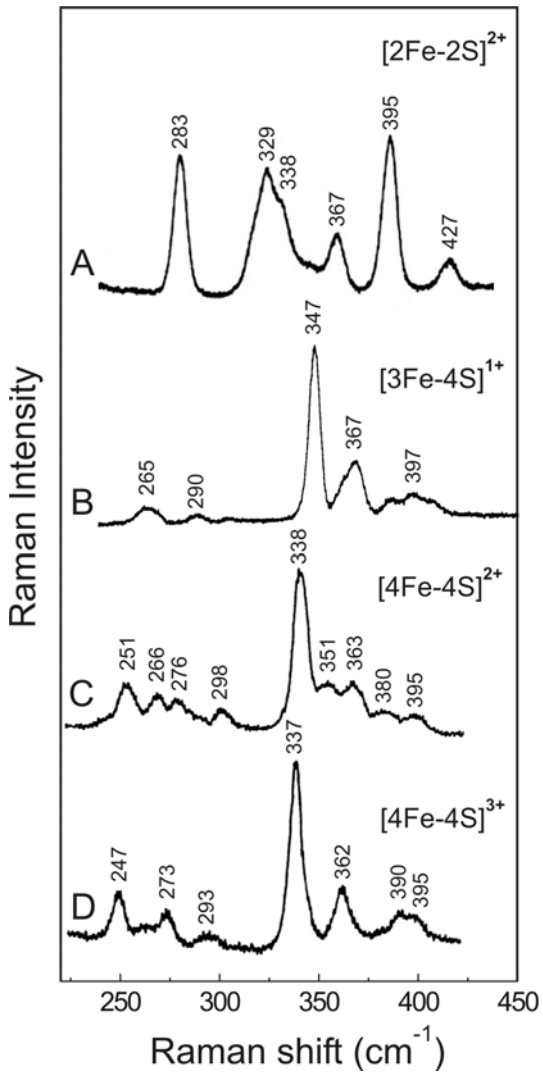

Figure 1-26: RR spectra of iron-sulfur clusters from different organisms.

(A) *Putidaredoxin* (B) $[3Fe\text{-}4S]^{+1}$ cluster from *Pyrococcus furiousus* ferredoxin

(C) $[4Fe\text{-}4S]^{+2}$ from *Clostridium pasteurianum* 4Fe ferredoxin

(D) $[4Fe\text{-}4S]^{+3}$ from *Chromatium vinosum*, HiPIP.

(Courtesy of Michael Johnson at the Center for Metalloenzymes, University of Georgia, Athens)

1.3 Statement of purpose

The research presented here is focused on the characterization of the iron-sulfur clusters that are present in the enzymes GcpE and LytB. These enzymes are involved in the last two steps of the alternative pathway of isoprenoid synthesis. The alternative pathway is utilized by various pathogenic organisms.

The ultimate goal of Dr. Duin's research is to design compounds that can inhibit GcpE and LytB enzymes that will eventually serve as anti-infective drugs in the treatment of the diseases caused by these pathogens. Before this can be achieved, a better understanding of the respective reaction mechanisms is necessary.

In this work, the purification and characterization of GcpE from *Thermus thermophilus* and LytB from *Aquifex aeolicus* will be discussed. The third enzyme studied is an accessory protein called YfgB. YfgB enzyme is not involved in the alternative pathway of isoprenoid synthesis. Genetic evidence (Heidi Sofia, personal communication) indicates that YfgB belongs to the class of radical SAM proteins and is probably an activating protein for GcpE enzyme.

The goal of this work is to characterize the iron-sulfur clusters present in these proteins using various spectroscopic techniques so as to establish their roles.

CHAPTER 2

MATERIALS AND METHODS

2.1 Biochemical and chemical reagents

Glucose, dithiothreitol (DTT), sodium sulfide, ampicilin, ferrous ethylenediammonium sulfate, neocuprine, ferrozine, imidazole, iron (III) chloride, Tris base, sodium dithionite, potassium permanganate, ammonium acetate, S-adenosyl methionine (SAM) and Isopropyl-β-D-thiogalactoside (IPTG) were purchased from Sigma-Aldrich (St. Louis, MO). Absolute ethanol, ethylene glycol, magnesium sulfate, magnesium chloride, tryptone, yeast extract, LB-agar, sodium chloride, hydrochloric acid and Tris-base were from Fisher Biotech (Pittsburgh, PA). Diethyl amino ethyl (DEAE) sepharose, Mono Quaternary ammonium (mono Q), XK 16/60 sephadex 200, PD-10 columns were purchased from Amersham Biosciences (Piscataway, NJ). Centricon ultrafiltration units were from Millipore.

MEcPP was synthesized at Justus-Liebig University at Giessen by Jochen Wiesner. All buffers, media and reagents were prepared using water that had been purified at a resistance of 18.2 MΩ/cm through a Millipore system (MilliQ, QPAK II).

Anaerobic buffers were used for all purifications and experiments. The buffers were filtered and subsequently boiled under nitrogen gas flow. The buffers were stirred under vacuum for 1-2 h. The buffer could then be used or stored under argon. For storage, 0.3 atmospheric over pressure was applied to the head space of the storage

bottles. All purification steps and experiments were performed under exclusion of dioxygen in an anaerobic tent under an atmosphere of 95% N_2 and 5% H_2 (Figure 2-1).

2.2 Construction of LytB plasmid

Expression plasmids were constructed at Justus-Liebig University at Giessen by Jochen Wiesner using the following procedure:

The *lytB* gene of *Aquifex aeolicus* was amplified by polymerase chain reaction (PCR) using *A. aeolicus* genomic DNA and the oligonucleotides Aa-LytB-cHis-for (5'-CCATGGTTGACATAATAATCGCA-3') and Aa-LytB-cHis-rev (5'-AGATCTGGAGGAAACCAATTGCCC-3'), introducing an *NcoI* and *BglII* restriction sites respectively.

The PCR product was ligated into the pCR-TOPO-T/A-vector (Invitrogen), verified by restriction endonuclease analysis and sequencing, and subsequently cloned into pQE60 vector (Qiagen) using the restriction enzymes *NcoI* and *BglII* resulting in the plasmid pQE60-Aa-LytB. This construct allowed the production of the *A.aeolicus* LytB protein in *Escherichia coli* with a carboxyl terminal extension of eight amino acids (*150*).

2.3 Expression and Purification of LytB protein

2.3.1 Expression of LytB protein

E.coli XL-1 blue cells were transformed with pQE60-Aa-LytB. Cells from frozen glycerol stocks were plated on LB-agar plates supplemented with 10 mg/mL ampicilin (LB-Amp). A single colony with the above construct was used to inoculate 2 mL SOC media containing 10 mg/ml ampicilin. The culture was incubated overnight for

Figure 2-1: Picture of the anaerobic tent.

approximately 17 hours with shaking at 37°C. The 2 mL culture was used to inoculate 30 mL SOC-Amp media which was subsequently incubated for 12 hours at 37°C. 50% of the 30 mL culture was used to inoculate two 100 mL SOC-Amp media containing 10 mM $FeCl_3$. The cultures were incubated for 12 hours at 37°C, and used to inoculate two 1L flasks of SOC-Amp media containing 100 Mm $FeCl_3$. When the O.D. of the culture at 600 nm reached a value of 0.4-0.5, which took about 1 h, isopropyl-β-D-thiogalactoside (IPTG) was added to a final concentration of 0.4 mM. The incubation continued at 37°C for 9 hours with shaking until the O.D at 600 nm reached 4.0-4.5. The cells were harvested by centrifugation at 10,000 rpm for 20 minutes and cell pellets were stored at -80°C.

2.3.2 Purification of LytB protein

Cells from a 1L growth were resuspended in 50 mL buffer A (30 mM Tris-HCl pH 8.0, 100 mM NaCl). Cell lysis was performed by sonication followed by centrifugation at 16,000 rpm for 20 minutes at 4°C to remove precipitated materials. This was followed by heat treatment of the supernatant at 65°C for 30 minutes in a water bath followed by centrifugation at 25,000 rpm for 25 minutes. The supernatant containing LytB protein was filtered using a 0.2 μm filter unit. The protein was purified by immobilized metal affinity chromatography using the Ni-His Trap column connected to a Pharmacia fast protein liquid chromatography (FPLC) device. The column was first washed with buffer A containing 30 mM Tris-HCl (pH 8.0), 100 mM NaCl (40 mL). The protein was then eluted using a linear imidazole gradient of 100% buffer B (70 mL) containing 30 mM Tris-HCl (pH 8.0), 100 mM NaCl, 500mM imidazole. The fractions

containing LytB protein (dark-brown color) as determined by sodium dodecyl sulfate-polyacrylamide gel electrophoresis (SDS-PAGE) were pooled and concentrated using a centricon ultrafiltration unit with 10 kDa cut-off when necessary and stored at -20°C.

2.4 Determination of protein concentration

Protein concentration of LytB protein was determined using the Bradford method. In this method, the absorption of protein samples with an unknown concentration was compared with a set of samples (as shown in the table below) with a known BSA (Bovine Serum Albumin) concentration. BSA solution (1.33 mg/ml) was used to prepare the calibration curve. Dye reagent was prepared by diluting 1 part Dye Reagent concentrate with 4 parts distilled D. I. water. 20 μL protein solution or BSA solution was added to 1mL of the dye reagent in a plastic cuvette. The solution was mixed and after 5 min the absorbance was measured at 595 nm. 50 μl BSA solutions were prepared as shown in table 2-1 for a calibration curve.

Table 2-1: Different volume of BSA and buffer used in the preparation of the calibration curve

Concentration (mg/mL)	Volume of BSA (μL)	Volume of buffer (μL)
0.0 (blank)	**0.0**	**50.0**
0.2	**7.5**	**42.5**
0.4	**15.0**	**35.0**
0.6	**22.6**	**27.4**
0.8	**30.0**	**20.0**
1.0	**37.6**	**12.4**

2.5 Absorption spectrophotometry

The absorption experiments were performed using an ocean optics USB 2000 miniature fiber optic spectrometer by transferring an aliquot of the purified protein into a closed cuvette containing the necessary buffer. Cluster reduction was carried out under anaerobic conditions by filling a syringe with sodium dithionite and then injecting it into the closed cuvette.

2.6 EPR measurements

EPR spectra at X-band (9 GHz frequency) were obtained with a Bruker EMX spectrometer. Sample cooling was performed with an Oxford Instrument ESR 900 flow cryostat with an ITC4 temperature controller. The cavity is fitted with either a liquid nitrogen finger dewar for measurement at 77 K or with a variable temperature helium flow cryostat for measurement in the 3.8 – 300 K.

Spin quantifications were carried out under non-saturating conditions using 10 mM copper perchlorate as the standard (10 mM $CuSO_4$; 2 mM $NaClO_4$; 10 mM HCl). Double integration of the signals and comparison to the signal of the standard were performed when necessary.

2.7 Plasmid construction for GcpE

The *gcpE* gene of Thermus thermophilus was identified by scanning the genome of *T. thermophilus* with the amino acid sequence of the *E.coli* GcpE protein. The *T. thermophilus* genome was at > 99.5% completion by genome sequencing. The amino acid sequence was back-translated into the codon usage of *E. coli* and produced as a fully

synthetic gene in order to overcome the G/C-rich codon bias of *T. thermophilus*.

The synthetic gene was cloned into the pQE60 expression vector (Qiagen) using the *NcoI* and *BglII* restriction sites. The carboxy-terminal His-tag was removed by digestion of the plasmid with *BglII* and *HindIII* and then relegated with T4 DNA ligase. The vector-derived sequences resulted in the addition of the sequence Gly-Ser-Ala at the carboxyl terminus (*7*).

2.8 Expression and Purification of GcpE protein

2.8.1 Expression of GcpE protein

Expression of GcpE protein was the same as for LytB protein except that the incubation of a 1 L culture of GcpE protein continued for 8 hrs with shaking until the optical density at 600 nm reached 4.5-5.0 and the cells were stored until needed at -80°C

2.8.2 Purification of GcpE protein

The cell pellet from 1L growth was resuspended in 80 mL buffer A containing 20 mM Tris-HCl (pH 8.0). Cell lysis was performed by sonication followed by centrifugation at 16,000 rpm for 20 minutes to remove precipitated materials. This was followed by heat treatment of the supernatant containing GcpE protein at 65°C for 30 minutes. Precipitated material was removed by centrifugation at 25,000 rpm for 25 minutes. The supernatant was filtered using a 0.2 μm filter unit. The protein solution was loaded onto a 1.6 × 40 cm diethylaminoethyl (DEAE) sepharose column (weak anion exchanger) equilibrated with buffer A. The protein was eluted using a linear gradient from 0 to 1 M NaCl in buffer A.

Fractions containing dark brown color were pooled and rebuffered in buffer A, washed in an Amicon filtration unit (cut-off) to lower the salt concentration for the binding of the protein to the next column. The protein was further purified on 1 × 10 cm source 15 Q (strong anion exchanger) column with a linear gradient of 0 to 1 M NaCl in buffer A. Fractions containing dark color were pooled and concentrated using a centricon ultrafiltration unit with 30 kDa cut-off. The protein was finally purified by gel filtration using an XK 16/60 superdex 200 column equilibrated with buffer A containing 100 mM NaCl. The dark brown color fractions were collected, concentrated and stored at -20^{0}C until further use.

2.9 Protein and iron determinations

2.9.1 Determination of protein concentration using the Bradford method

The protein determination was similar to LytB described above.

2.9.2 Protein determination using amino acid analysis

Amino acid analysis of GcpE protein was done to determine the precise concentration at the Molecular Structural Facility at University of California at Davis. Samples containing 0.5 mg/mL of protein were weighed and dried for tared hydrolysis. Liquid phase hydrolysis was performed using 6N HCl in 0.1% phenol at 110°C for 24 hours and the samples were dried. The samples were dissolved in Norleu dilution buffer to a final volume of 800 μL. 50 μL sample was loaded onto L-8800 amino acid analyzer for the analysis after vortexing and centrifugation.

2.9.3 Iron determination by AAS

The graphite furnace Atomic absorption spectrometry (AAS) experiment was performed on protein samples to determine the iron content of the protein. Iron content was determined using an AA 240 (Varian, CA). Samples containing 0.5 mM protein was diluted 10,000 times in 20 mM Tris–HCl (pH 8.0), and loaded on the atomic absorption instrument. The samples were dried for 60 s at 50 - 150°C followed by ashing for 30 s at 900°C. The samples were atomized for 7 s at 2600°C and cleaned for 3 s at 3000°C. The concentrations (μg/L) were recorded and the peaks were analyzed using spectral AA software.

2.9.4 Iron determination by Colorimetry method

The iron content was also determined by using a rapid colorimetric method (*151*). The iron standard was prepared using 0.0523 M of ferrous ethylenediammonium sulfate in 0.01 M HCl for the calibration curve. 0.25 mL of freshly prepared iron releasing reagent which contained 0.6 M HCl and 0.142 M potassium permanganate ($KMnO_4$) were added to 0.5 mL of the protein sample and the standards. The digested mixture was incubated in a capped tube for 2 hours at 60°C. Following the digestion, 0.1 mL of reducing, iron chelating reagent which contained 6.5 mM ferrozine (disodium 3-(2-pyridyl)-5,6-bis(4-phenyl sulfonate)-1,2,4-triazine), 13.1 mM neocuprine (2,9-dimethyl-1,10-phenanthroline), 2 M ascorbic acid and 5 M ammonium acetate were added to the digested mixture and mixed. The solution was left to stand at room temperature for at least 30 min. After this, the absorbance of standards and protein samples were measured at 562 nm. The calibration curve was prepared as shown in table 2-2.

Table 2-2: Volume of standard and water used in preparing the calibration curve

Volume of standard (mL)	**Amount of water(mL)**	**Concentration (mM)**
0.0	**1.0**	**0.0 (blank)**
0.2	**0.8**	**0.01096**
0.4	**0.6**	**0.02092**
0.6	**0.4**	**0.03138**
0.8	**0.2**	**0.04184**
1.0	**0.0**	**0.05230**

2.10 Resonance Raman Spectroscopy (RR) of GcpE enzyme

The resonance Raman spectra on GcpE protein were recorded by Heather Hernandez at the Center for Metalloenzymes, University of Georgia, Athens, GA using a SA Ramanor U1000 double monochromator fitted with a cooled RCA 31034 photomultiplier tube with 90° scattering geometry was used. A schematic diagram of RR spectrometer is shown in Figure 2-2.

Experiments were performed on GcpE protein as isolated using 0.5 mM protein and in the presence of 1.9 mM MEcPP. Plasma lines are filtered out by passing incident light through a premonochromator. The filtered light is focused on the sample by a focusing lens. The sample is loaded inside an anaerobic box onto a gold-plated copper holder as a droplet (a volume of about 10 μL at a time), it is then shrouded with a glass bulb and the whole holder is frozen under vacuum by attachment to a cryogenic helium refrigeration system. The sample was cooled down to about 17 K. The spectra were recorded digitally by using a computer interfaced to a printer. Each spectrum is the sum

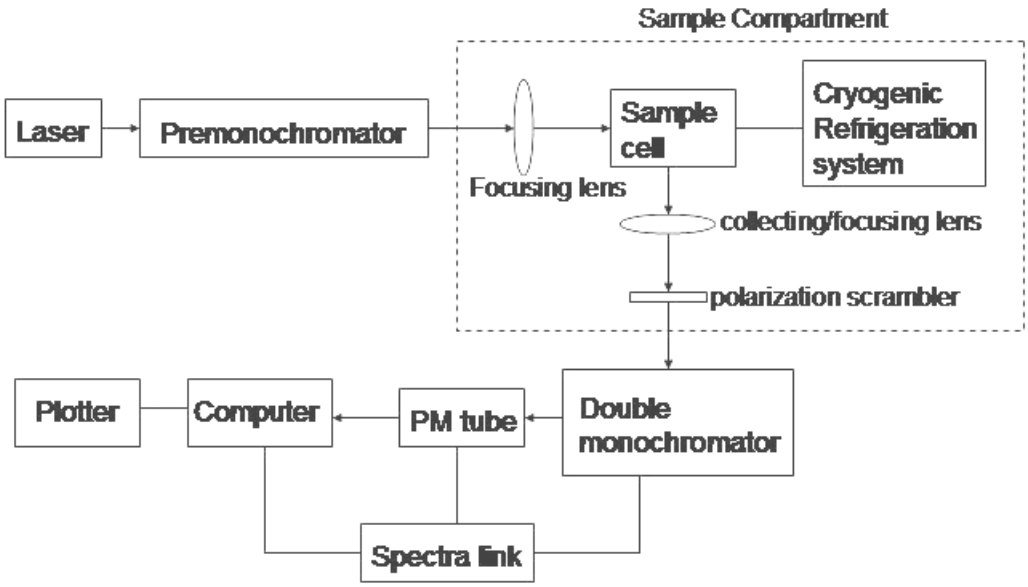

Figure 2-2: Schematic representation of a low-temperature Raman spectrometer (*148*)

of 40 scans, with 6 cm^{-1} spectral bandwidth to improve the signal to noise ratio. The excitation frequency and a Na_2SO_4 standard which are accurate to ±1 cm^{-1} were used for the calibration of band positions. Raman spectra were collected with approximately 70-100 mW laser power at the sample at 457.9 nm excitation wavelength.

2.11 EPR experiment on GcpE

The EPR spectra were recorded at 77 K. Samples containing GcpE enzyme, substrate and dithionite were prepared at 55°C in which the dithionite solution was used to initiate the reaction. Samples were frozen in cold ethanol (200 K). For kinetic studies, the samples were frozen in cold ethanol at different time intervals.

2.12 ENDOR of GcpE protein

The ENDOR samples were prepared as described above. The sample solutions were transferred into an ENDOR tube and frozen in cold ethanol after 22 s. Another sample was prepared using the same molar concentration of MEcPP and dithionite, transferred into an ENDOR tube and frozen after approximately 5 min in cold ethanol. The two samples were then transferred into EPR tubes. EPR measurements were performed on the samples to check the signal intensity. The ENDOR experiments were carried out at North Western University at Chicago by Nick Lees.

2.13 Rapid Freeze quench kinetic experiment coupled with EPR of GcpE

Rapid Freeze quench kinetic analyses were carried out to trap the radical intermediate in the reaction mechanism at Emory University, Atlanta Georgia. We drove

there by ourselves and the experiment was performed with the help of Dr. Vincent Hynh in the department of physics at Emory University.

The Freeze quench set up is shown in figure 2-3. In this experiment, the GcpE protein (0.4 mM) and the substrate (5.5 mM) were filled into syringe 1. The solution from syringe 1 was rapidly mixed with 25 mM dithionite in syringe 2. From the mixing chamber, the mixture flows through the aging tube into a collection funnel filled with cold isopropanol causing a rapid quench of the reaction. By changing the speed with which the syringes are emptied and the length of the aging tube, samples that are frozen at different time interval can be prepared enabling kinetic analysis of EPR active species. After the filled syringes were put in place the whole system was flushed with Ar to remove oxygen from the tubes and syringe head spaces. The 'snow' that was collected in the cold isopropanol was packed in EPR tubes which were stored in liquid nitrogen.

2.14 Activity assay of GcpE protein

The activity assay was carried out by monitoring the oxidation of methyl viologen at 732 nm with GcpE protein at 55°C. MEcPP was added with the aid of a syringe in a closed cuvette to the resulting solution of methyl viologen, dithionite, GcpE in 20 mM Tris-HCl, pH 8.0 to initiate the reaction. The oxidation of methyl viologen was monitored spectrophotometrically by measuring the decrease in absorbance at 732 nm which is observed by a color change from intense blue to colorless

2.15 Plasmid construction for YfgB

The plasmid for YfgB was constructed using the same procedure as for GcpE.

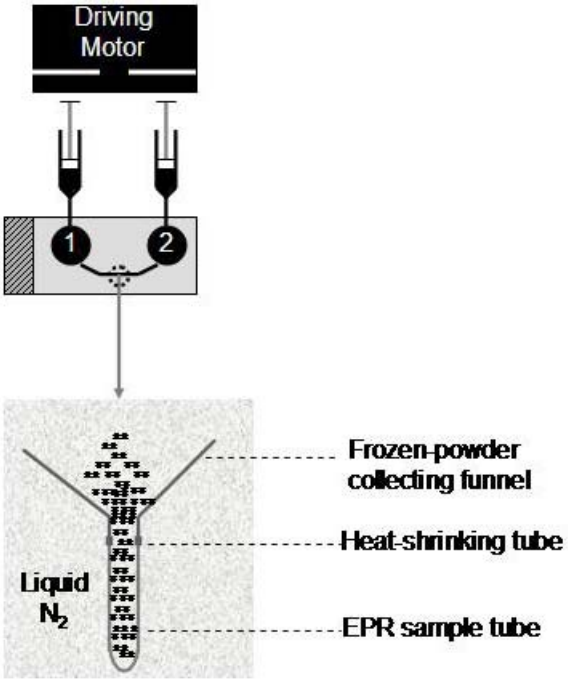

Figure 2-3: Schematic representation of a rapid freeze quench instrument (*152*)

2.16 Expression and purification of YfgB protein

2.16.1 Expression of YfgB protein

YfgB protein expression was the same as described above for the LytB and GcpE enzymes except that the incubation was stopped when the optical density at 600 nm reached 5.0-6.0 after 11 hours.

2.16.2 Purification of YfgB protein

YfgB protein was purified using a similar procedure as GcpE with the following changes. The protein solution was loaded onto DEAE sepharose column equilibrated with buffer A (20 mM Tris-HCl, pH 8.0). The protein was eluted using a linear gradient of 0 to 100 % buffer B containing (1 M NaCl, 20 mM Tris-HCl, pH 8.0). The fractions containing the YfgB protein as determined by SDS-PAGE were pooled, concentrated and loaded onto a 1 × 10 cm source 15 Q column for further purification.

The protein was eluted with a linear gradient of 0 to 1 M NaCl. Fractions containing the YfgB protein as determined by SDS-PAGE were collected. The protein was concentrated using a centricon ultrafiltration unit with a 10 kDa cut off and stored at -20°C.

2.17 Reconstitution of YfgB protein

Reconstitution of the iron-sulfur cluster was carried out in the anaerobic tent using a procedure described previously (*151*). The enzyme concentration was 660 μM. Dithiothreitol (DTT) in 50 mM Tris-HCl (pH 8.0) was added to the enzyme to a final concentration of 5 mM. $FeCl_3$ and Na_2S (dissolved in anaerobic water) in a five-fold

molar excess with respect to the enzyme concentration were added to the solution. After 3 hours, the mixture was centrifuged at 4500 rpm for 5 minutes and desalted on a PD-10 column equilibrated with 50 mM Tris-HCl (pH 8.0). The reconstituted protein was stored at -20°C. An alternative method using L-cysteine resulted into precipitation of the protein.

2.18 Protein and iron determination of reconstituted YfgB

Protein determination was carried out before and after reconstitution of the cluster using the Bradford method described above.

Iron determination was carried out using the colorimetry method as previously described for GcpE protein above.

2.19 EPR of reconstituted YfgB protein

Samples containing 87 μM YfgB were first reduced by 50 mM dithionite dithionite, 20% ethylene glycol was added to the sample. The protein solution was transferred into EPR tubes and frozen in liquid nitrogen. The spectra were recorded at 10K under non-saturating conditions.

2.20 Effect of SAM on YfgB protein

Effect of SAM on YfgB protein was determined using both the UV-visible and EPR spectroscopy. Twenty fold molar excess concentration of SAM with respect to the YfgB enzyme was prepared and added to the sodium dithionite reduced YfgB protein in

50 mM Tris-HCl, pH 8.0 with the aid of a syringe in a closed cuvette at 25°C. The UV-visible and the EPR spectra were recorded. Alternative experiments were performed in which excess dithionite was removed using the desalting PD-10 column before SAM were added.

2.21 GcpE protein in the presence of reduced-YfgB and SAM

Reconstituted YfgB was first reduced with the dithionite solution followed by the addition of SAM (twenty fold molar excess). GcpE enzyme was then added to the resulting solution. Both absorption and EPR spectra were recorded.

CHAPTER THREE

RESULTS ON LytB PROTEIN

3.1 Protein expression and purification

The LytB gene of *Aquifex aeolicus* was expressed in *E. coli* XL-1 blue cells as recommended by Jochen Wiesner from the Justus-Liebig University, Giessen, Germany. The expression of the LytB was first carried out at 37°C without induction with IPTG. This yielded low amounts of protein after purification. Optimal protein production was observed when cultures were grown with induction of IPTG at 37°C to a final concentration of 0.4 mM. Figure 3-1 shows the growth curve for the *E. coli* cells in the presence of IPTG. The protein was present in the cytosol and was purified as described in chapter 2. After a rough purification step using a heat treatment at 65°C the protein solution was loaded unto a nickel affinity chromatography column. Figure 3-2 shows the purification profile for this column. The highest peak represents protein elution and this occurred when 100% buffer B (500 mM imidazole) has been used. Over 80% pure LytB protein was obtained as determined by SDS-PAGE gel. Figure 3-3 shows the different purification steps for LytB protein. The molecular weight of LytB was determined as approximately 32 kDa from SDS-PAGE. The purification of LytB protein yielded 20 mg of protein from a 1L cell culture with an optical density at 600 nm of 4.0-4.5.

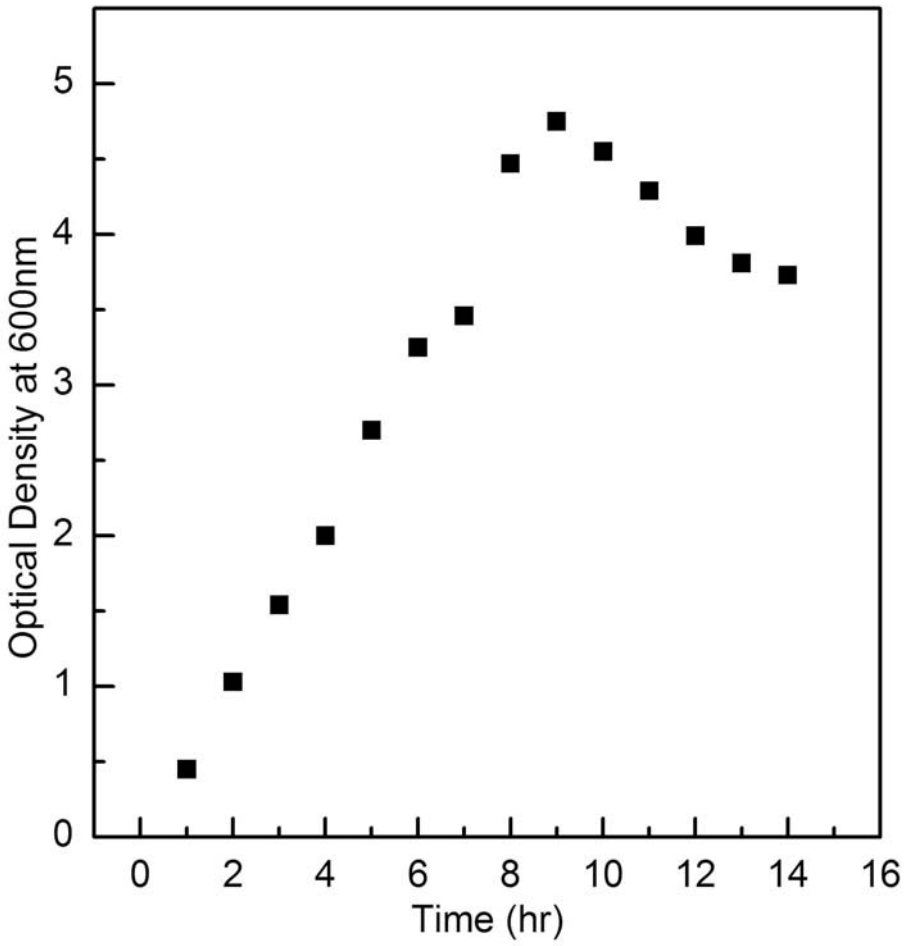

Figure 3-1: Growth curve of recombinant *E. coli* XL-Blue cells in the presence of IPTG

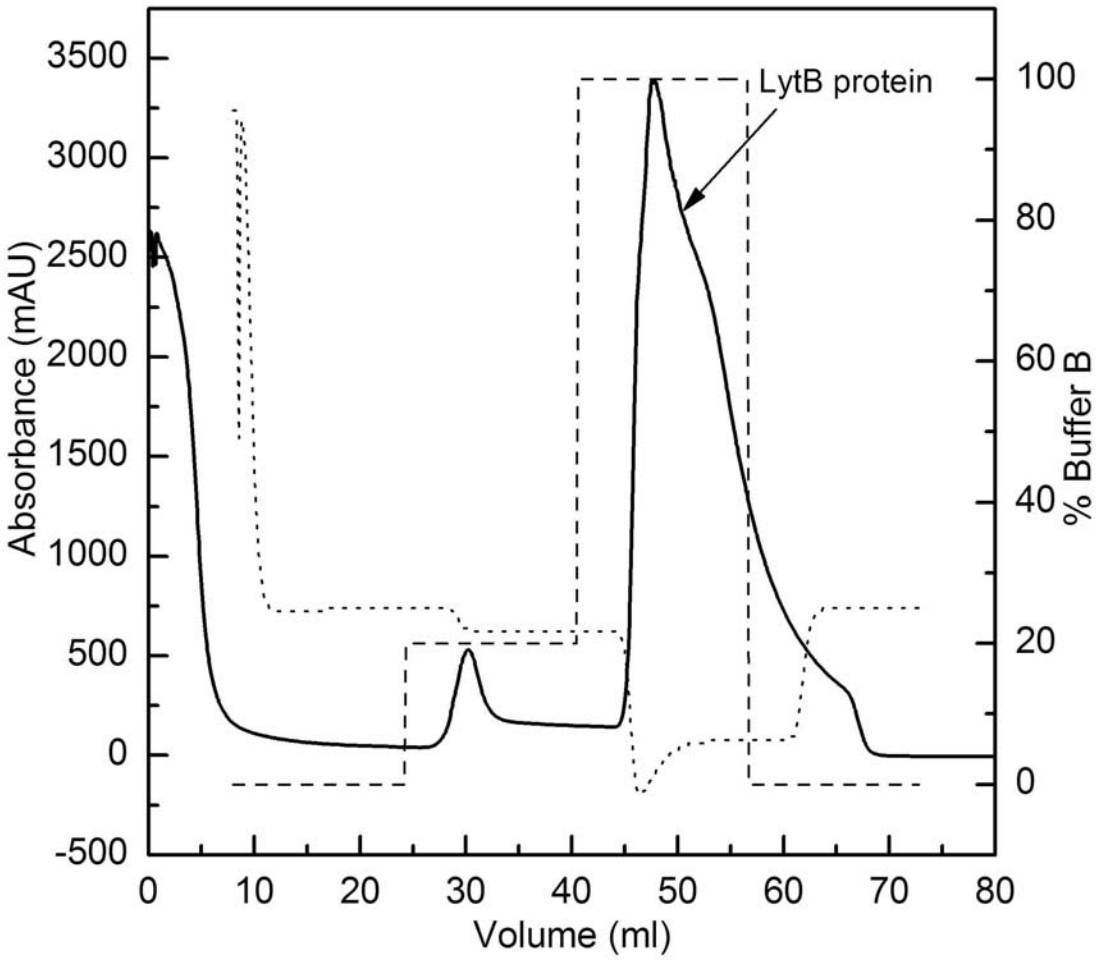

Figure 3-2: The nickel histidine trap column profile of the LytB purification. The dashed lines represent the % concentration of buffer B. The dotted lines represent the conductivity. The high intense peak is where LytB protein came off the column when 100% buffer B was used.

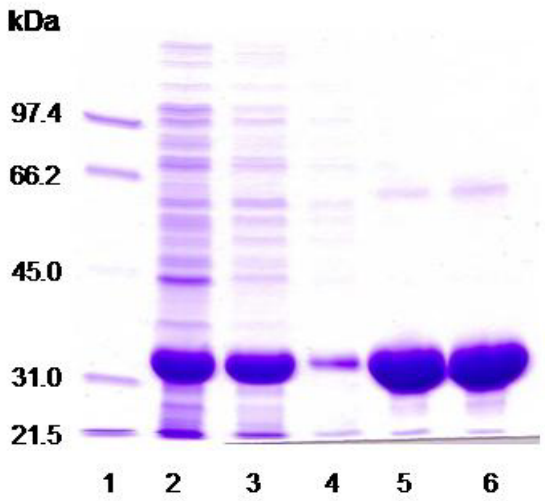

Figure 3-3: SDS-PAGE of purification steps of LytB protein. Lane 1, protein standard; Lane 2, Cell extract; Lane 3, Sample after heat treatment; Lane 4, Flow through of the nickel His-trap column; Lane 5-6, Samples after elution from the nickel His-trap column.

3.2 Spectroscopic measurements of LytB protein

3.2.1 UV-Visible absorption spectra

The absorption experiment was performed to determine the type of cluster contained in the LytB protein. The absorption spectrum of the as-isolated LytB protein showed a pronounced shoulder at 420nm which indicates the presence of $[4Fe\text{-}4S]^{2+}$ and/or $[3Fe\text{-}4S]^{1+}$ clusters. After reduction with sodium dithionite solution, the absorption at 420 nm decreases, indicating that the cluster has been reduced (Figure 3-4). The spectra were recorded at 0, 5, 10, 15 and 20 min after the addition of the dithionite solution.

3.2.2 Electron paramagnetic resonance (EPR) of LytB protein

EPR measurements on the as-isolated LytB protein solution showed the presence of an isotropic EPR signal that can be attributed to a $[3Fe\text{-}4S]^{1+}$ cluster (Figure 3-5). Reduction of the cluster in LytB enzyme with sodium dithionite solution in the presence of ethylene glycol induced the appearance of an EPR signal with g values at 4.3, 5.1 and 5.8 which are typical of an S = 3/2 $[4Fe\text{-}4S]^{1+}$ and g = 1.861, 1.919 and 2.043 which are typical of an S = ½ $[4Fe\text{-}4S]^{1+}$ cluster (Figure 3-6 and 3-7). Spin quantification by double integration of the signal was performed by recording the copper-sulfate standard under the same conditions. It was confirmed that in a 2 mM protein sample, 14.5% of the cluster was $[3Fe\text{-}4S]^{1+}$as determined from the as-isolated LytB protein, 41% contained $[4Fe\text{-}4S]^{1+}$ as determined from the reduced preparation (for both high and low spin) and, therefore, 35% contained no cluster.

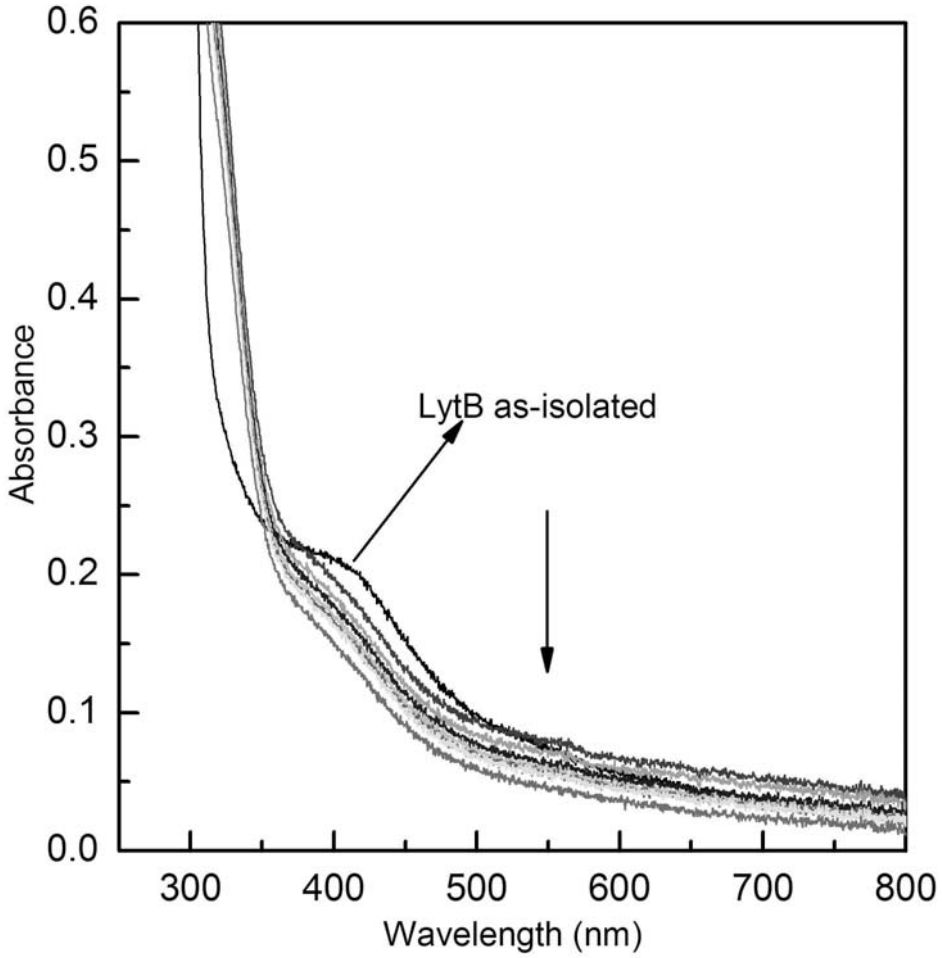

Figure 3-4: UV-visible absorption spectral of the LytB protein. The upper spectrum is LytB (0.6 mM) as purified; the lower spectra were recorded 0, 5, 10, 15 and 20 min after reduction with 50 mM sodium dithionite.

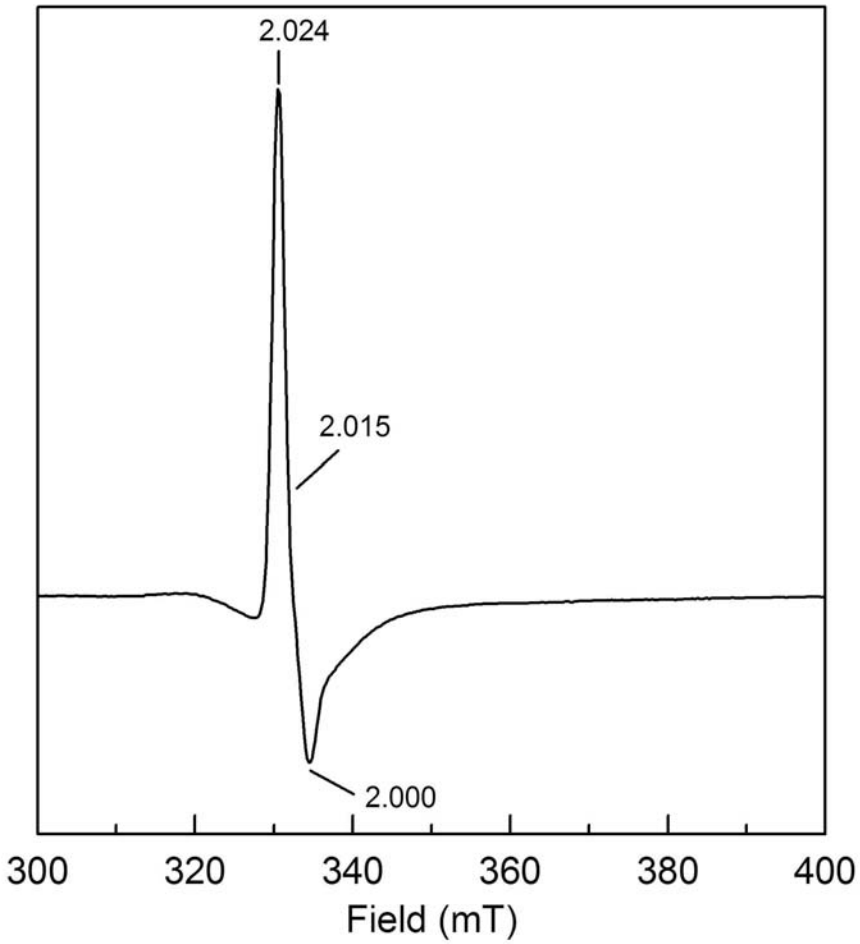

Figure 3-5: EPR spectrum of LytB protein (0.6 mM) as-isolated at 10 K with ethylene glycol. EPR conditions: microwave frequency, 9.3809 GHz; microwave power, 1.992 mW; field modulation, 0.6 mT; modulation frequency, 100 kHz.

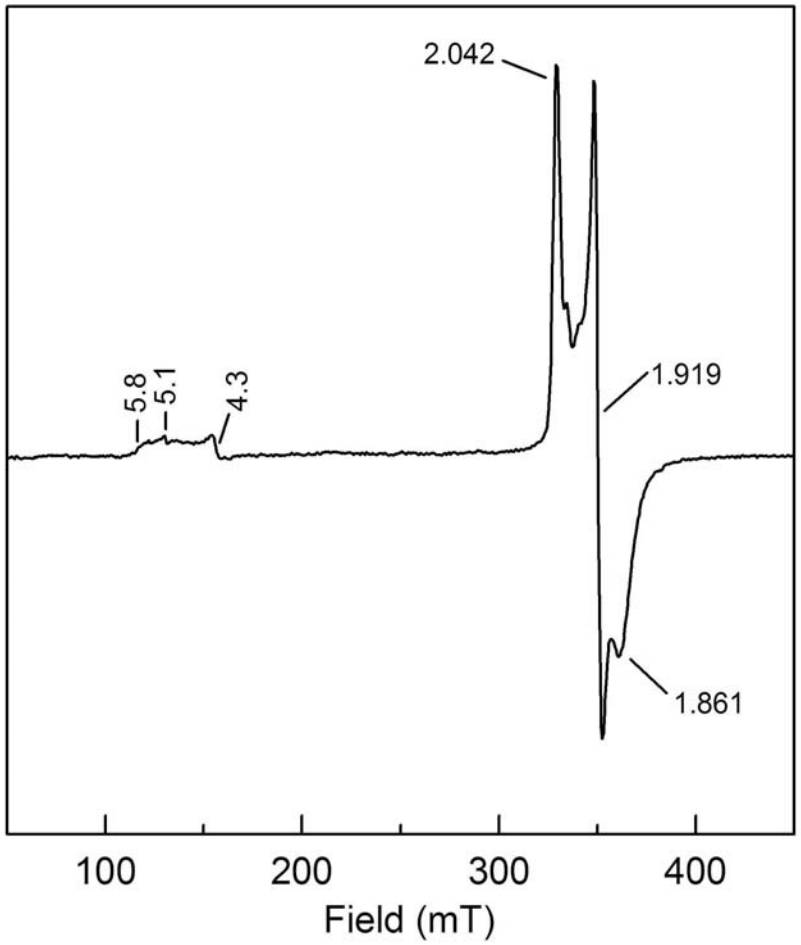

Figure 3-6: EPR spectrum of LytB (0.44 mM) in the presence of dithionite (3.7 mM) and ethylene glycol (20%) at 10 K. The spectrum is for both spin 3/2 and spin ½. The EPR conditions are microwave frequency is 9.384 GHz, microwave power is at 0.199 mW, modulation amplitude is 0.6 mT and modulation frequency is 100 kHz.

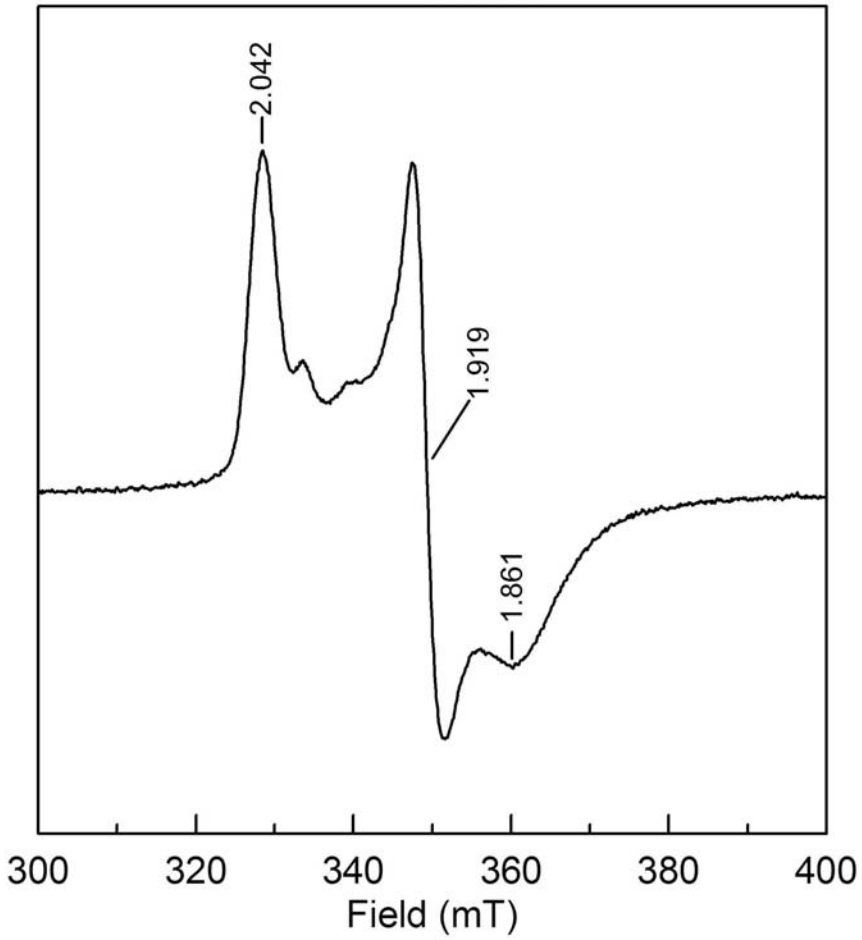

Figure 3-7: EPR spectrum of LytB protein (0.44 mM) in the presence of dithionite (3.7 mM) and 20% ethylene glycol. The spectrum is for S = ½ only. EPR conditions: microwave frequency, 9.385 GHz; microwave power, 0.199 mW; modulation frequency, 100 kHz; modulation amplitude, 0.6 mT.

This EPR result together with the absorption spectra confirmed that LytB contains a $[4Fe\text{-}4S]^{+1}$ cluster that can be reduced by dithionite solution. This is in line with the previous work where the activity related to the presence of the 4Fe cluster. The 3Fe is probably due to breakdown of the 4Fe cluster. This might be due to instability of the cluster in the cell.

3.3 Problems encountered

Although the obtained spectroscopic data obtained on LytB protein is of high quality, the presence of only 50% of the intact cluster is a concern. In addition the yield of several purifications was collected to produce the EPR spectra observed. Before there was a chance to improve the cluster content and protein yield, other problems occurred.

In comparison with the *E. coli* strains that overexpress the GcpE and YfgB protein, the *E. coli* strain that expresses the LytB protein has a very short life expectancy, approximately two weeks. It also turned out that the back up glycerol stocks were not viable after some weeks. Since good progress was made with the GcpE protein (Chapter 4), the project on LytB protein was terminated.

New constructs were sent by Jochen Wiesner since it was suspected that genetic leakage due to use of the *lac* promoter might be a problem. The expression in the new constructs was under regulation of the *tet* promoter. *E. coli* cells transformed with the new plasmids coding for either *A. aeolicus* or *Plasmodium falciparum* do not show any instability as observed with the old plasmid.

Weiya Xu is now working on the characterization of LytB protein from these two organisms.

CHAPTER FOUR

RESULTS FOR THE GcpE PROTEIN

4.1 Expression and purification of GcpE enzyme

The GcpE gene was overexpressed in *E.coli* X-L1 blue cells. Initial expression in the absence of IPTG at 37°C did not give a good yield. Optimal protein yield was observed when expressed by induction with IPTG at 37°C. Cells were harvested when an optical density at 600 nm reached 4.0-4.5 (Figure 4-1). The protein was purified under anaerobic conditions by applying three chromatographic steps that include both weak and strong anion exchange chromatography and size exclusion chromatography to the supernatant after heat treatment at 65°C. Figures 4-2 and 4-3 show the profile for the chromatographic steps for DEAE, and mono Q 200 columns from each respective purification step. The peaks with highest intensity indicate the elution of the GcpE protein as judged by SDS-PAGE. From the sequence alignment of GcpE , the weight of the protein was known as 42 kDa by taking the number of amino acid residues present and multiplying this by the average molecular weight of an amino acid (110 g/mol). We were able to achieve 95% purity for GcpE as determined by SDS-PAGE. We do not always include the last column in our purification, since only a very small increase in purity was achieved and no other EPR-active species are present after the first two column steps.

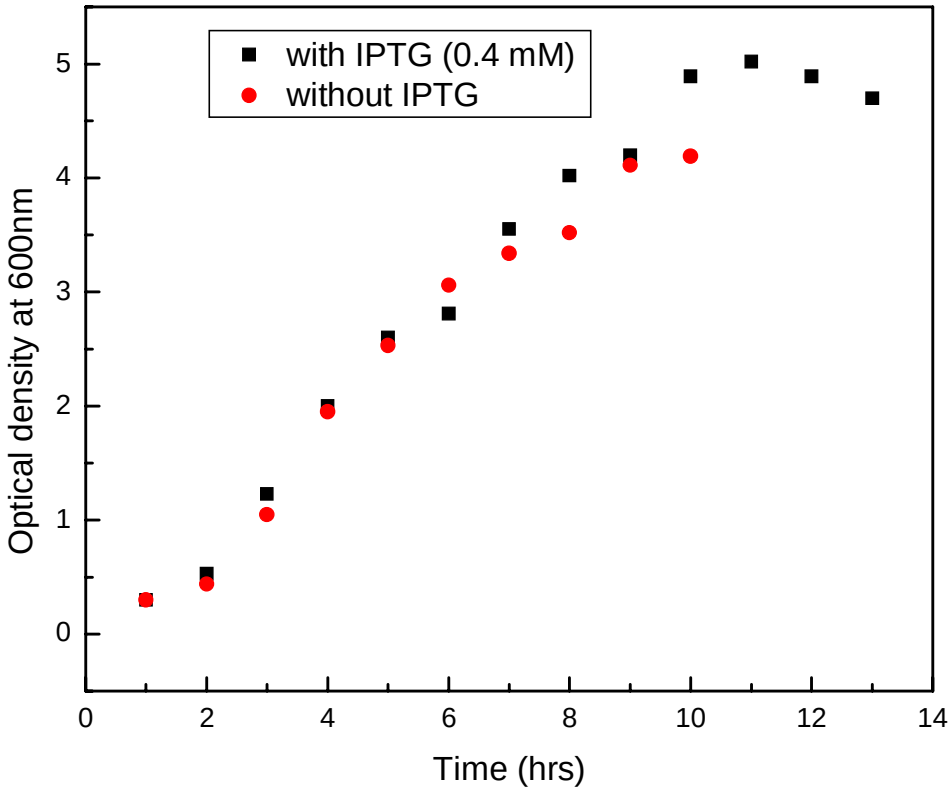

Figure 4-1: Growth curve of recombinant *E. coli* XL-1 blue cells in the absence (circle) and presence (square) of IPTG (0.4 mM)

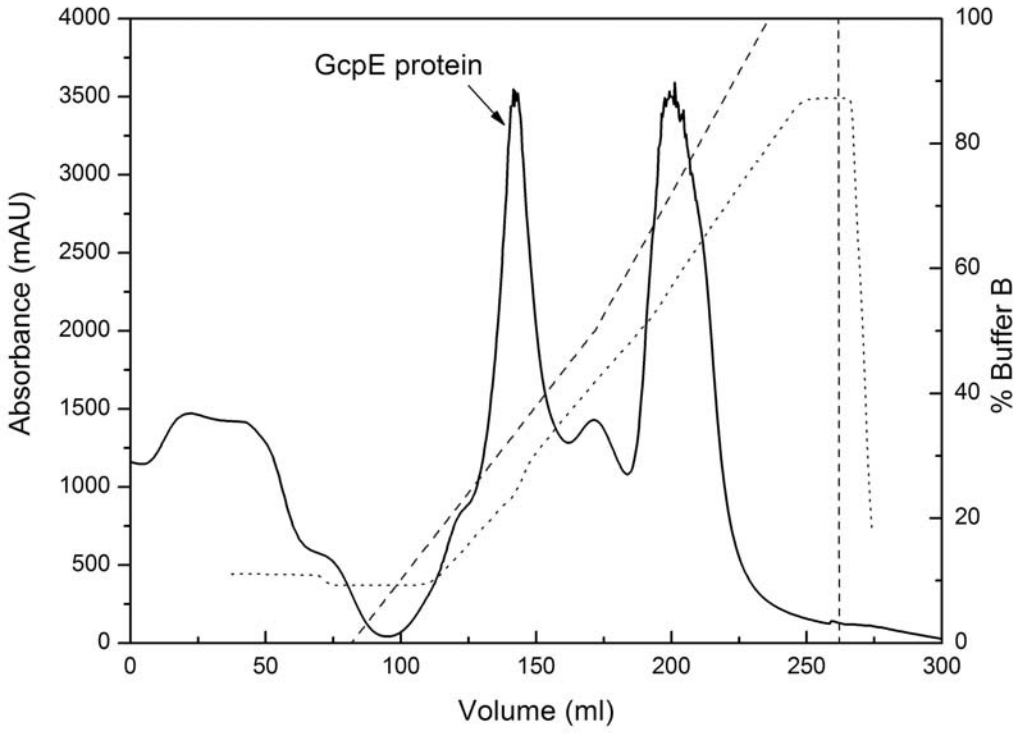

Figure 4-2: DEAE column profile of the purification of the GcpE protein. The solid line is the absorbance at 280 nm. The dashed lines represent the % conductivity; the dotted lines represent the % concentration of buffer B used. The protein was eluted between 18% and 32% buffer B.

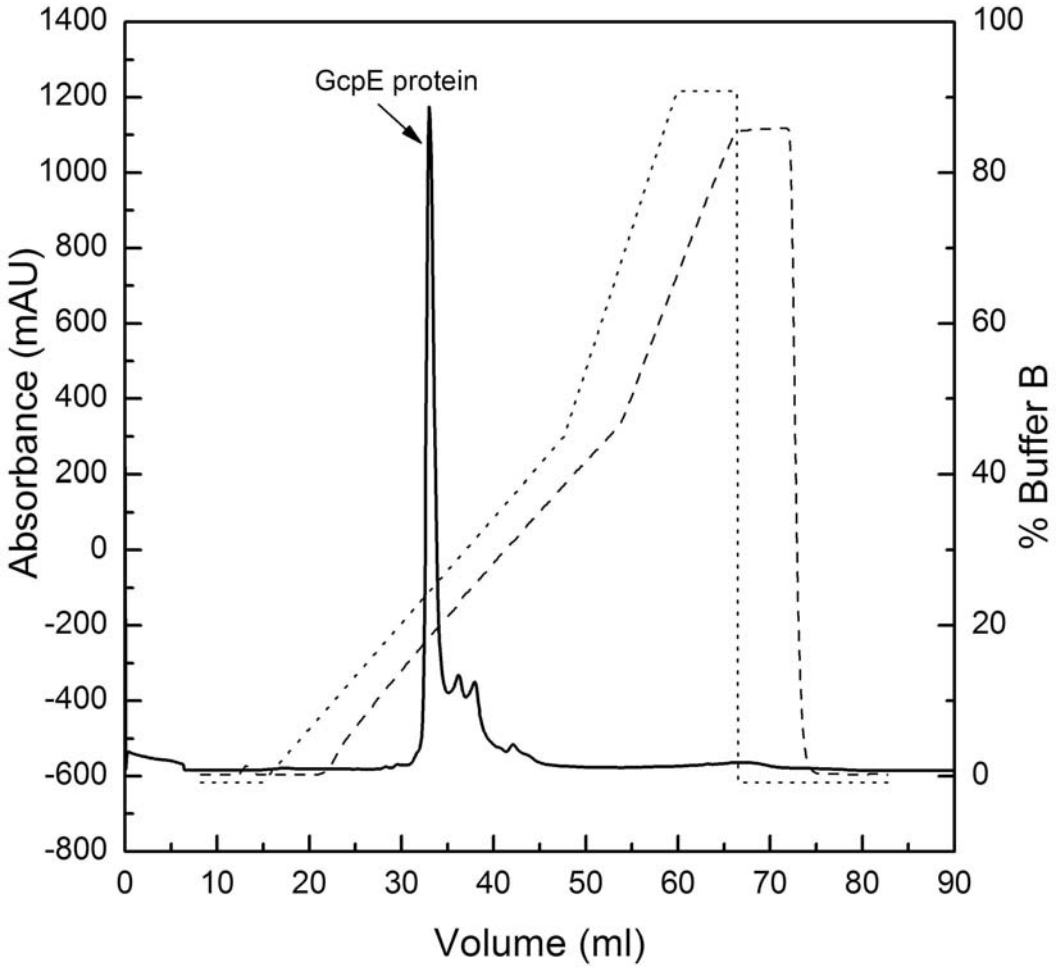

Figure 4-3: Mono Q column profile during GcpE purification. The solid line is the absorbance at 280 nm. The dotted lines represent the % conductivity; the dashed lines represent the % concentration of buffer B. The sharp peak indicates the position where GcpE is eluted which is between 18% and 20% of buffer B.

Figure 4-4 shows the SDS-PAGE analysis of the different fractions obtained during purification. Generally 25 mg of GcpE protein is obtained from a 1L growth.

4.2 Absorption spectroscopy

The absorption spectrum of GcpE was recorded to detect the presence of iron-sulfur clusters. The protein was brown in color as purified and the absorption spectra revealed a pronounced shoulder at 420 nm indicating the presence of a $[4Fe\text{-}4S]^{2+}$ and/or $[3Fe\text{-}4S]^{1+}$ cluster. A $[2Fe\text{-}2S]^{2+}$ cluster containing protein would show additional peaks at about 320 nm and 500 nm.

EPR and MCD spectroscopy of the samples demonstrated the presence of only the diamagnetic S = 0 $[4Fe\text{-}4S]^{2+}$ cluster since there were no signals detected in either the presence or absence of dithionite solution. The protein as purified did not show any EPR signal (not shown) which eliminates the presence of a $[3Fe\text{-}4S]^{1+}$ cluster.

Reduction of the cluster was performed by using sodium dithionite as a reductant. The spectra were recorded for a total time of 60 min in the presence of 0.28 mM dithionite and 1.66 mM dithionite for a period of 1 hr. The 420 nm band did not disappear even in the presence of excess dithionite solution, thus showing the cluster can not be reduced with excess dithionite (Figure 4-5).

An alternative method for cluster reduction was performed using a titanium (III) citrate solution. This resulted in the bleaching of the 420 nm peak which indicates reduction of the iron-sulfur cluster (Figure 4-6). For further confirmation of the reduction of the cluster, the EPR spectrum of the GcpE protein in the presence of titanium citrate

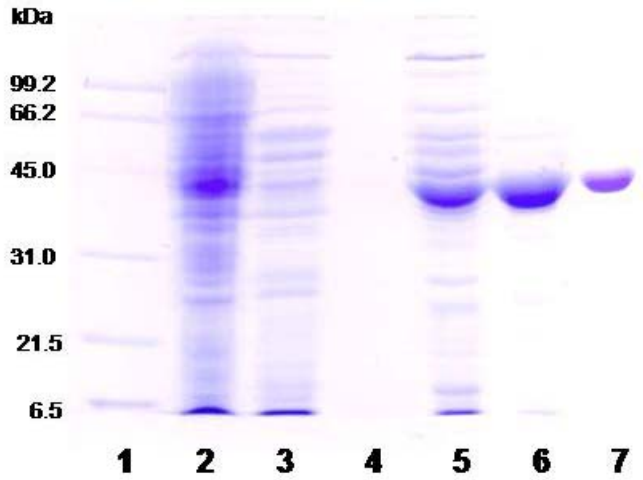

Figure 4-4: SDS-PAGE of different fractions obtained during purification of GcpE protein. Lane 1, protein standard; Lane 2, Cell lysate; Lane 3, heat stable protein; Lane 4, flow through; Lane 5, Sample after DEAE sepharose column (weak anion exchanger); Lane 6, Sample after 15 Q sepharose column (strong anion exchanger); Lane 7, Sample after superdex 200 gel filtration column.

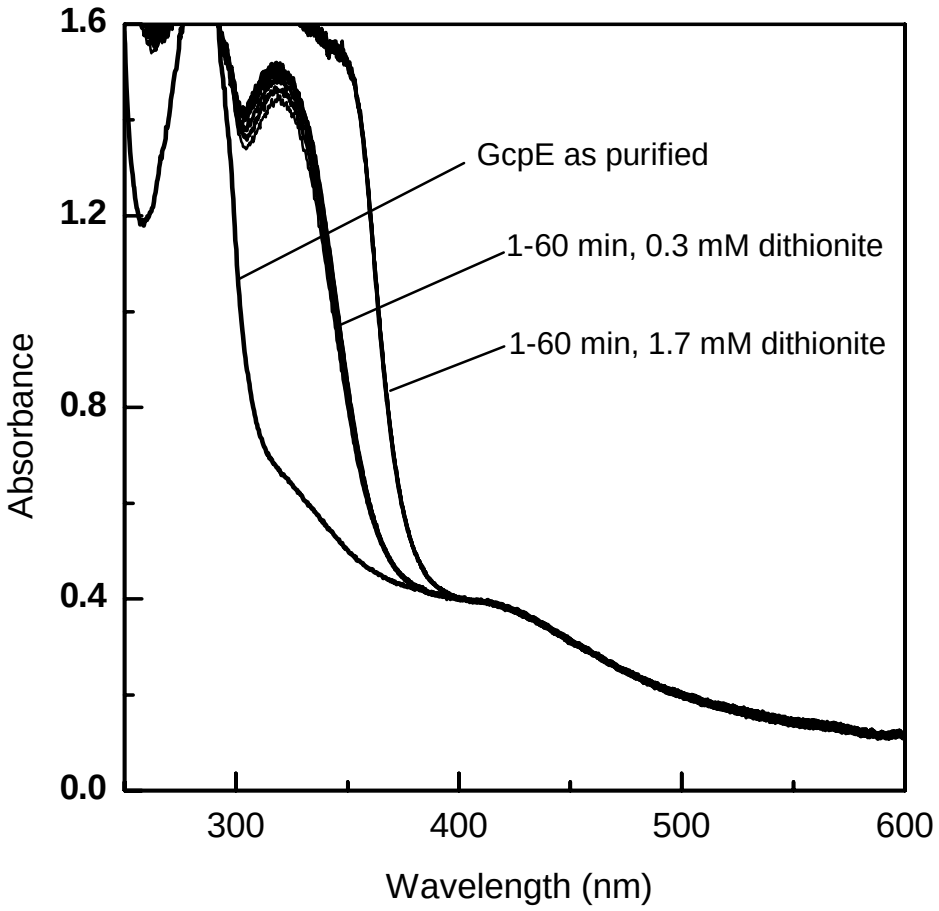

Figure 4-5: Absorption spectra of GcpE. The as-isolated enzyme (0.040mM) incubated for a total time of 60 min in the presence of 0.28 mM dithionite and subsequently for a total time of 60 min in the presence of 1.66 mM dithionite. Spectra were taken after 1, 2, 5, 10, 15, 30, 45 and 60 min. The band at 330 nm is due to dithionite.

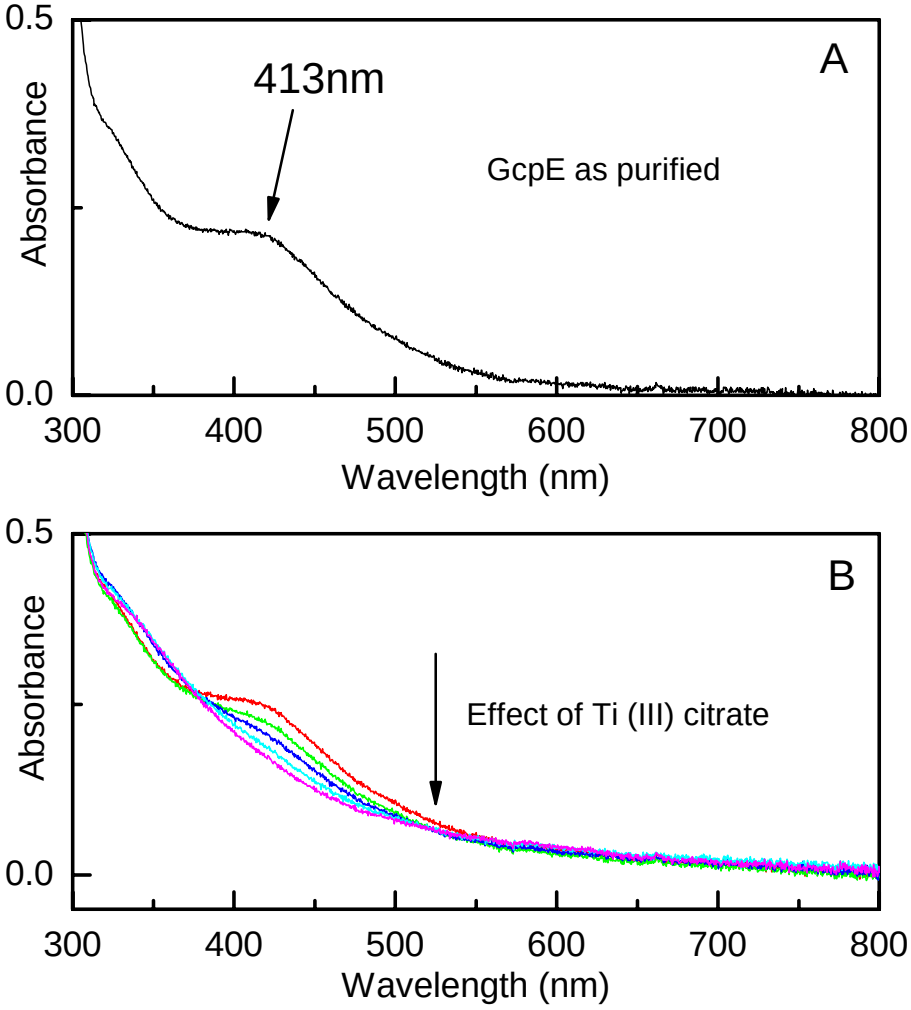

Figure 4-6: Absorption spectra of GcpE protein. Panel A shows the GcpE protein (0.044 mM) as-purified. Panel B shows GcpE in the presence of 0.25 mM titanium citrate incubated for a total time of 10 min. The spectral were taken after 1, 2, 5 and 10 min.

solution was recorded, but there was no signal detected that could confirm the reduction of the cluster due to the presence of the Ti (III) citrate signal at around g = 2. This indicates that the cluster may have been broken down under these conditions.

4.3 Protein and Iron determinations of the GcpE protein

Accurate determination of the protein concentration was performed via amino acid analysis because the BSA based assay seemed to give a high estimate. The A_{420}/A_{280} ratio would indicate full cluster content, but comparison of the iron content with that of the protein concentration determined with Bradford assay would indicate that only 60-70% of the cluster is intact.

The amino acid analysis gave both the type and amount of amino acids present which was used to calculate the exact protein concentration. Table 4-1 shows the type of amino acids present and their concentrations (not all amino acid were determined). The sample protein concentration was calculated by using the corrected amino-acid concentration and divide by the amount of corresponding amino-acid residue present (as determined from the sequence). The corrected amino-acid concentration was calculated by using:

[AA]mmol × [Norleu standard] × Dilution factor × 1/sample weight(g)

For Glx,

$$3.874 nmol \times 1000 mmol \left(\frac{2.0}{2.065}\right)\left(\frac{800}{50}\right)\left(\frac{1}{95.4 mg \times 1000 g}\right) = 0.630 mM$$

$$= \frac{0.630}{48} = 0.0133 mM$$

Table 4-1: Amino acids present in GcpE protein and their corresponding concentrations

Amino acid	Average Concentration (nmol)	Amount of residue present
Cysteine (Cys)	0.046	3
Asparagine (Asx)	1.586	20
Threonine (Thr)	1.472	21
Serine (Ser)	1.183	16
Glutaminic acid (Glx)	3.874	48
Glycine (Gly)	2.831	35
Alanine (Ala)	3.749	46
Valine (Val)	2.699	36
Methionine (Met)	0.109	10
Isoleucine (Ile)	1.228	16
Leucine (Leu)	3.605	45
Norleu (Nor)	2.065	Standard
Tyrosine (Tyr)	0.479	7
Phenylalanine (Phe)	0.688	9
Histidine (His)	0.794	10
Lysine (Lys)	1.757	22
Arginine (Arg)	2.534	32
Proline (Pro)	2.151	27

Each amino-acid concentration was calculated as above and the protein concentration was determined by finding the average of the concentrations of all amino-acids present. The Bradford method overestimates the protein by a factor of 1.5.

Iron determination was performed by using both the atomic absorption spectrometry (AAS) and a rapid ferrozine-based colorimetric method. The purified GcpE enzyme contains 3.9 mole Fe per mole of enzyme as determined both by AAS and the colorimetric method.

4.4. Effect of ferricyanide solution on GcpE protein

Electron paramagnetic resonance (EPR) spectral was recorded at 5K for GcpE protein to determine if the cluster can be oxidized to give the EPR active $[4Fe\text{-}4S]^{3+}$ cluster. A spectrum that can be assigned to a $[3Fe\text{-}4S]^{1+}$ (Figure 4-7) was observed indicating that the cluster was probably broken down in the presence of excess ferricyanide solution since this signal was not observed in the native protein.

4.5 Resonance Raman (RR) spectroscopy of GcpE protein

Since no 3Fe EPR signal is detected in the protein as purified it appears that GcpE contains a $[4Fe\text{-}4S]^{2+}$ cluster that cannot be reduced or oxidized. To confirm the presence of a $[4Fe\text{-}4S]^{2+}$ cluster a RR spectrum was measured for GcpE as purified (Figure 4-8, upper panel). The results confirmed the presence of a $[4Fe\text{-}4S]^{2+}$ cluster because of the positions and relative heights of the bands in the 325-400 cm^{-1} region which are typical for regular $[4Fe\text{-}4S]^{2+}$ clusters with either 3 or 4 cysteine ligands (*153*,*154*).

No bands were detected that can be assigned to a 3Fe or 2Fe cluster. The low-frequency region is different. The typical 250 cm^{-1} band has a very low intensity, while the 265 cm^{-1} band is more intense. The reason for this difference is not clear since these bands are associated with internal Fe-S bonds (*153*).

RR spectroscopy of the GcpE protein in the presence of MEcPP was also recorded to test if MEcPP binds to the $[4Fe\text{-}4S]^{2+}$ cluster. This experiment was intended to check binding of substrate to the oxidized cluster since we have reasons to believe that

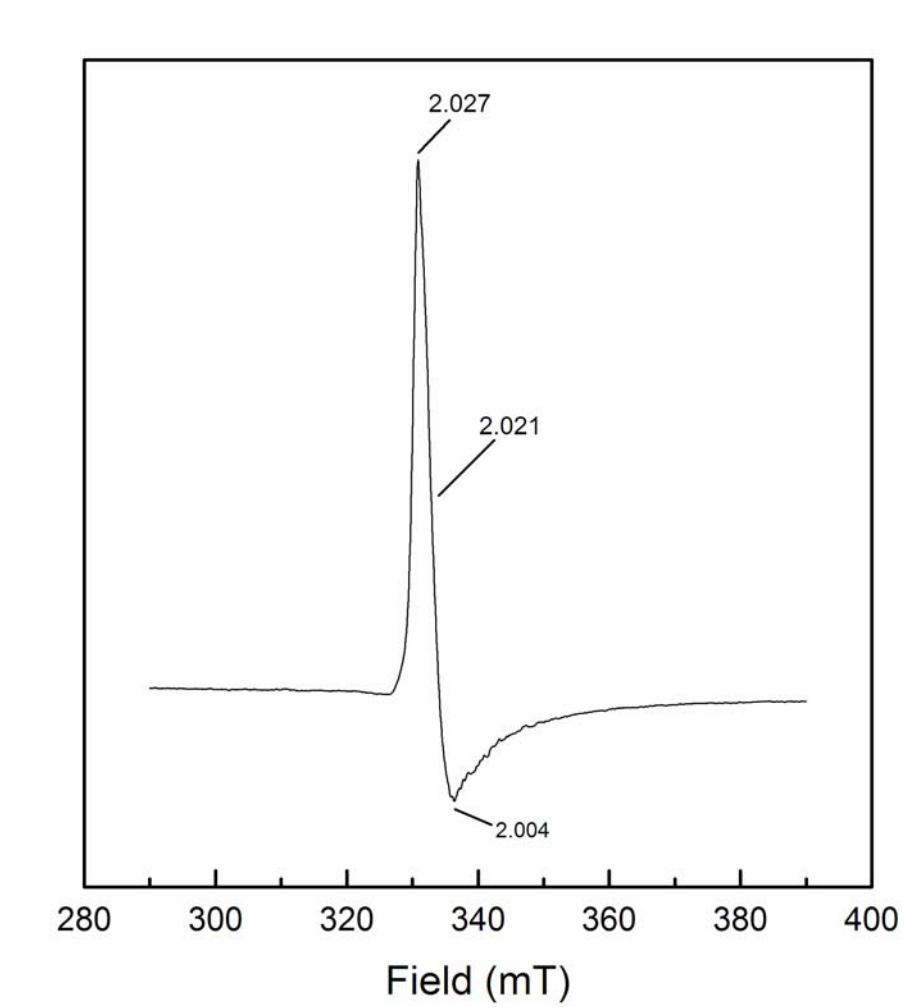

Figure 4-7: EPR spectrum of GcpE (0.21 mM) in the presence of excess ferrycyanide (2.5 mM). Temperature; 5 K. Microwave frequency is 9.385 GHz, microwave power incident to the cavity is 1.994 mW.

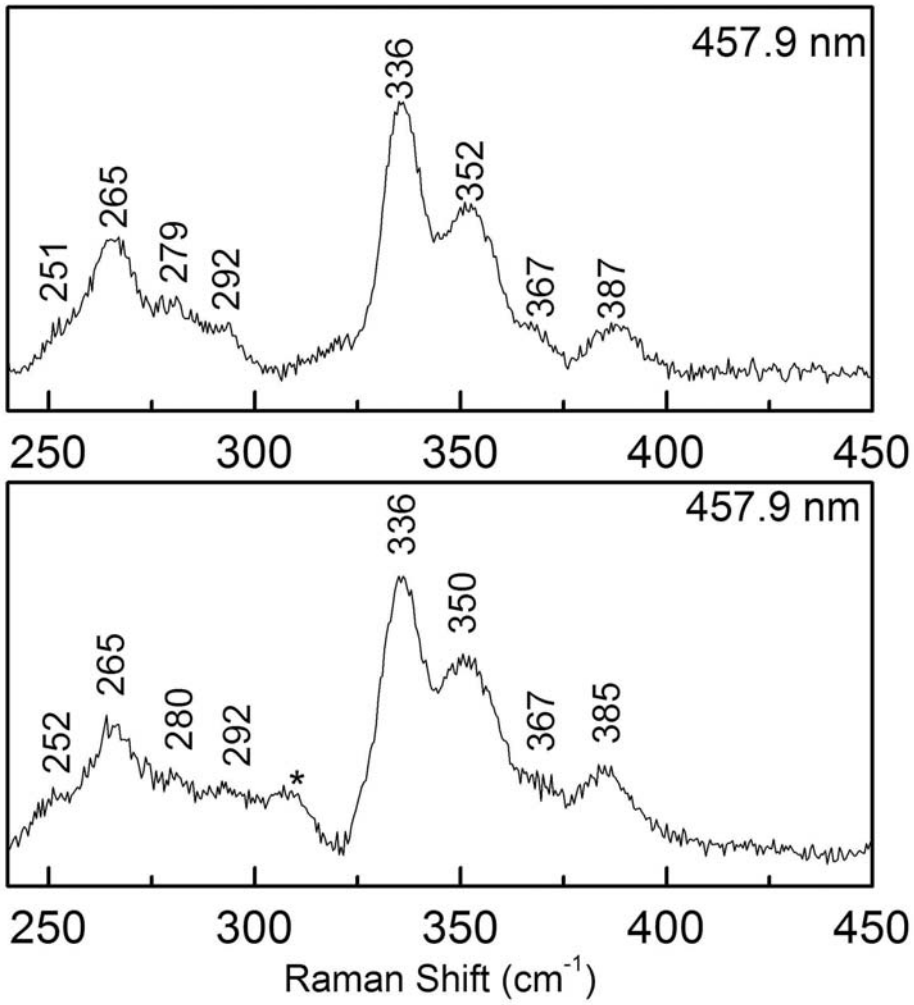

Figure 4-8: Resonance Raman spectra of GcpE. Upper panel: GcpE as isolated, 0.50 mM. Lower panel: GcpE in the presence of 1.9 mM MEcPP. Each spectrum is a sum of 40 scans, with 6 cm^{-1} spectral bandwidth. The peak marked with an asterisk is due to frozen water.

substrate binds to the reduced cluster (See below). The spectrum (Figure 4-8, lower panel) is also similar to the RR spectrum in the absence of substrate. This might indicate that MEcPP is probably not binding to the cluster. However, we cannot exclude that a water molecule might be present as a fourth ligand. Replacing this ligand with an oxygen from the substrate would not lead to any detectable changes.

4.6 Electron Paramagnetic Resonance (EPR) spectroscopy of GcpE protein

The finding that the dithionite solution can not reduce the 4Fe cluster in the GcpE protein (Figure 4-5) is unexpected since dithionite is the electron donor in the activity assay. EPR spectra of GcpE protein in the presence of dithionite and substrate were recorded under steady-state conditions to test the effect of both compounds on the GcpE enzyme. For the experiment, GcpE and MEcPP were incubated at 55°C. The reaction was started by addition of dithionite with an end concentration of 4.7 mM in total volume of 2 ml in 100 mM Tris-HCl buffer, pH 8.0.

Since the maximal specific activity of GcpE is 0.6 μmol min^{-1} mg^{-1} (*7*), the complete reaction should last about 3 min. The development of an EPR active species was followed by transferring aliquots of the solution into an EPR tube and flash freezing the sample in cold ethanol (200K) at different time intervals. During the first minute of the reaction, a transient EPR signal was detected that has its highest intensity in samples that were frozen within 10-12 s (Figure 4-9). The spectrum shows a rhombic EPR signal with g_{xyz} = 2.000, 2.019 and 2.087 and has a spin intensity of 0.6 relative to the protein concentration. The shape of the EPR signal is similar to that of a HiPIP-type $[4Fe\text{-}4S]^{3+}$ cluster. The signal intensity decreases over time and is lost after 1.5-2 min (Figure 4-10).

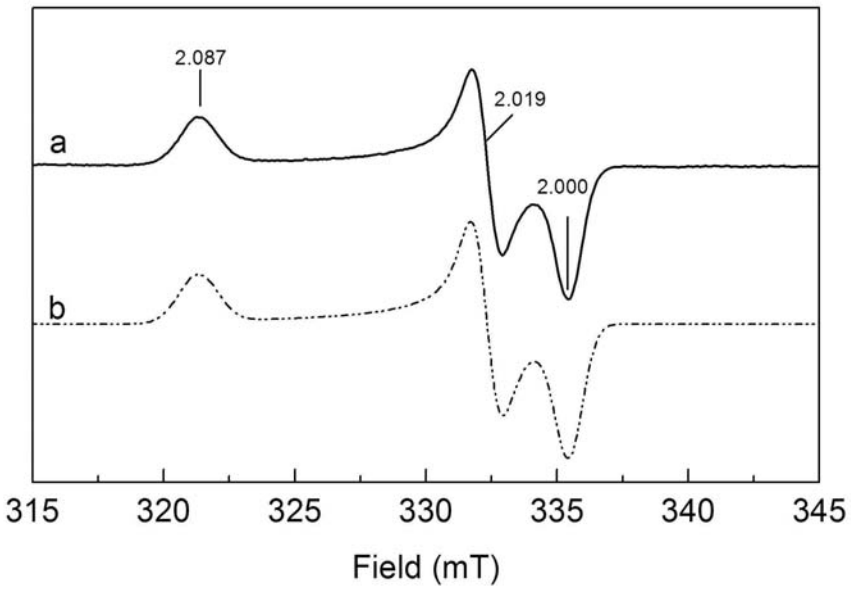

Figure 4-9: HiPIP-like EPR signal detected in GcpE during turn-over experiments (a) and (b) the simulated spectrum. The starting solution contained 0.10mM GcpE, 4.0mM MEcPP and 4.7 mM dithionite solution in 2 mL of 100 mM Tris-HCl buffer, pH 8.0. The sample was frozen after 10 s. EPR conditions: microwave frequency, 9.388 GHz; microwave power incident to the cavity, 2.01 mW; field modulation frequency, 100 kHz; modulation amplitude, 0.6 mT. Simulation parameters: g_{xyz} = 1.9999, 2.0185 and 2.0874; W_{xyz}: 1.05, 0.95 and 1.50 mT; Temperature: 77 K.

In addition to the Fe-S signal that was observed, two more signals were detected in the time-dependent studies. The HiPIP-like signal is replaced by a radical type signal that reaches its maximum intensity at about 3-4 min when all the substrate has been converted to product (Figure 4-10), also another signal similar to the first HiPIP-like signal was observed.

The temperature behavior of the first HiPIP-like signal is not the same as what has been detected previously for that type of cluster (*153,155*). At temperature below 20 K, it is difficult to measure the signal without saturation. From 20 K to 100 K, the signal can be measured without saturation.

The HiPIP-like signal is also different from real HiPIP signal in that it can only be observed under reducing conditions as opposed to strongly oxidizing conditions (*156*). Figure 4-11 shows the temperature behavior of the EPR active species in the sample frozen after 4'05". The figure shows an overlap of the spectra taken at different temperatures. The intensity of the spectra has been corrected for temperature differences and power. This way the Curie-behavior of the different signals can be detected.

At low temperature, the radical signal that can be detected at 77 K is not detectable due to power saturation, a HiPIP-like signal is detected with $g_{\perp} = 1.986$ and $g_{//} = 2.081$. This signal can be measured without saturation up to 20 K. Above 20 K, the signal starts to broaden. For the discussion we will call this signal HiPIP-B.

The radical signal is saturated at lower temperatures. It can be measured without saturation in the 50-80 K temperature region. The signal starts to broaden at higher temperature (above 100 K) until it cannot be detected anymore at 160 K.

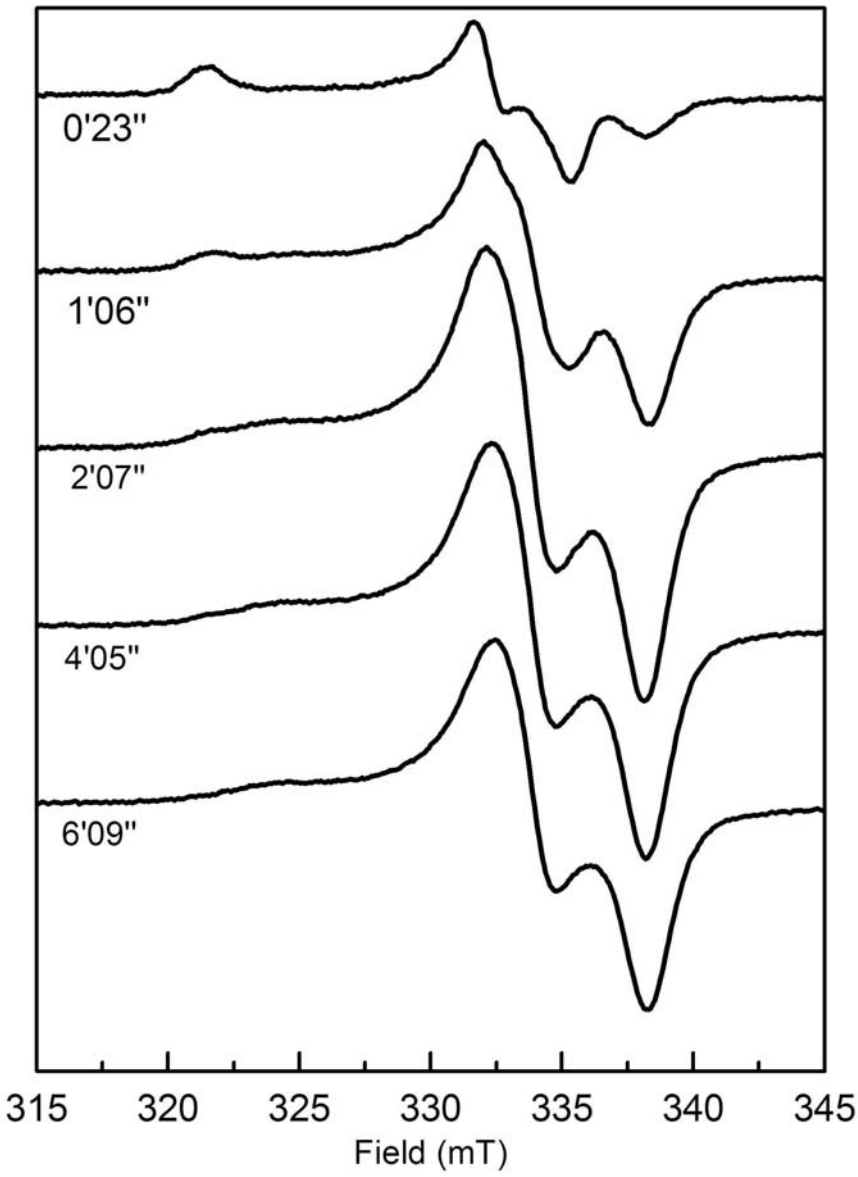

Figure 4-10: Time-dependent electron paramagnetic resonance spectra obtained during the reaction of GcpE in the presence of dithionite and MEcPP for samples frozen in cold ethanol (200 K) at different time intervals from 23 s-6 min. The samples were made under the same conditions as in Figure 4-9. EPR conditions are the same as for Figure 4-9.

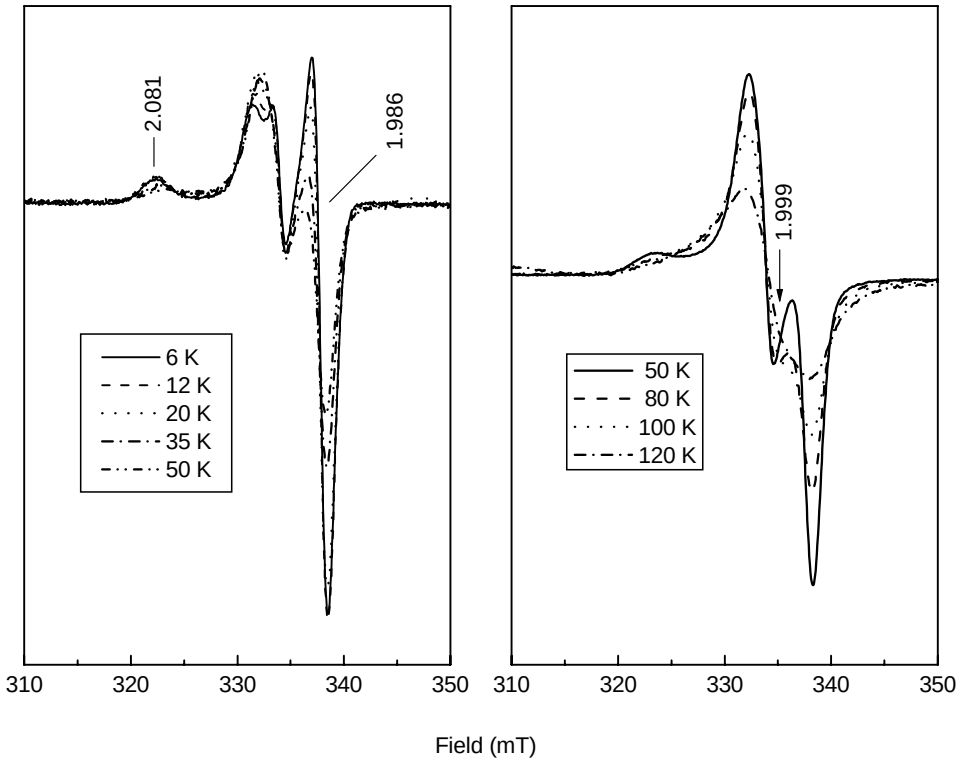

Figure 4-11: Temperature overview of the EPR active species in GcpE protein. EPR conditions: field modulation frequency, 100 kHz; modulation amplitude, 0.6mT; microwave power, 2.01 mW; microwave frequency, 9.388 GHz.

Similar signal was detected in ferredoxin thioredoxin reductase (FTR) (*156*). This enzyme is involved in a two one-electron step reduction of a disulfide bond. The [4Fe-4S]$^{2+}$ cluster present in the active site of FTR is involved in mediating electron transfer to the active site disulfide and stabilization of the cystenyl radical. The cystenyl radical results from an initial one-electron reduction of the active-site disulfide. The radical is stabilized by coordination of the sulfur ion to an iron on the resultant oxidized [4Fe-4S]$^{3+}$ cluster (*157*).

With only three conserved cysteine residues present in GcpE that are involved in the coordination of the 4Fe it can be assumed that there is no active-site disulfide present in GcpE. In contrast to the EPR signals found in FTR all the g values of the EPR signal in GcpE are equal to 2 or higher (*156*). This might be due to the presence of one or two oxygen ligands from MEcPP instead of the two cysteine sulfur atoms in FTR.

Figure 4-12 shows the EPR spectra of two samples that were prepared for ENDOR experiments. The samples were prepared after 22 s and 5 min incubations. The sample incubated for 22 s contained mainly the HiPIP-like signal. A small amount of a radical-type was also present. There are several species that were present in the 5 min incubation sample. The species present are the radical type signal and the HiPIP-B signal. Presence of HiPIP-B signal was verified at low temperature (data not shown).

Spectra were also obtained at 35 GHz (Q-band) by Nick Lees at North Western University, Chicago for both rapid (22 s) and slow (5 min) incubations. The spectra are similar to those recorded at 9 GHz, ignoring the slight shift in g-value (field not calibrated). The signals have different saturation characteristics for samples with 22 s incubation as seen from the change in relative intensities at the two different microwave

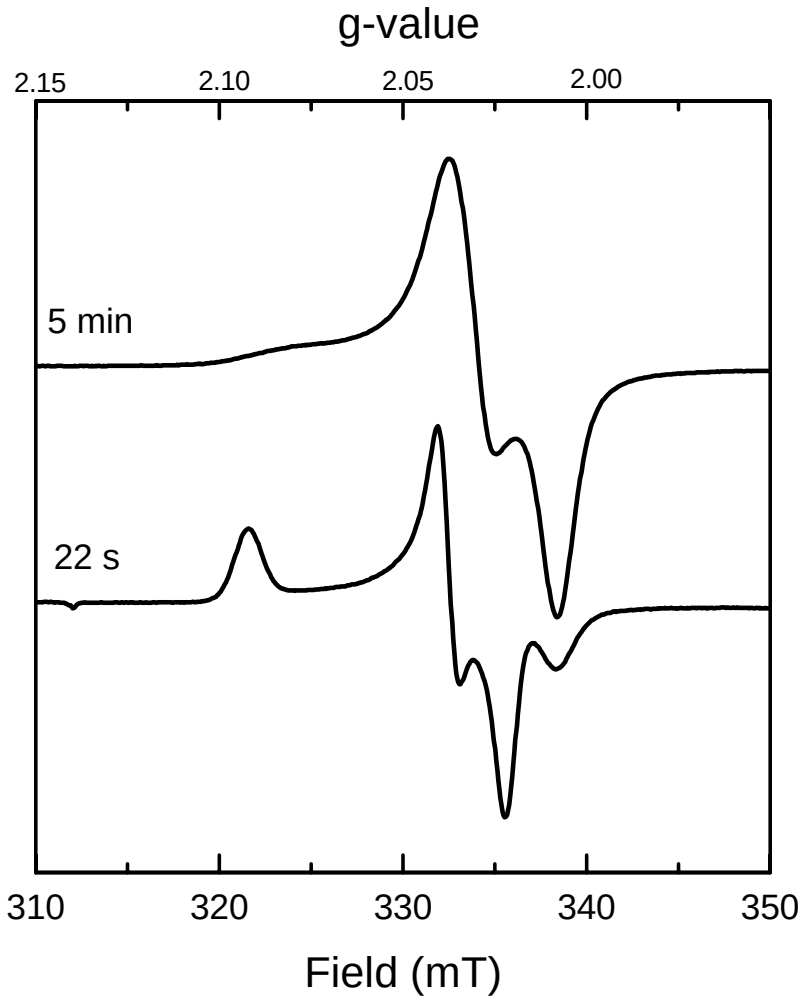

Figure 4-12: EPR spectrum of GcpE in the presence of dithionite and MEcPP for samples frozen in cold ethanol at 5 min (upper spectrum) and 22 s (lower spectrum) at 77 K.

powers shown (Figure 4-13, upper panel). This indicates the presence of different EPR active species. For the sample at 5 min incubation, the signals were similar to those obtained at 9 GHz (Figure 4-13, lower panel) with slight intensity ratio differences.

4.7 Electron nuclear double resonance (ENDOR) of GcpE protein

GcpE in the presence of dithionite and MEcPP was measured using ^{31}P ENDOR spectroscopy to probe the exact mode of binding of MEcPP to the 4Fe cluster. The spectra were recorded for both the 22 s (Figure 4-14) and the 5 min (Figure 4-15) incubations. The results indicate a weak isotropic coupling (< 0.5 MHz) for ^{31}P ENDOR that can be observed across the EPR spectrum in both samples.

It is not possible to draw a clear conclusion. It is possible that only the radical signal and the HiPIP-B signal show the ^{31}P-coupling. Since the signals are present in both samples, the coupling is detected in both samples. In that case, the HiPIP-like signal might not show any coupling. The other option is that the HiPIP-like signal and one of the other two signals show identical coupling. We can only solve this problem by making a sample that only shows the HiPIP-like signal.

The size and nature of ^{31}P coupling suggests a weak interaction with a fairly distant coordinated phosphorous that is likely to be at least three or four bonds away from the source of the electron spin density.

4.8 Freeze Quench in conjunction with EPR spectroscopy of GcpE

A freeze quench technique was employed to acquire more kinetic information on the radical intermediate occurring during the reaction of GcpE with dithionite and

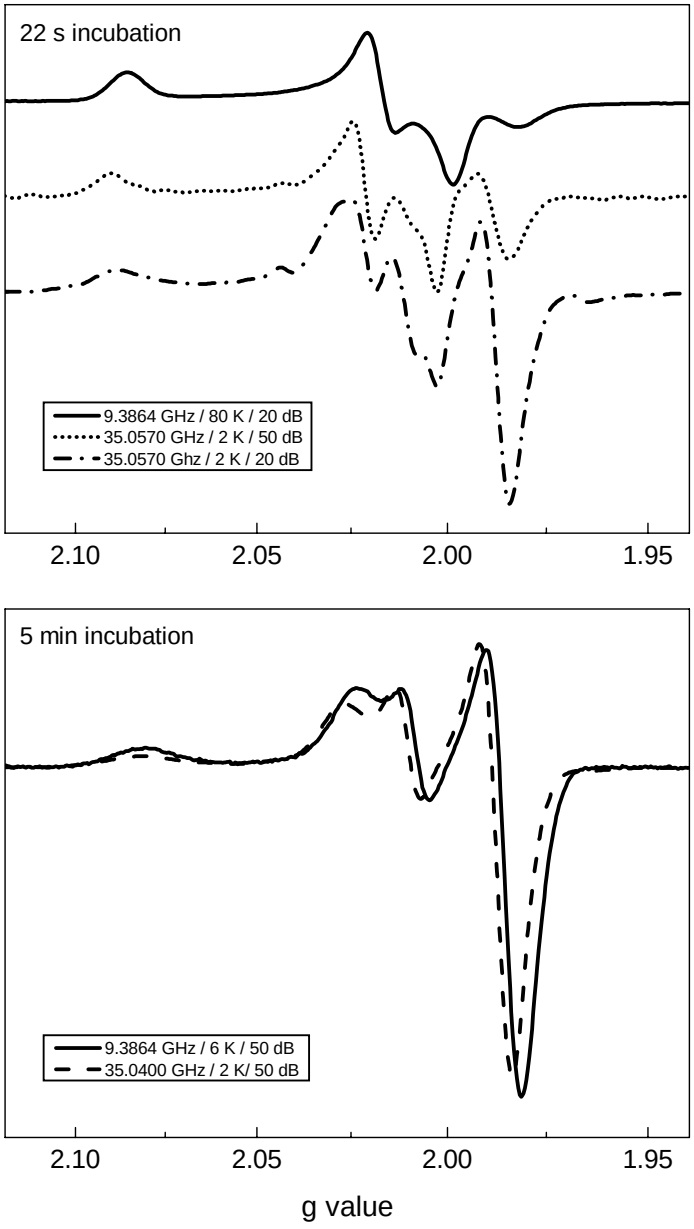

Figure 4-13: X-band (9 GHz) and Q-band (35 GHz) EPR spectroscopy of 22 s incubation (upper panel) and 5 min incubation (lower panel) of GcpE enzyme compared.

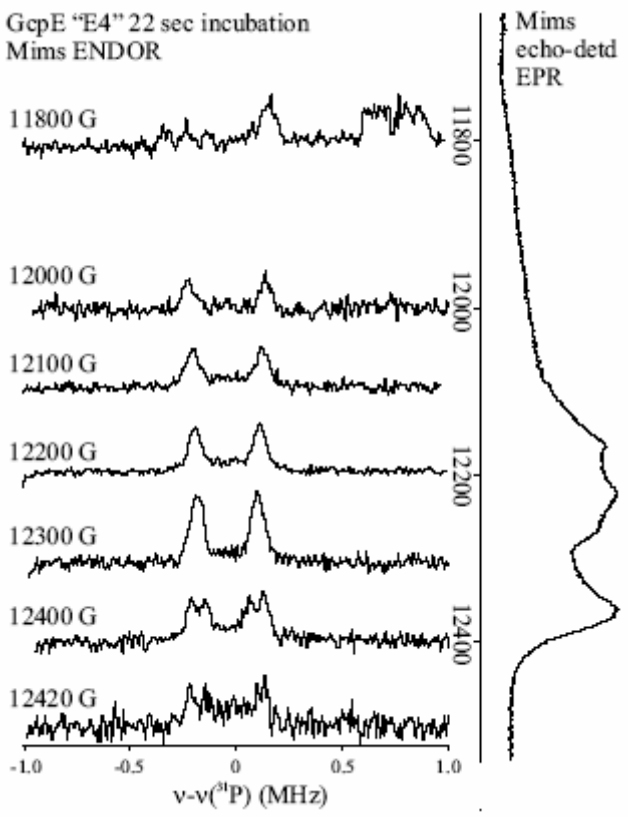

Figure 4-14: ^{31}P ENDOR spectra of GcpE enzyme incubated for 22 s at RT. The spectra were taken at different field positions as indicated on the left. Conditions: T = 2 K; microwave frequency = 35 GHz.

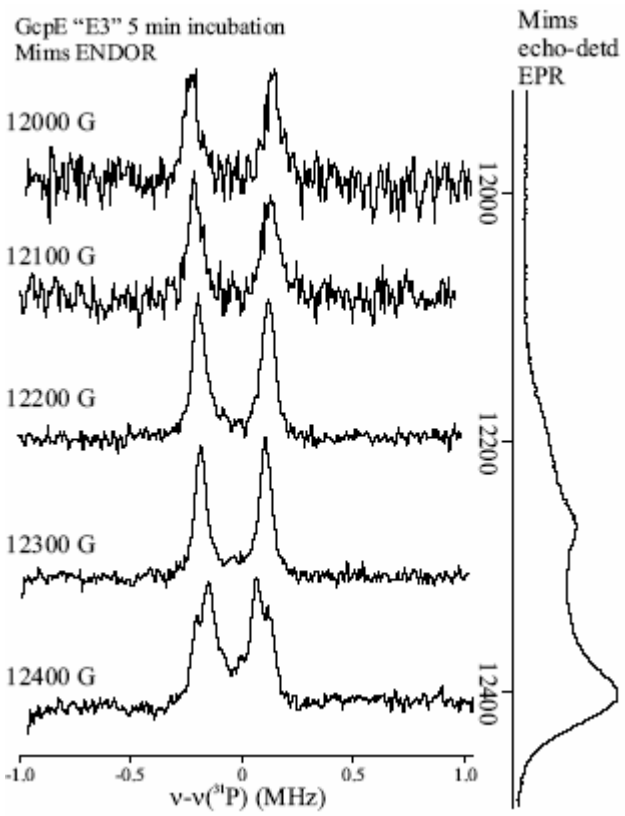

Figure 4-15: ^{31}P ENDOR spectra of GcpE enzyme incubated for 5 min at RT. The spectra were taken at different field positions as indicated on the left.

Conditions: T = 2 K; microwave frequency = 35 GHz.

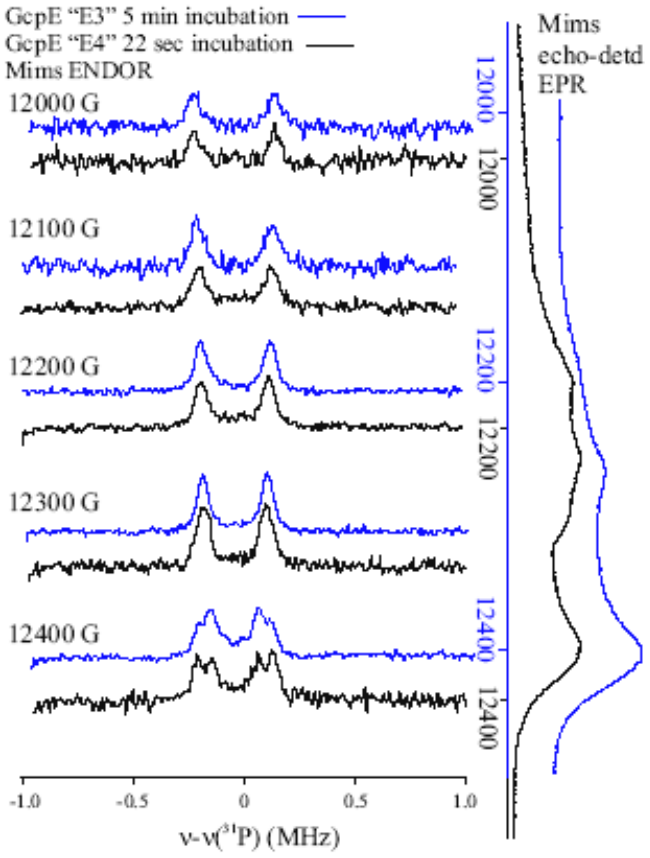

Figure 4-16: Overlay of figure 4-15 (top, 5 min incubation) and Figure 4-14 (bottom, 22 s incubation) of ^{31}P ENDOR spectra of GcpE enzyme.

MEcPP. EPR samples were made at different quench times (the time between the injection of the solution and cessation of the reaction) from 28 ms-60 s at room temperature (Figure 4-17). The results show the presence of the iron-sulfur (HiPIP-like) that started to develop at 1.2 s and reaches its maximum intensity at 30 s.

Another feature (at around g = 2) that may be attributed to an intermediate signal was also present, since it appeared at the beginning of the series and was lost after 8 s. It is not clear if this radical is part of the reaction or is due to dithionite.

4.9 Activity studies of GcpE enzyme

An activity assay for GcpE in the presence of substrate and dithionite was performed to determine if the protein that showed the two new EPR signals after 4 min incubation is still active when new substrate was added. This was accomplished by monitoring the absorption of methyl viologen at 732 nm for 10 min.

The experiment was performed for protein sample (as such) and a sample that was incubated with MEcPP and dithionite for 3-4 min (since the maximum intensity was reached around 3-4 min although the radical signal is still present till 16 min). A parallel EPR sample was taken to check for the presence of both iron-sulfur and the radical-type signals. The result shows that the new species were not active after addition of new substrate because there is no change in absorbance. This indicates that these EPR active species probably do not represent reaction intermediates (Figure 4-18).

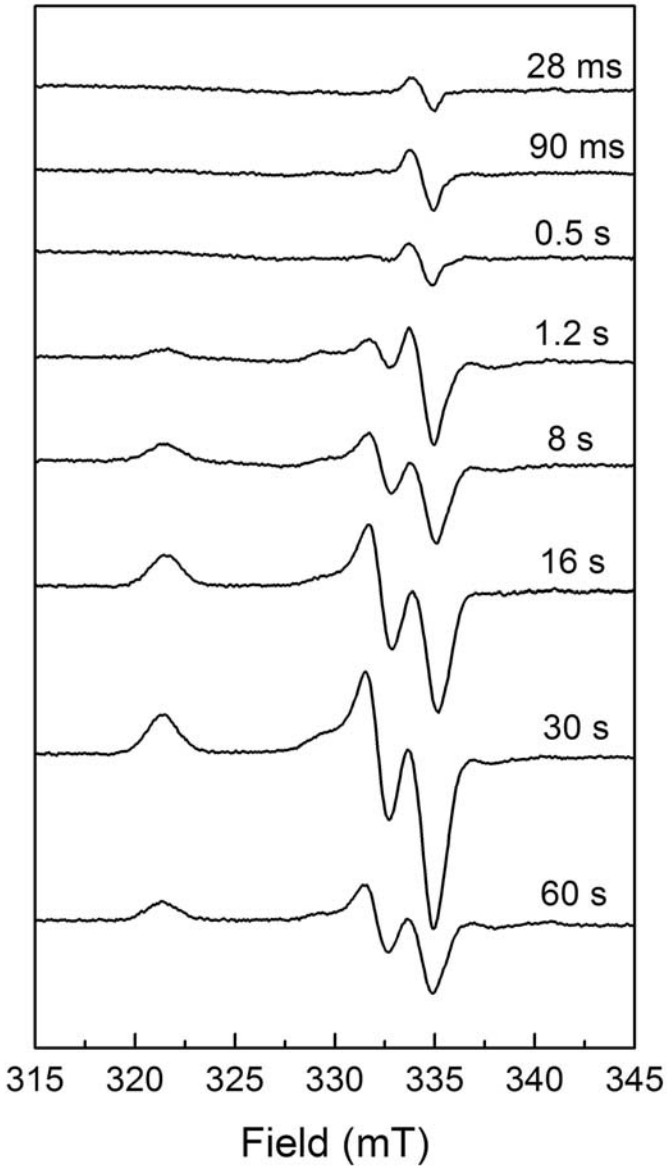

Figure 4-17: EPR spectroscopy of freeze quench samples at different quench times. Each sample tube contained 0.4 mM GcpE, 5.5 mM MEcPP and 25 mM dithionite. EPR conditions: microwave power, 0.199 mW; microwave amplitude, 0.6 mT; frequency, 9.385 GHz; Temperature, 10 K.

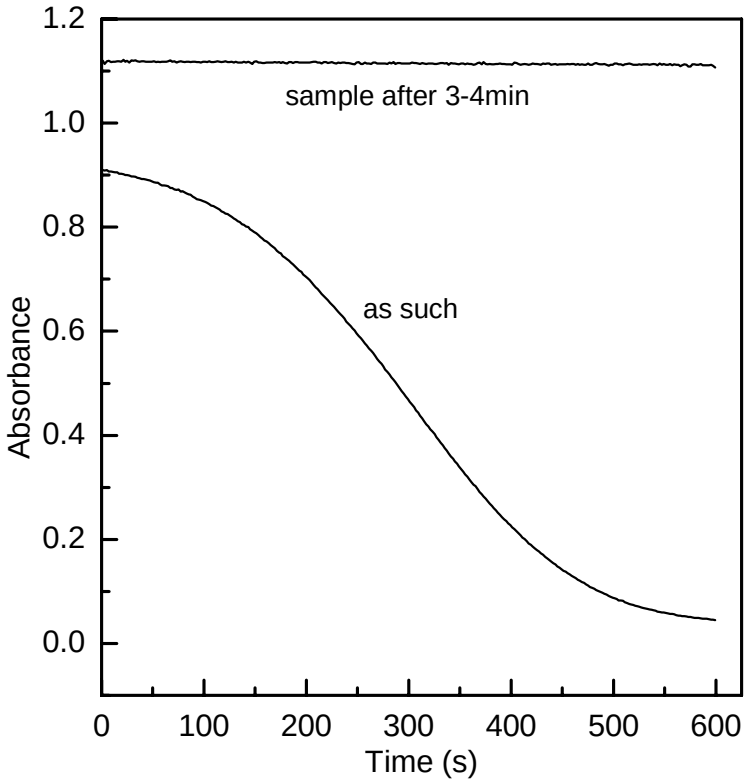

Figure 4-18: Activity studies of GcpE protein in the presence of dithionite, substrate and methyl viologen. The reaction was initiated by addition of substrate at 55°C. Oxidation of methyl viologen was monitored at 732 nm. As such indicates the curve obtained with fresh protein. Sample after 3-4 min is the curve obtained for a protein sample that was pre-incubated for 4 min in the presence of 5.5 mM MEcPP and 25 mM dithionite

4.10 Summary

The combination of EPR and resonance Raman (RR) spectroscopy showed that GcpE protein contains only a [4Fe-4S] cluster. EPR studies showed that the GcpE protein contains an unusual paramagnetic species under turnover conditions that resembles a HiPIP cluster. This paramagnetic species can only be observed in the presence of substrate (MEcPP) and dithionite, in which dithionite serves as an artificial reductant. The conditions used to induce the signal and its temperature behavior is similar to that of the EPR active species in FTR. In that case, the signal was due to a cluster-substrate complex.

CHAPTER FIVE

RESULTS FOR THE YfgB PROTEIN

5.1 Protein expression and purification

The YfgB gene of *Thermus thermophilus* was over expressed in *E.coli* XL-1 blue cells. Optimum protein expression was obtained at 37°C and induction with 0.4 mM (end concentration) IPTG. The cells were harvested when the optical density at 600 nm reached 4.0-5.0 (Figure 5-1). In the absence of IPTG, the protein was expressed but the amount was minimal. The protein was purified using heat treatment at 65°C followed by both weak (DEAE sepharose column) and strong (mono Q column) anionic exchange chromatography.

The protein was eluted from the DEAE column at around 25% buffer B (Figure 5-2) and from the mono Q column at around 20% buffer B (Figure 5-3). (Buffer B contains 20 mM Tris-HCl and 1 M NaCl). The high intensity peak signifies the position where the protein is being eluted. Purification was followed with SDS-PAGE since no assay is available. More than 80% purity was achieved for YfgB as determined by SDS-PAGE. Figure 5-4 shows the SDS-Page analysis of the different steps. The yield from a 1L growth culture was about 20 mg. The YfgB protein is about 32 kDa in size as judged by SDS-PAGE.

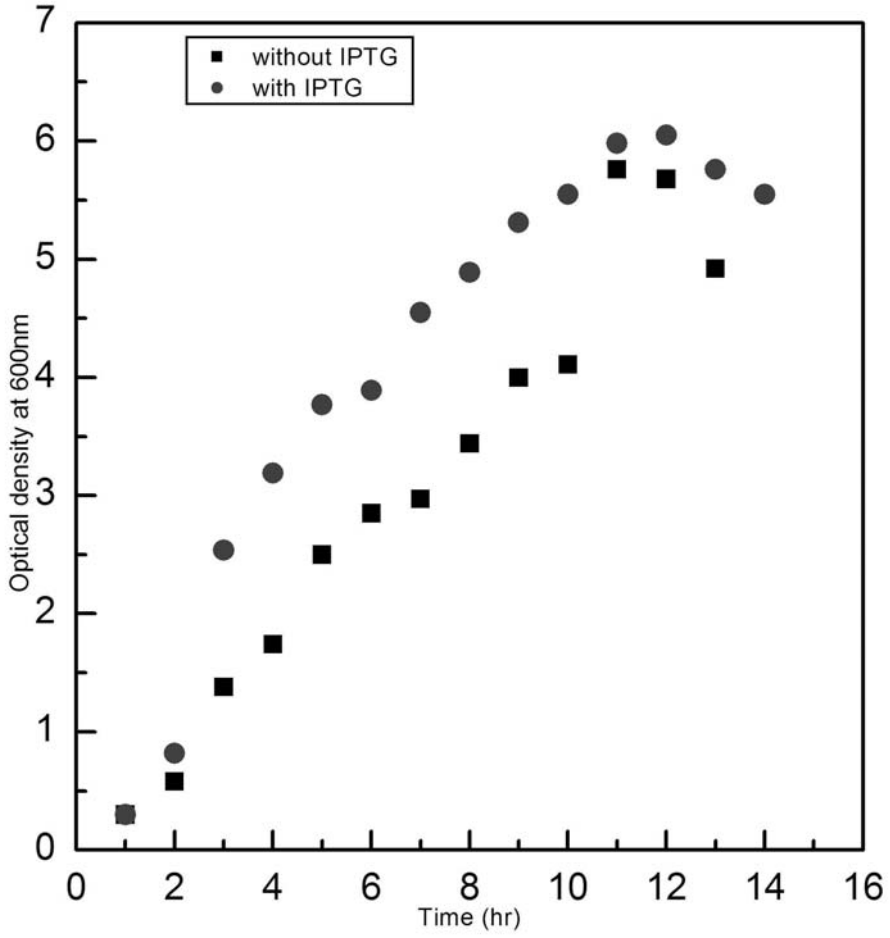

Figure 5-1: Growth curve of *E. coli* XL blue cells in the absence and presence of IPTG (0.4 mM).

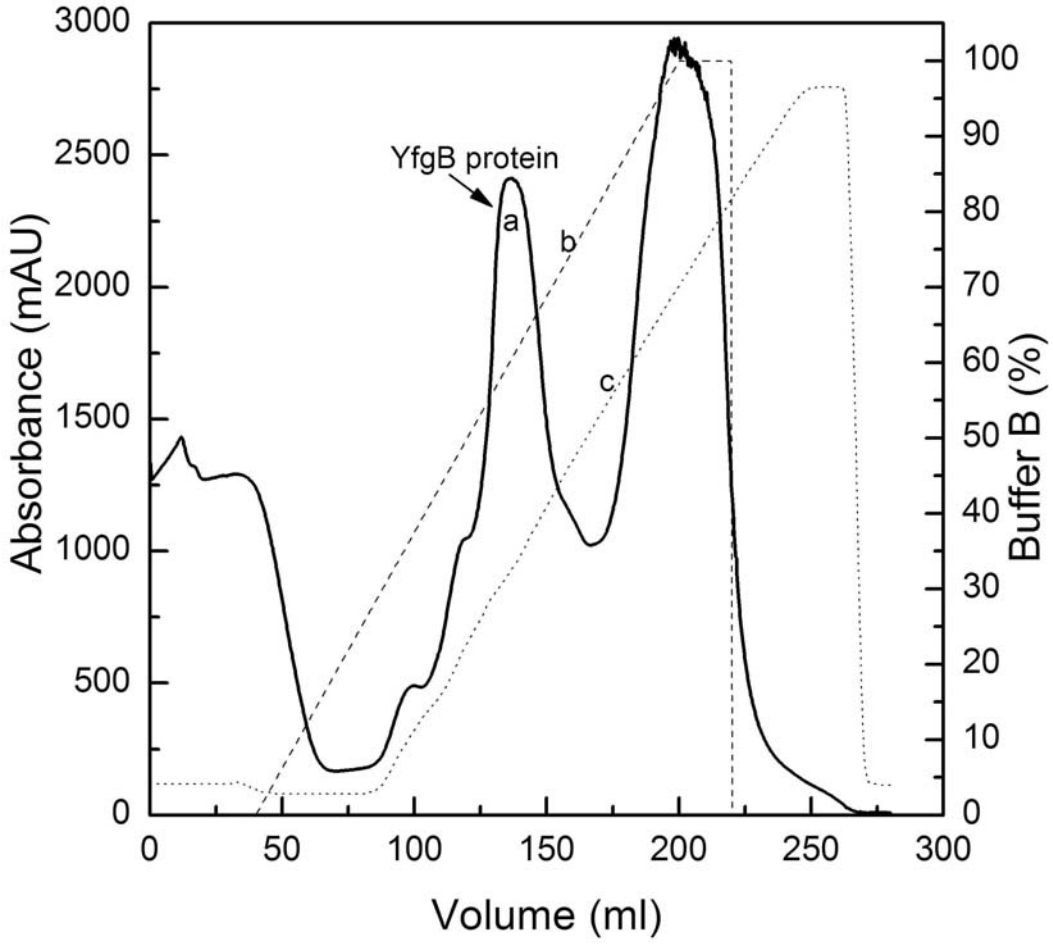

Figure 5-2: DEAE column profile for purification of the YfgB protein. Letter a denotes the absorption peak for YfgB protein, b denotes the % conductivity and c is the % concentration of buffer A. Protein eluted between 20% and 45% buffer A concentration.

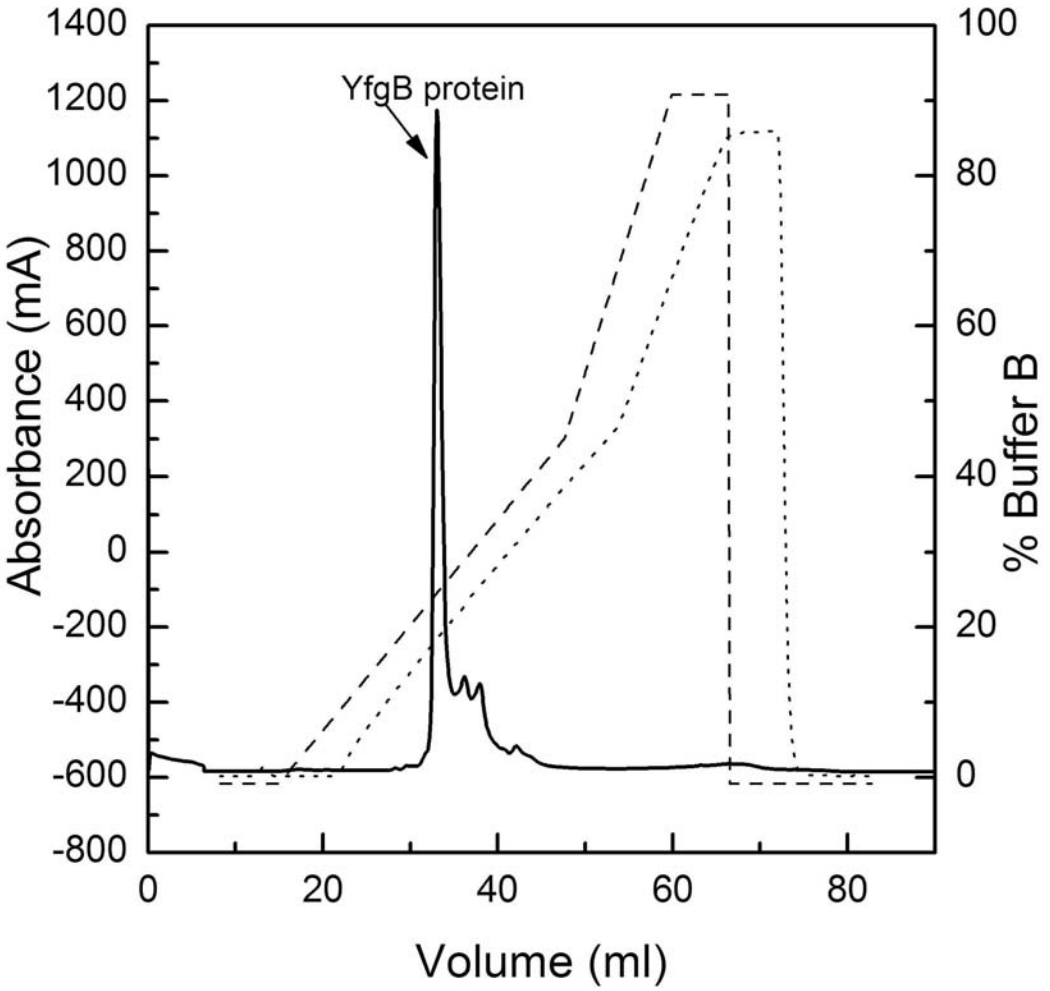

Figure 5-3: Mono Q column profile for the YfgB purification. The high intensity peak is the YfgB protein. The dashed line represents the % conductivity; the dotted line represents the % concentration of buffer used. The protein eluted between 20% and 23% buffer B.

5.2 Absorption spectroscopy of YfgB protein

The absorption spectrum of YfgB was measured after purification to check for the presence of an iron-sulfur cluster. There was no absorbance peak at around 420 nm (Figure 5-5) which indicated that there was no iron-sulfur cluster present. Reconstitution of the cluster was performed according to a procedure previously described (*158*) and the spectrum of the reconstituted cluster was recorded as shown in figure 5-6. The absorption band at around 420 nm indicates the presence of a $[4Fe\text{-}4S]^{2+}$ and/or $[3Fe\text{-}4S]^{1+}$ cluster.

Reduction of the cluster was performed using dithionite. The bleaching of the 420 nm band indicates reduction of the cluster. To further confirm the presence of the iron-sulfur cluster, EPR experiments on the YfgB protein were performed.

The reconstituted YfgB enzyme contains 3.6 mole of Fe per mole of enzyme as determined by the ferrozine-based colorimetric method.

5.3 Electron paramagnetic resonance (EPR) of reconstituted YfgB protein

EPR spectroscopy of YfgB was obtained for reduced-YfgB in the presence of ethylene glycol at 10K. In this experiment, YfgB protein is first reduced with dithionite solution, transferred into an EPR tube, and then frozen in liquid nitrogen. The EPR signal shows the presence of $[4Fe\text{-}4S]^{1+}$ cluster with both high spin (spin 3/2, minor component) and low spin (spin ½, major component) present (Figure 5-7). In the presence of ethylene glycol, a sharp signal for the spin ½ was obtained (figure 5-8). Figure 5-9 shows only the spin ½ signal with g values at 2.034, 1.915 and 1.858 which is typical for a $[4Fe\text{-}4S]^{1+}$ cluster.

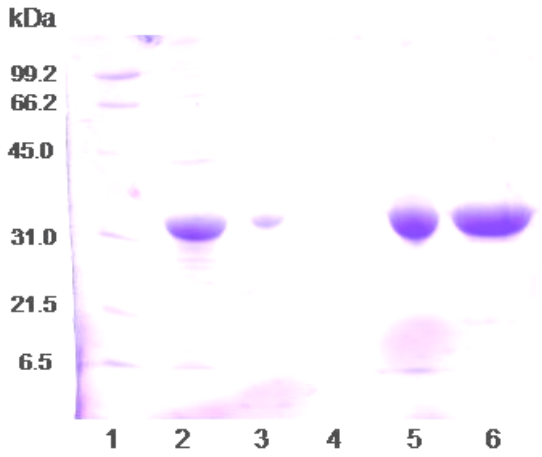

Figure 5-4: SDS-PAGE gel of different fractions obtained during purification of YfgB protein. Lane 1, protein standard; Lane 2, Cell extract; Lane 3, Heat stable protein; Lane 4, Flow through; Lane 5, Sample after DEAE sepharose column (weak anion exchanger); Lane 6. Sample after 15 Q sepharose column (strong anion exchanger).

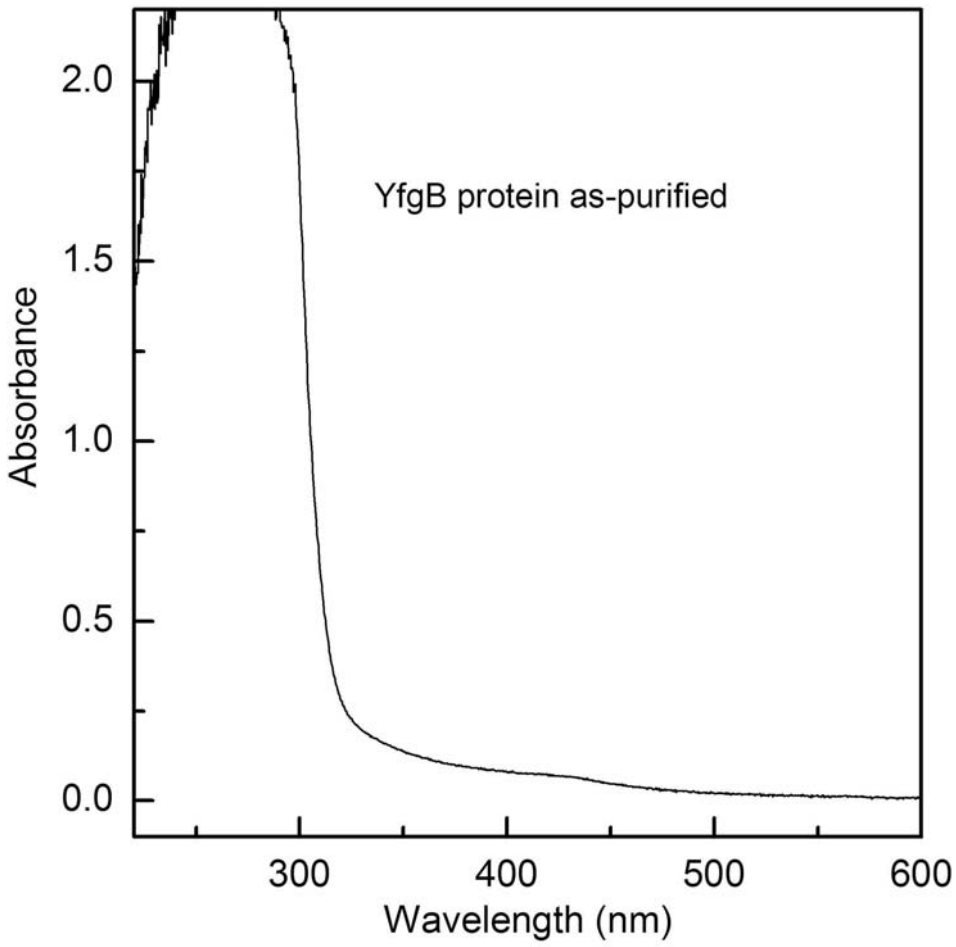

Figure 5-5: Absorption spectra of YfgB protein after purification. Absence of pronounced absorbance band at 420 nm is indicative of the absence of iron-sulfur clusters.

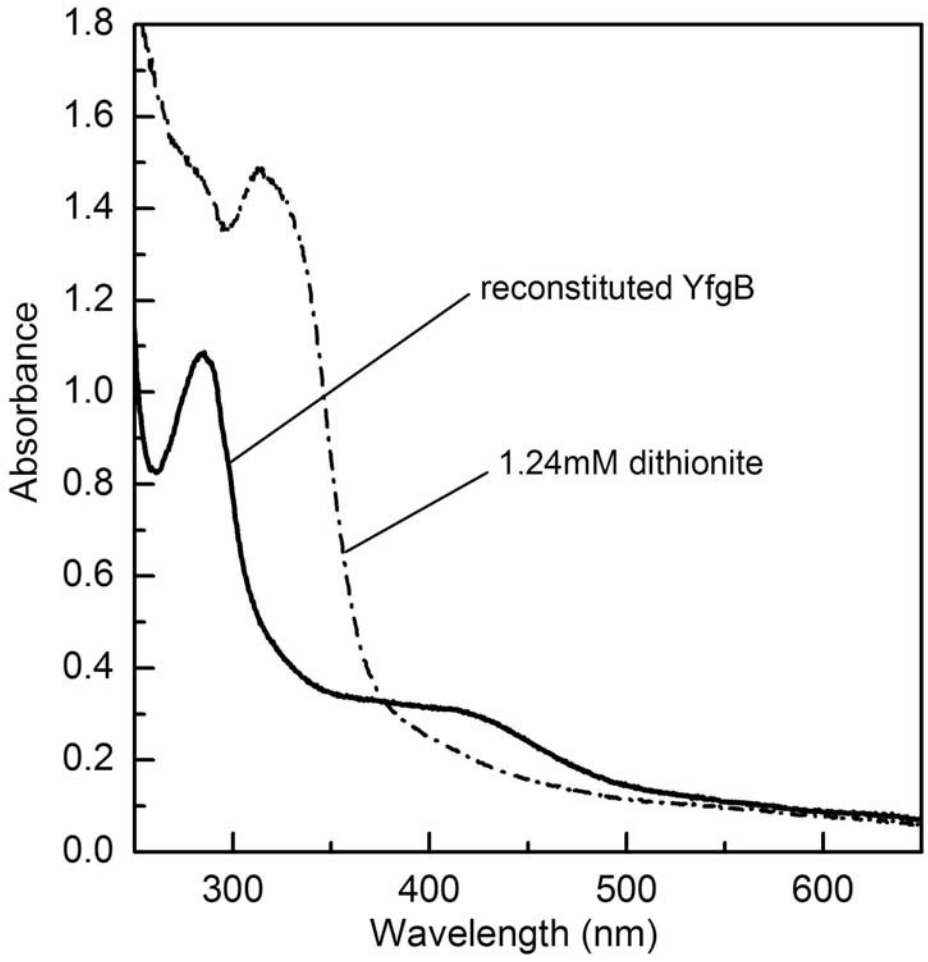

Figure 5-6: Absorption spectra of reconstituted YfgB protein. The reconstituted (solid line) enzyme (0.011 mM) in the presence of 1.22 mM dithionite (dash-dot line). The band at 330 nm is due to dithionite.

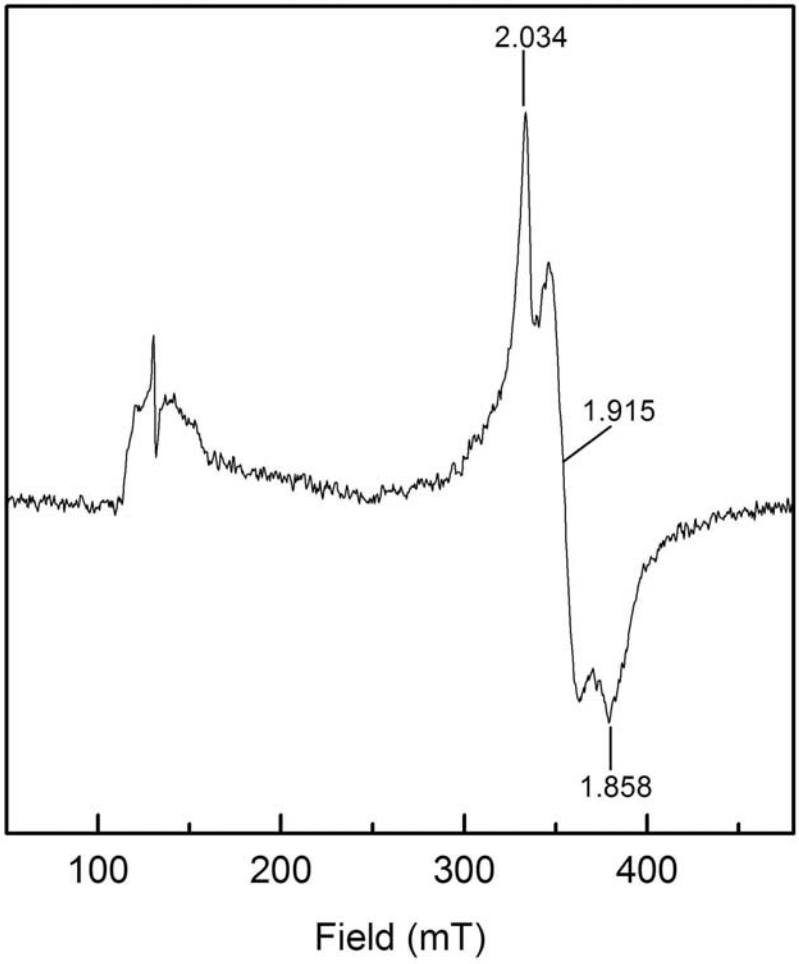

Figure 5-7: EPR spectrum of YfgB protein in the absence of ethylene glycol showing both the spin 3/2 (minor component) and spin ½ (major component) at 10 K. EPR conditions: Microwave power, 0.01993 mW; microwave frequency, 9.3858 GHz; modulation amplitude, 0.6 mT; field modulation at 100 kHz.

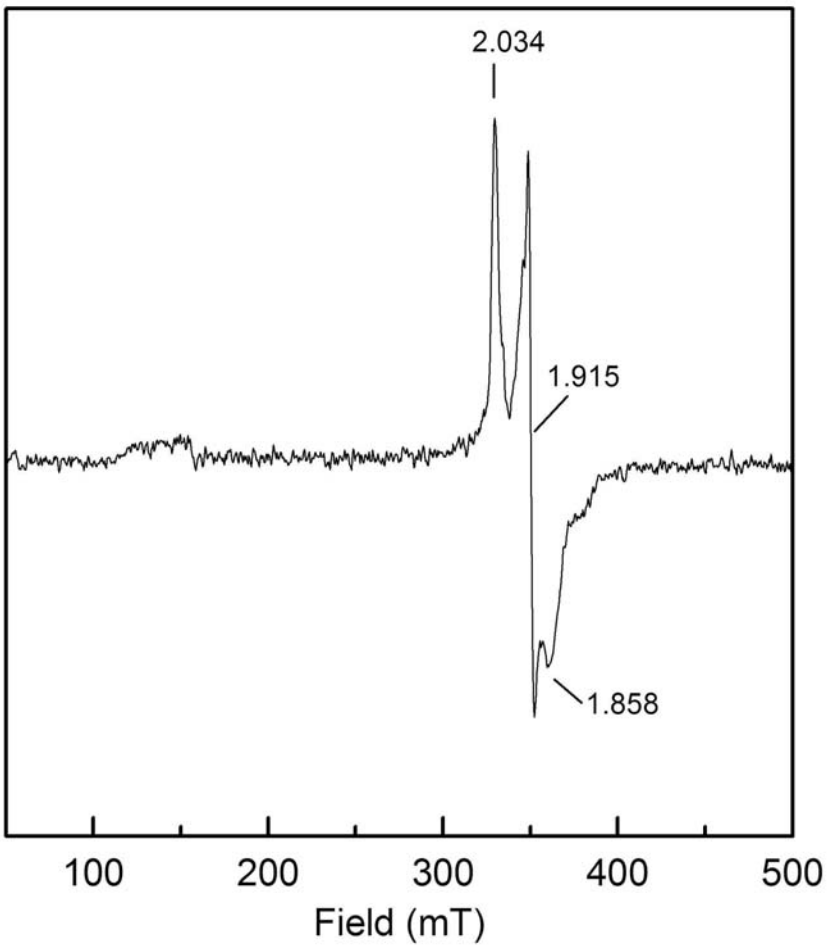

Figure 5-8: EPR spectrum of dithionite reduced YfgB (0.081mM) in the presence of 20% ethylene glycol at 10 K showing both spin 3/2 and spin 1/2. EPR conditions: Microwave power, 0.01993 mW; microwave frequency, 9.3858 GHz; modulation amplitude, 0.6 mT; field modulation at 100 kHz.

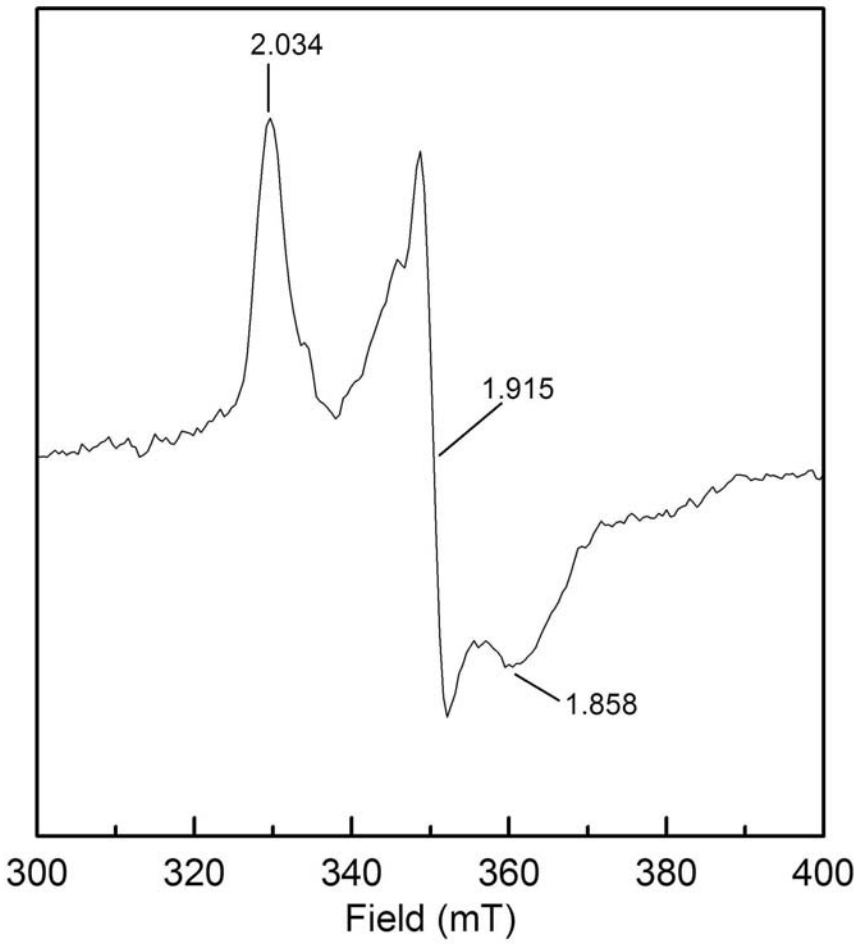

Figure 5-9: EPR spectrum of dithionite reduced YfgB (0.081 mM) in the presence of 20% ethylene glycol at 10 K. Microwave power is 0.01992 mW, microwave frequency is 9.3859 GHz, modulation amplitude is at 0.6 mT and field modulation at 100 kHz

5.4 Effect of SAM on YfgB protein

A twenty fold molar excess of SAM with respect to enzyme concentration was added to YfgB protein that has been reduced with dithionite solution. We could not see any effect of SAM on both the absorption and the EPR spectra of the reduced YfgB protein that would indicate binding of SAM to the 4Fe cluster.

Two possible effects could be expected when SAM binds; either SAM binds without being converted which is expected to be observed as a change in g-values in EPR or when SAM is converted, the Fe-S EPR signal is lost due to oxidation and a radical signal might be detected due to an amino-acid based radical species. None of these changes were detected (not shown).

5.5 GcpE in the presence of YfgB protein

We propose that YfgB might be acting as an activating protein for GcpE (Figure 5-10). Following the example of other radical SAM proteins, YfgB might transfer a low potential electron to GcpE. On GcpE, a radical could be formed that is needed to activate the substrate before binding to the cluster.

Several experiments were performed by first reducing YfgB with dithionite and removing the excess dithionite on a PD-10 column followed by the addition of SAM and GcpE enzyme. No oxidation of the reduced cluster present in YfgB was detected in EPR and absorption spectroscopy.

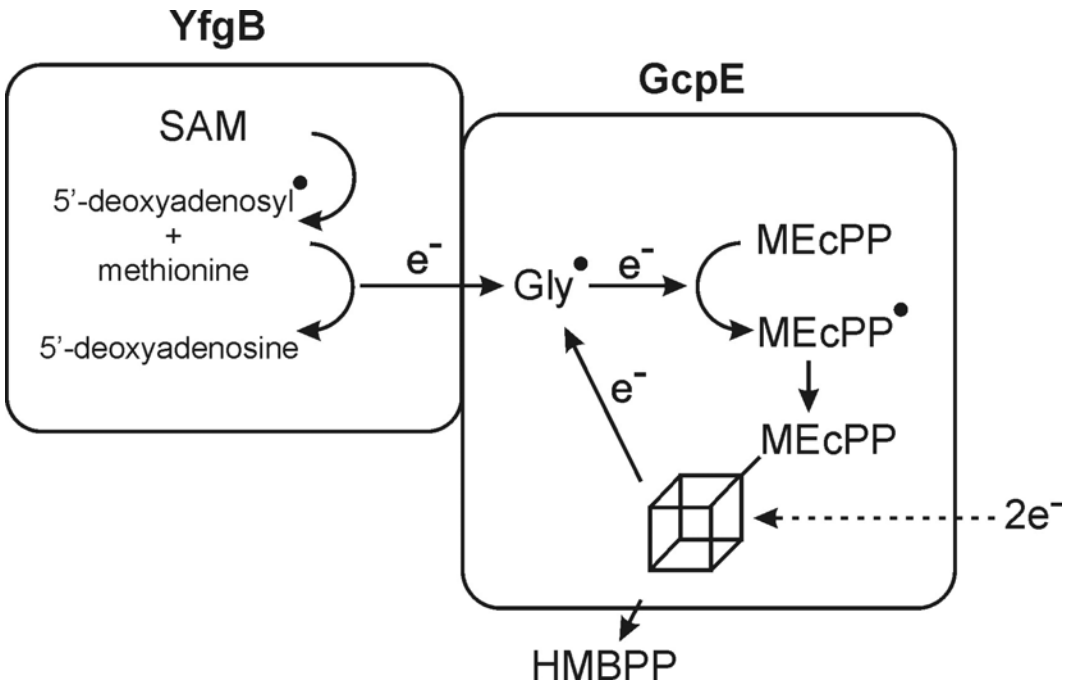

Figure 5-10: Proposed YfgB/GcpE model in which YfgB is acting as an activating protein to create a glycyl radical on GcpE for MEcPP activation before binding to the iron-sulfur cluster.

CHAPTER SIX

DISCUSSION

6.1 LytB protein

LytB catalyzes the conversion of HMBPP to IPP and DMAPP in the ultimate step of isoprene synthesis (Figure 1-1). In this work, we determined the type of iron-sulfur cluster present in LytB protein using both absorption and EPR spectroscopic techniques.

The *lytb* gene from *Aquifex aeolicus*, a hyperthermophillic organism was expressed in *E. coli* cells. Expression of LytB protein in the presence of IPTG provided a significant amount of protein and purification was carried out in the absence of oxygen in a Coy glove box to ensure iron-sulfur cluster stability.

LytB protein as purified contained both $[3Fe\text{-}4S]^{+1}$ and $[4Fe\text{-}4S]^{+2}$. This showed that the LytB protein contained an unstable 4Fe cluster. The purification had a A_{420}/A_{280} ratio (< 0.1) which showed that the cluster content of LytB protein is on the low side when compared to GcpE enzyme. This indicates instability of the cluster in the cell despite purification in the absence of oxygen (Figure 6-1). The instability of the 4Fe cluster is in line with the protein sequence data: the sequence alignment of LytB showed the presence of only three conserved cysteines (Figure 6-2) in which the fourth iron is coordinated by a different amino acid side chain, water or is not coordinated at all. This can cause the unique iron atom to be easily removed during purification.

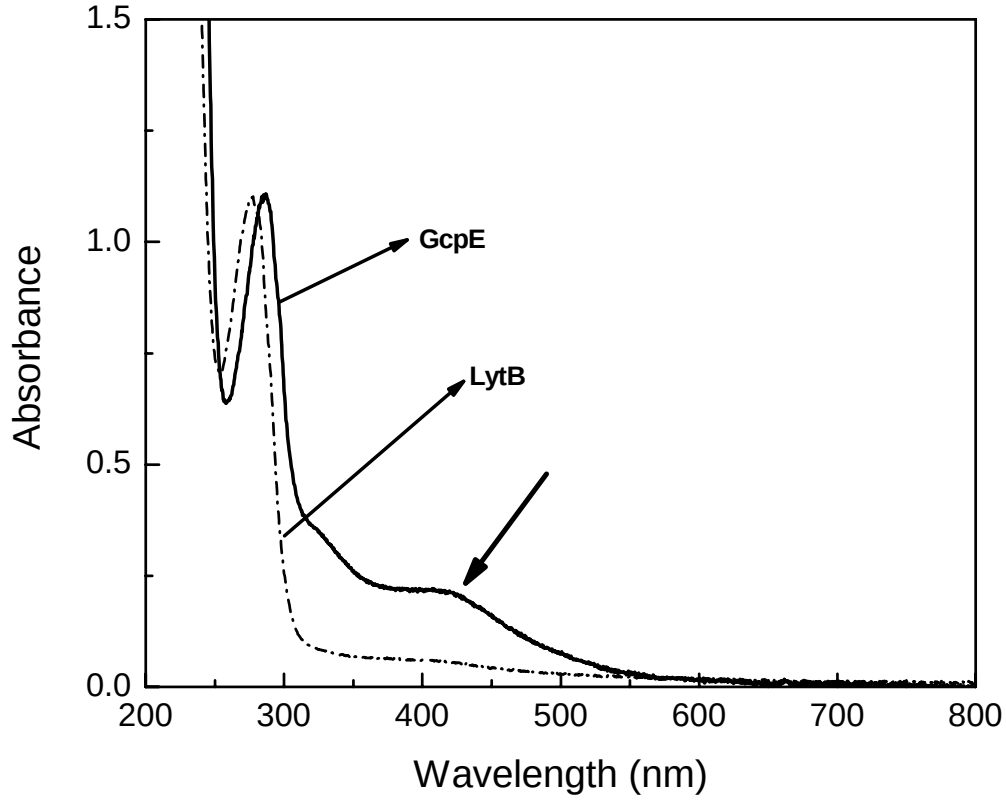

Figure 6-1: Comparison of the amount of cluster content in GcpE and LytB enzymes. The shoulder at 420 nm indicates the relative amount of cluster present.

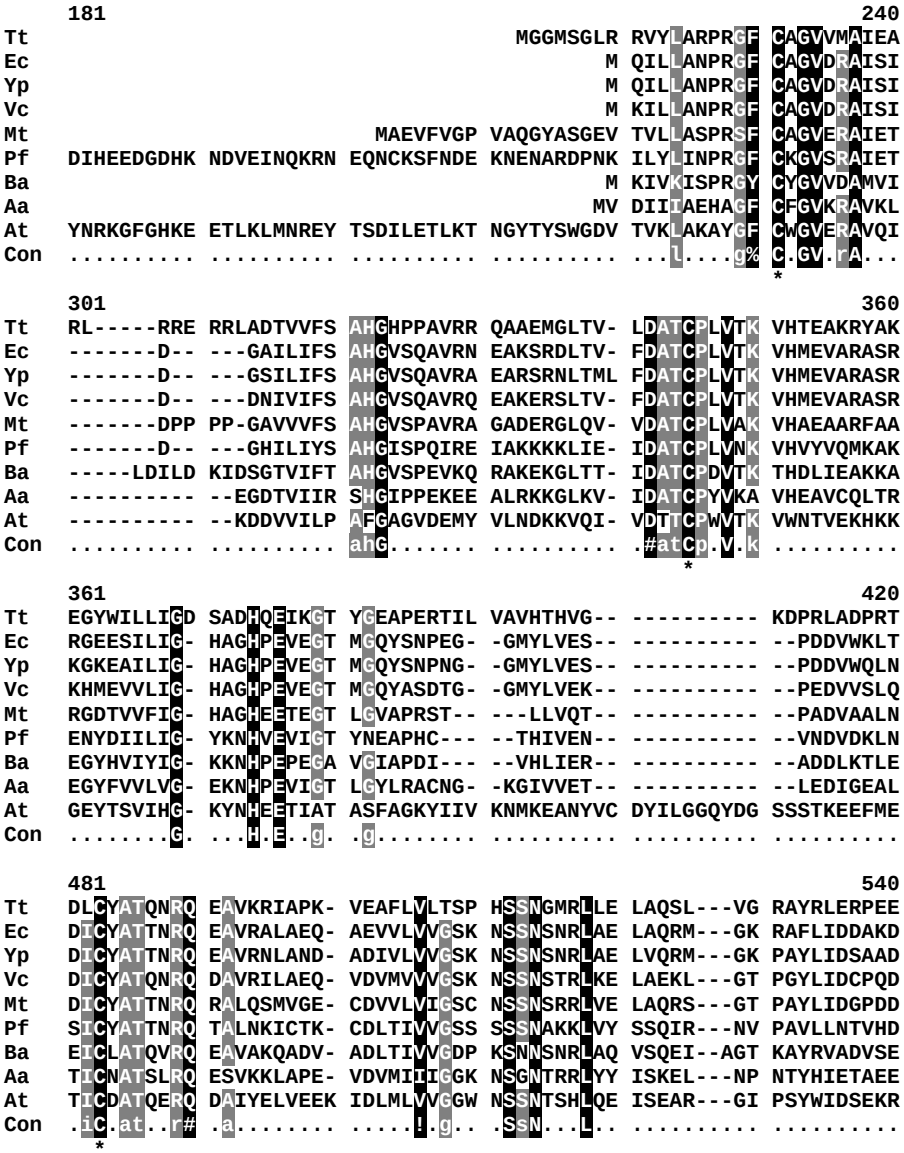

Concensus sequence based on alignment (Blosum62-12-2) of 75 unique sequences (only 9 shown).

Tt, Thermus thermophilus HB27; EC, Escherichia coli K12; Yp, Yersinia pestis; Vc, Vibrio cholerae; Mt, Mycobacterium tuberculosis H37Rv; Pf, Plasmodium falciparum 3D7; Ba, Bacillus anthracis A2012; Aa, Aquifex aeolicus; At Arabidopsis thaliana.

Black background, 100% conserved. Gray background 80% conserved. Asterisks indicate the position of the conserved Cys residues. Numbering is from the P. falciparum gene that contains an extra N-terminal domain.

Figure 6-2: Sequence alignment of LytB protein from different organisms. The asterisk shows the conserved cysteine residues.

Reconstitution of the cluster can be carried out to obtain full cluster content. Since LytB has only three conserved cysteines available to coordinate the 4Fe cluster, there is the possibility that the substrate will bind to the uncoordinated cluster-iron during the reaction cycle as seen in aconitase. This may indicate that the [4Fe-4S] cluster in LytB protein is probably involved in substrate binding.

Further characterization of the cluster in LytB protein was not carried out because of the problems encountered. One possible explanation is that due to genetic leakage of the *lac* promoter, LytB protein is expressed in the absence of IPTG. For some unknown reasons, this made the cell lines unstable. Replacing the *lac* promoter with a *tet* promoter removed the problems with the cell lines.

Although cell lines are available in the lab for the expression of lytB from *A. aeolicus* and LytB from *P. falciparum*, Weiya Xu continued to work with the *P. falciparum* enzyme since it is expressed with a high cluster content, removing the need for reconstitution procedures.

Reduced $[4Fe\text{-}4S]^{+1}$ cluster is detected in the presence of dithionite only and the EPR spectra confirmed the presence of $[4Fe\text{-}4S]^{+1}$. In the presence of both dithionite and substrate (HMBPP), a HiPIP-like signal (data not shown) was observed for LytB protein from *P. falciparum* that was identical to the signal found in GcpE from *T. thermophilus.*

6.2 GcpE enzyme

The GcpE enzyme catalyzes the conversion of 2-C-methyl-erythritol-2,4-cyclodiphosphate (MEcPP) into (E)-4-hydroxy-3-methyl-but-2-enyl diphosphate (HMBPP) in the second to the last step of the DOXP pathway for isoprenoid synthesis

(Figure 1-1). *E.coli* cells were transformed by gcpe gene from *Thermus thermophilus,* expressed and purified under exclusion of molecular oxygen. The absorption spectra of purified GcpE protein showed a high intensity band at 280 nm and a pronounced band at 420 nm. This indicates the presence of an iron-sulfur cluster which may contain either $[4Fe\text{-}4S]^{+2}$ and/or $[3Fe\text{-}4S]^{+1}$. The ratio of 420 nm/280 nm is above 0.2, indicating a significant amount of iron-sulfur cluster content. The purified protein contains 3.9 mole Fe per mole of enzyme.

Addition of dithionite solution did not have any effect on the iron-sulfur cluster in the protein, which would indicate that the cluster in GcpE enzyme cannot be reduced by dithionite. Reduction with titanium citrate probably resulted into cluster breakdown. Resonance Raman (RR) spectroscopy further confirmed the presence of only $[4Fe\text{-}4S]^{2+}$ cluster in the GcpE protein. There is no evidence for the presence of any other type of iron-sulfur cluster present in the GcpE enzyme apart from [4Fe-4S], so we conclude that the GcpE enzyme solely contains a [4Fe-4S] cluster. Sequence alignment (Figure 6-3) of GcpE showed the presence of three conserved cysteine residues which in principle can coordinate a 4Fe cluster and the unique iron atom could function in binding the substrate during the reaction cycle.

Generally in iron-sulfur cluster, the uncoordinated iron atom is easily removed under oxidative conditions leading to relative instability of the cluster upon purification. This is rarely the case for GcpE. We found out that after purification, the iron-cluster is not very sensitive to oxygen. It was reported (*159*) that the iron-sulfur cluster in GcpE enzyme is oxygen-sensitive and therefore reconstitution of the cluster is needed.

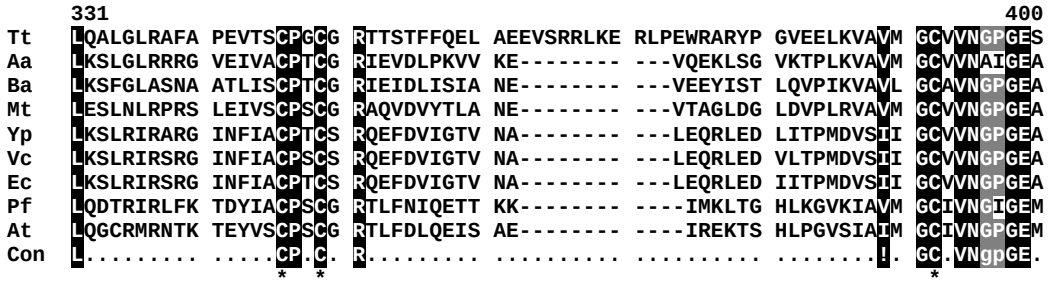

Concensus sequence based on alignment (Blosum62-12-2) of 63 unique sequences (only 9 shown).
Tt, Thermus thermophilus HB27; Aa, Aquifex aeolicus; Ba, Bacillus anthracis A2012; Mt, Mycobacterium tuberculosis H37Rv; Yp, Yersinia pestis; Vc, Vibrio cholerae; Ec, Escherichia coli K12; Pf, Plasmodium falciparum 3D7; At Arabidopsis thaliana.
Black background, 100% conserved. Gray background 80% conserved. Asterisks indicate the position of the conserved Cys residues.

Figure 6-3: Sequence Alignment of GcpE protein from different organisms

In metalloproteins, two types of iron-sulfur cluster can be generated either under strongly oxidizing or reducing conditions. Under reducing conditions, conversion of $[4Fe\text{-}4S]^{2+}$ to $[4Fe\text{-}4S]^{1+}$ is possible for clusters known as standard type clusters. Under strongly oxidizing condition conversion from $[4Fe\text{-}4S]^{2+}$ to $[4Fe\text{-}4S]^{3+}$ is possible for HiPIP clusters. Neither of these changes occurs in the iron-sulfur cluster of GcpE.

The HiPIP-like signal can easily be observed at 77 K but a real HiPIP can only be seen at temperature below 20 K. Measurement in EPR at temperatures below 20 K for the cluster in GcpE is not possible without saturation of the GcpE signal.

Time-dependent studies on GcpE revealed the presence of two additional signals apart from the first HiPIP-like signal observed. The first additional signal is a radical intermediate which is observed after 1-2 min when the HiPIP-like signal is replaced by the radical-type signal (Figure 4-10). Another signal that resembles a HiPIP signal was also observed. The origin of both signals is not clear.

The freeze quench experiment confirmed the role of the HiPIP-like signal as a transient reaction intermediate. In addition it revealed the presence of another EPR species. The EPR is isotropic, which is a characteristic for a radical species.

Several hypothetical mechanisms can be found in the literature that proposes a radical-type mechanism for GcpE. Figure 6-4 shows a mechanism that has been proposed by several groups that in principle does not need a direct role for the Fe-S cluster. The proposal was based on the fact that the cluster in GcpE can be reduced with titanium citrate in which the reaction may be initiated by ring opening of the cyclodiphosphate to yield a tertiary carbocation that is relatively stable. The carbocation can then be reduced by two consecutive one-electron transfer steps under the concerted

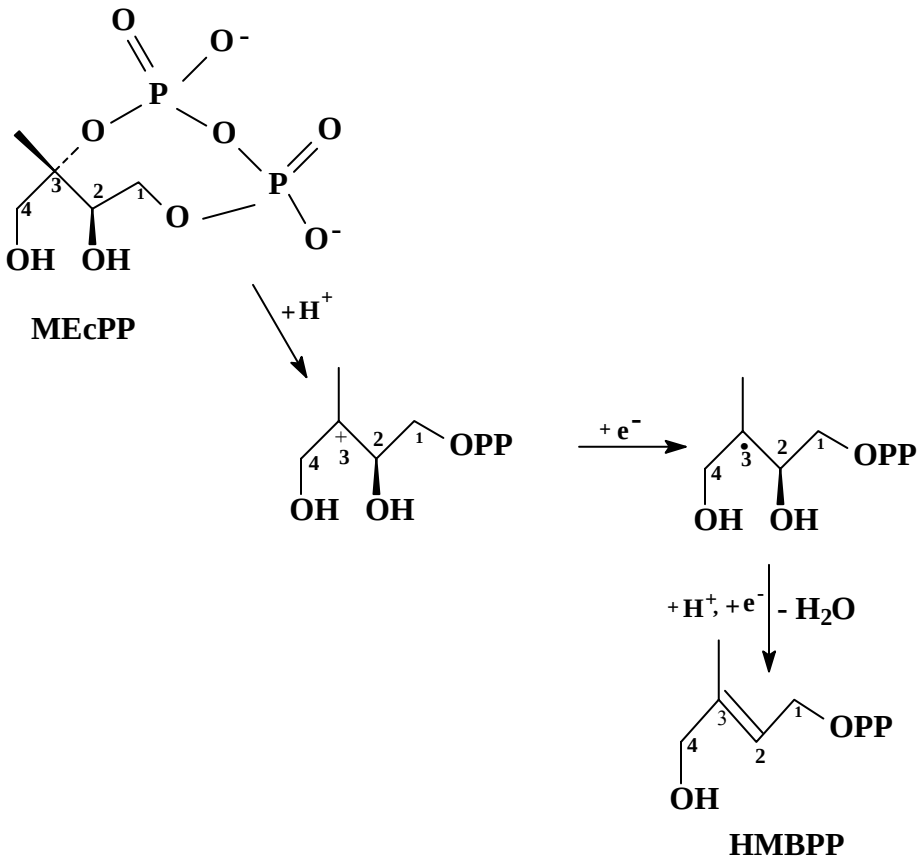

Figure 6-4: Hypothetical mechanism I the conversion of MEcPP into HMBPP by the GcpE enzyme (*7*)

elimination of the hydroxyl group as water to give the product, HMBPP.

Our EPR data indicates the binding of the substrate to the cluster with different possibilities. The binding of the substrate to the cluster could take place through the phosphate group, however, the ENDOR data excludes this option due to low ^{31}P coupling. This indicates that the mode of binding of the iron-sulfur cluster to the substrate is most likely through a hydroxyl group.

The binding of the cluster to the C2 carbon atom with the elimination of the C2 hydroxyl group has been proposed for GcpE enzyme (*159*) (Figure 6-5). But the opening of the cyclodiphosphate and the elimination of the hydroxyl group still remain to be solved. The Lewis acid character of the iron-sulfur cluster, which may coordinate to the hydroxyl group has been established for aconitase enzyme but it is not known whether the Fe-S cluster or other acidic groups are involved. The evidence for a weak isotropic coupling in phosphorous atom shows that the iron-sulfur cluster in GcpE enzyme is directly involved in substrate binding and catalysis.

Knowing the mode of binding of substrate to the cluster is important; this will lead to a better understanding on the reaction mechanism and help in designing potential inhibitors that mimic the substrate-transition state. These compounds might probably show high specificities and high binding constants that will make them good candidates for anti-infective drugs.

The sequence alignment of GcpE shows the presence of two highly conserved glycine residues (Figure 6-3). The radical-type signal present at incubation time of 3 min and longer may be attributed to a glycyl species that might have developed due to the

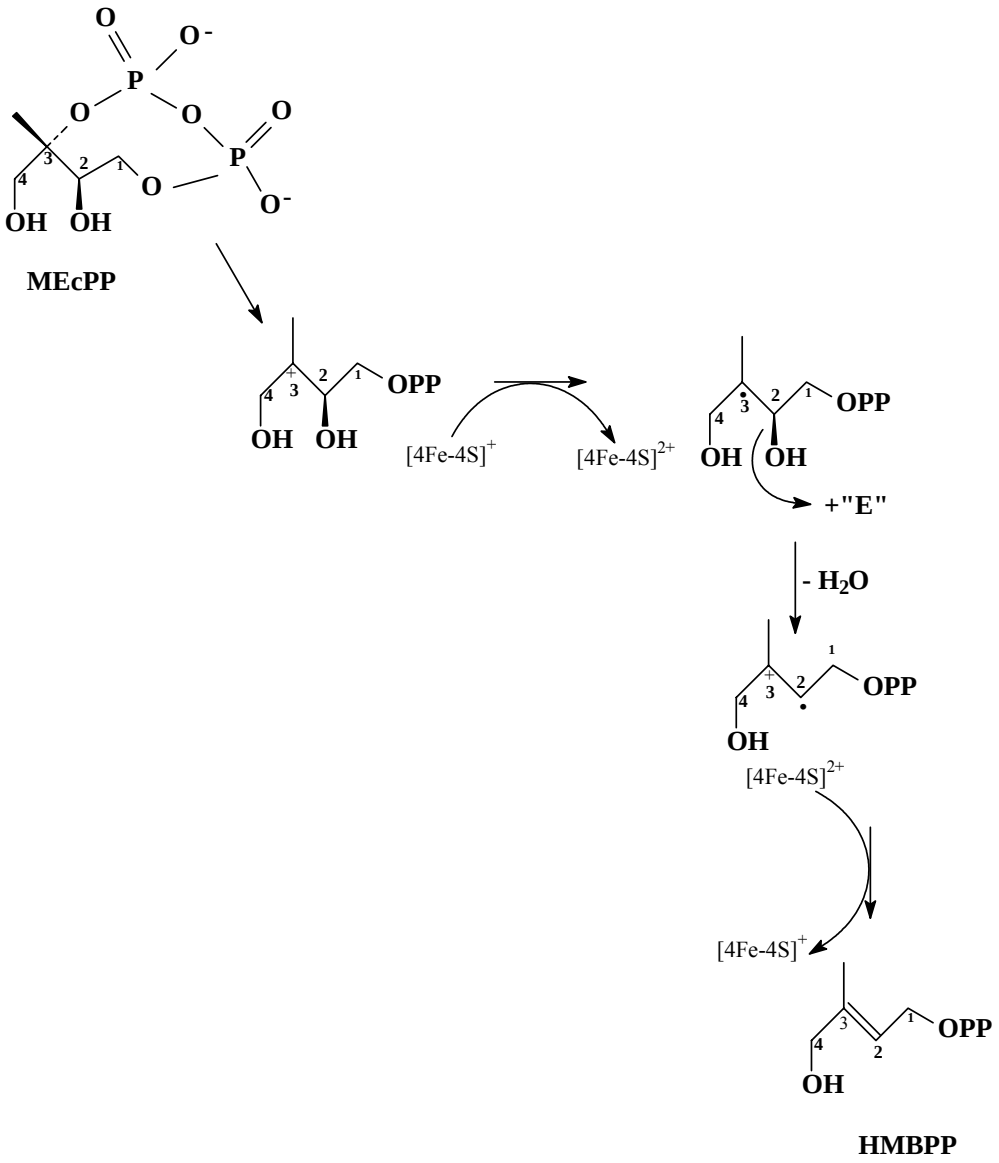

Figure 6-5: Hypothetical mechanism II for the reaction catalyzed by the GcpE enzyme (*159*)

presence of the glycine residues in the close vicinity of the Fe-S cluster. However, the activity studies on GcpE revealed that the enzyme that showed this EPR signal is not active in our assay.

These results suggest that they are not intermediates in the reaction mechanism, but might be part of the side reactions. This shows that a better understanding of the reaction mechanism of the GcpE enzyme is essential to explain the various signals observed.

6.3 YfgB protein

The LytB and GcpE proteins are directly involved in the DOXP pathway. As can be expected there is an additional need for accessory proteins that assist in the synthesis, folding and function of the proteins that constitute the pathway. Besides the obvious role of proteins that function in Fe-S cluster synthesis and insertion, genetic evidence (Heidi Sofia, personal communication) indicates that there is a gene, *yfgB*, that codes for a protein that belongs to radical SAM family. This gene seems to be associated with the *gcpE* gene.

The presence of the defining CxxxCxxC motif in the YfgB protein sequence indicates that YfgB belongs to the radical SAM enzymes. This motif is highly conserved in YfgB proteins from different organisms as shown by the sequence alignment in Figure 6-6.). The binding site for SAM is also present (not shown). The length of the amino acid chain and the absence of any other motif that would indicate the presence of another metal center would indicate that YfgB functions as an activating protein (not shown).

```
        151    *   *   *                                    200

E. coli     QVGCALECKF CSTAQQGFNR NLRVSEIIGQ VWRAA----- --KIVGAAKV
S. flex     QVGCALECKF CSTAQQGFNR NLRVSEIIGQ VWRAA----- --KIVGAAKV
S. enter    QVGCALECKF CSTAQQGFNR NLRVSEIIGQ VWRAA----- --KIVGAAKV
S. typhi    QVGCALECKF CSTAQQGFNR NLRVSEIIGQ VWRAA----- --KIVGAAKV
Y. pestis   QVGCALECKF CSTAQQGFNR NLRVSEIIGQ VWRAA----- --KIIGSLKS
Y. pseudo   QVGCALECKF CSTAQQGFNR NLRVSEIIGQ VWRAA----- --KIIGSLKS
E. carot    QVGCALECKF CSTAQQGFNR NLRVSEIIGQ VWRAA----- --KIIGAFKV
W. gloss    QIGCALNCKF CATSYQGFNR NLNSYEIISQ IWYAM----- --KIINDRNN
P. aeru     QAGCALDCSF CSTGKQGFNS DLTAAEVIGQ VWIAN----- --KSFGTVPA
B. amphid   QIGCSLKCHF CATGQEGFQR NLKVSEIIAQ IWQAN----- --KRLKEKNI
B. pseudom  QAGCAVNCRF CSTGKQGFSR NLSTGEIVGQ LRMAEFALRA SLGRAPGPNG
N. menin    QVGCALECTF CSTGRQGFNR NLTAAEIIGQ LWWAN----- ---KAMGVTP
C. jeju     QVGCKSGCSF CLTAKGGLKR NLSAGEIVGQ ILW------- ----IKKQNN
M. bovis    QAGCGMACPF CATGQGGLTR NLSTAEILEQ VRAG------ ----AAALRD
C. diphte   QAGCGMACPF CATGQGGLDR NLSTGEIVDQ VRAA------ ----SATMQA
 Consensus  Q.GC...C.F C.T...G..r #L...E!..Q .......... ..........
```

Figure 6-6: Sequence Alignment of the cluster binding motif of YfgB protein

The evidence that YfgB might be acting as an activating protein for GcpE is that both *yfgB* and *gcpE* genes are clustered together in the genomes of most organisms (Figure 6-7). The genes, however, are not present in the same operon. This makes sense since much more GcpE is needed in the cell than its activating enzyme.

Figure 6-7a depicts the gene cluster pattern in the genomes of *Candidatus* species in which both *gcpE* and *yfgB* genes are next to each other (The gene cluster patterns for a particular gene can be found on the KEGG website (www.genome.jp/kegg/) using the 'SSDB Gene Cluster Search' command). The figure also shows that the genes coding for the proteins involved in isoprene synthesis are not clustered together. The *gcpE* and *yfgB* genes are enclosed by the *hisS* and *ndk* genes that code for the enzymes histydyl-tRNA synthetase and nucleoside diphosphate kinase respectively.

In several organisms like *E. coli* strains and *Shigella* species, there is another gene, *yfgA*, a hypothetical gene, that is present between *gcpE* and *yfgB* genes as shown in figure 6-7b. Both *hisS* and *ndk* genes are also present.

In *Photobacterium* species, the two genes are further separated by two hypothetical genes (designated as hyp) present between the *gcpE* and *yfgB* (Figure 6-7c). Also present are both *hisS* and *ndk* genes. The two genes from Thermophilus used in our plasmids are not even clustered together in the genomes of *Thermus* species (Figure 6-7d).

As a comparison we also looked at the gene clustering pattern for pyruvate formate lyase and pyruvate formate lyase activating enzyme. In the *E. coli* genome, several pyruvate formate lyases can be found that are associated with their activating

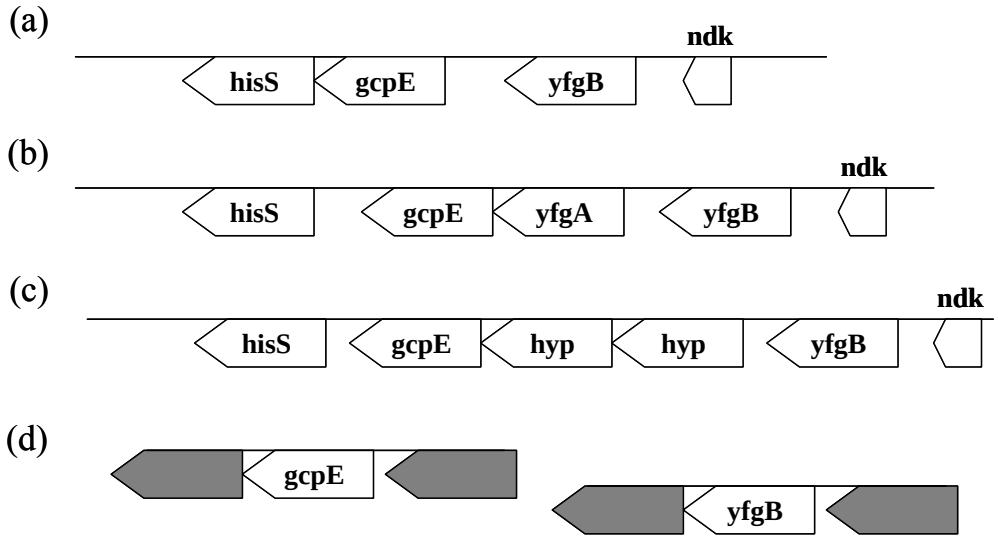

Figure 6-7: Schematic representation of operons in the genome of different organisms (a) *Candidatus* species (b) *E. coli* species (c) *Photobacterium* species (d) *Thermus* species

enzyme. An example is the *pflF* gene and gene that codes for the activating enzyme, *pflE*. The gene clustering pattern shows that in most genomes these two genes are next to each other (but not in the same operon). In several genomes, there is one other gene placed in between *pflF* and *pflE* genes.

The other example is the *pflB* gene and the gene that codes for the activating enzyme, *pflA*. In *E. coli* the genes are next to each other but in other genomes one, two or even three genes can be found in between these two genes. This shows that the different relative positions of the *yfgB* gene and the *gcpE* are still in line with a role for YfgB as an activating protein for GcpE.

The *yfgB* gene from *Thermus thermophillus* was used. *E. coli* cells were transformed using pQE60 expression vector, the cells were expressed in the presence of IPTG and has been purified in the absence of oxygen. Purification under anaerobic condition still led to the loss of the iron-sulfur cluster which might suggest that the iron-sulfur cluster in YfgB protein is relatively unstable. This is very common for the radical SAM protein.

Reconstitution of the iron sulfur cluster under anaerobic conditions followed by desalting resulted in ~3.7 mole Fe per mole of enzyme indicating that YfgB protein contained a $[4Fe\text{-}4S]^{2+}$. This was confirmed by absorption spectroscopy in which there is a pronounced shoulder at 420 nm. The final preparation gave a good A_{420}/A_{280} ratio (> 0.2). Reduction of the reconstituted protein by dithionite solution resulted in the disappearance of the 420 nm band. EPR spectra of the reconstituted YfgB on reduction showed the presence of both a high and low spin $[4Fe\text{-}4S]^{+1}$ cluster with spin ½ as the major component.

Our working hypothesis is that in the presence of SAM two different effects could be detected: Binding of SAM to the reduced cluster in YfgB could result in changes of the g-values of the EPR signal. Alternatively, binding of SAM could lead to oxidation of the cluster due to the reductive cleavage of SAM and the concomitant generation of the deoxyadenosyl radical. The radical could, subsequently, abstract a hydrogen atom from the protein to yield a glycyl radical that could be observed by EPR. However, the absorption and EPR experiments provided no evidence that SAM binds to the reduced cluster in YfgB protein. It has to be noted however that, not all radical SAM proteins show these effects.

Addition of GcpE enzyme to YfgB in the presence of SAM did not result in any detectable spectroscopic changes either. Therefore the role of the YfgB protein is still unclear.

6.4 Conclusions

All three enzymes that have been studied, LytB, GcpE and YfgB are iron-sulfur cluster containing proteins. They all contain a [4Fe-4S] cluster in their active site. Kinetic studies, in particular freeze-quench (Figure 4-17) and rapid freeze (Figure 4-10) experiments carried out for GcpE in the presence of dithionite and substrate resulted in the detection of several paramagnetic species of which at least two might play a role in the reaction mechanism. An isotropic radical signal was detected in the 30 ms to 2 s time range. The HiPIP-like signal develops in the 2 s to 30 s time range. To determine if this species are relevant for the reaction mechanism the turn-over number for GcpE has to be

determined at room temperature. Only if the turn-over number is comparable with the time intervals in which these two species develop will they be part of the reaction path towards product formation. Additional signals developed after 2 min, that is after exhaustion of substrate: A radical-type signal that seems to show a two-fold split, and another HiPIP-like signal, HiPIP-B. These two signals seem to develop together.

The spectroscopic properties of the HiPIP-like signal indicate that the [4Fe-4S] cluster is directly involved in substrate binding and stabilization of a radical-type intermediate. ENDOR measurements revealed a ^{31}P-hyperfine coupling of the cluster to the substrate due to the close vicinity of the MEcPP phosphate groups. (NOTE: New ENDOR data is now available that was obtained with a GcpE sample that showed only the HiPIP-like signal. The ^{31}P hyperfine coupling is present in this sample.) We hypothesize that the leaving hydroxy group from MEcPP is probably the group that binds to the cluster during the reaction. To prove this, labeling studies of MEcPP will be needed using either ^{18}O or ^{13}C labeling, These nuclei will introduce additional hyperfine couplings that can be detected with EPR and ENDOR spectroscopy.

The direct involvement of the cluster in substrate binding is an important finding since several mechanisms have been proposed in the literature (*7,10,160-162*) but in only two publications was a direct role proposed for the [4Fe-4S] cluster in GcpE enzyme (*159,163*).

This work was based on the application of various spectroscopic techniques in the understanding of the role of the iron-sulfur clusters involved in LytB, GcpE and YfgB enzymes. Based on the results in this work, the following recommendations can be made

for better understanding of the role of iron-sulfur clusters in the DOXP pathway of isoprenoid synthesis:

- Reconstitution of LytB protein from *Aquifex aeolicus* for full cluster content under anaerobic conditions.
- Labelling studies (^{13}C, ^{17}O) to know the exact binding mode of the cluster to the substrate.
- Mössbauer spectroscopy to identify the coordination around the iron center when the substrate binds.
- Synthesis of substrate analogs that can serve as specific inhibitors.
- Use of reduced flavodoxin as a biological reductant to know if SAM binds to the YfgB protein.
- Interactions of GcpE with YfgB to establish the role of YfgB protein.

REFERENCES

1. Sacchettini, J. C. and Poulter, C. D. (1997) *Science 277*, 1788-1789.

2. Croteau, R., Kutchan, T. M., and Lewis, N. G. (2000) *Biochemistry and Molecular Biology of Plants* ASPD, Rockville, MD.

3. Goldstein, J. L. and Brown, M. S. (1990) *Nature 342*, 425-430.

4. McGarvey, D. J. and Croteau, R. (1995) *Plant Cell 7*, 1015-1026.

5. Qureshi, N. and Poreter, J. W. (1981) *Biosynthesis of Isoprenoids Compounds* John Wiley, New York.

6. Bacher, A., Friesen, J. A., Stauffacher, C. V., and Rodwell, V. W. (1999) *Comprehensive Natural Product Chemistry* Pergamon, Oxford.

7. Kollas, A. K., Duin, E. C., Eberl, M., Altincicek, B., Hintz, M., Reichenberg, A., Henschker, D., Henne, A., Steinbrecher, I., Ostrovsky, D. N., Hedderich, R., Beck, E., Jomaa, H., and Wiesner, J. (2002) *FEBS Letters 532*, 432-436.

8. Andersson, D. I. (2003) *Curent Opini. Microbiol. 6*, 452-456.

9. Eisenreich, W., Rohdich, F., and Bacher, A. (2001) *Trends Plant Sci. 6*, 78-84.

10. Eisenreich, W., Bacher, A., Arigoni, D., and Rohdich, F. (2004) *Cell. Mol. Life Sci. 61*, 1401-1426.

11. Rohmer, M., Grosdemange-Billiard, C., Seemann, M., Tritsch, D., and (2004) *Curr. Opin. Invest. Drugs 5*, 154-162.

12. Schwarz, M. K. and Arigoni, D. (1999) *Comprehensive Natural Product Chemistry* Pergamon, Oxford.

13. Rohdich, F., Bacher, A., Hecht, S., and Eisenreich, W. (2004) *Bioorganic Chemistry 32*, 292-308.

14. Rohdich, F., Hecht, S., Bacher, A., and Eisenreich, W. (2003) *Pure Appl. Chem 75*, 393-405.

15. Rohmer, M. (1999) *Nat. Prod. Rep. 16*, 565-574.

16. Boucher, Y. and Doolittle, W. F. (2000) *Molecular Microbiology 37*, 703-716.

17. Lange, B. M., Rujan, T., Martin, W., and Croteau, R. (2000) *Proc. Natl. Acad. Sci. USA 97*, 13172-13177.

18. Rohdich, F., Kis, K., Bacher, A., and Eisenreich, W. (2001) *Curent Opini. Chem. Biol. 5*, 535-540.

19. Rohdich, F., Bacher, A., and Eisenreich, W. (2005) *Coenzymology: biochemistry of Vitamins biogenesis and Cofactor* 785-791.

20. Shankey-Dubey, V. (2002) *Current Science 83*, 685-688.

21. Phillips, R. (2001) *Clin. Microbiol. Rev. 14*, 208-226.

22. Falkow, S. and Kennedy, D. (2001) *Science 291*, 397.

23. Karson, K.-A. (2000) *Glycobiology 10*, 761-771.

24. Missinou, M. A., Borrmann, S., Schindler, A., Issifou, S., Adegnika, A. A., Matsiegui, P.-B., Binder, R., Lell, B., Wiesner, J., Baranek, T., Jomaa, H., and and Kremsner, P. G. (2002) *The Lancet 360*, 1941-1942.

25. Borrmann, S., Issifou, S., Esser, G., Adegnika, A. A., Ramhert, M., Matsiegui, P.-B., Oyakhirome, S., Mawili-Mboumba, D. P., Missinou, M. A., Kun, J. F. J., Jomaa, H., and Kremsner, P. G. (2004) *Journal of Infectious Diseases 190*, 1534-1540.

26. Kuzuyama, T., Schimizu, T., Takahashi, S., and Seto, H. (1998) *Tetrahedron Lett. 39*, 7913-7916.

27. Zeidler, J., Schwender, J., Muller, C., Wiesner, J., Weidemeyer, C., Beck, E., Jomaa, H., and Litchtenthaler, H. K. (1998) *Z. Naturforsch 53c*, 980-986.

28. Rodríguez-Concepcíon, M. (2004) *Current Pharmaceutical Design 10*, 2391-2400.

29. Averill, B. A. (1998) in *ACS symposium series: Metal Clusters in Proteins* (Que, L., Ed.) pp 258-292, American Chemical Society, Washington, DC.

30. Harrison, P. M. (1995) *Metalloproteins; Metals Proteins with Redox Roles* Verley Chemie, Florida.

31. Palmer, G. and Reedojk, J. (1991) *Eur. J. of Biochem. 200*, 599.

32. Cammack, R. (1992) in *Advances in Inorganic Chemistry* (Cammack, R., Ed.) pp 281-322, Academic press, Inc., California.

33. Kennedy, M. C. and Stout, C. D. (1992) in *Advances in Inorganic Chemistry* (Cammack, R., Ed.) pp 323-339, Academic Press, Inc, California.

34. Moura, I., Huynh, B. H., Hausinger, R. P., LeGall, J., Xavier, A. V., and Münck, E. (1980) *J. Biol. Chem. 255*, 2493-2498.

35. Johnson, M. K. (1994) *In Encyclopedia of Inorganic Chemistry* Wiley, New York.

36. Cammack, R., Patil, D. S., Fernandez, D. C., and Victor, M. (1985) *Biochemical Society Transactions 13*, 572-578.

37. Gillium, W. O., Mortenson, J. S., and Chen, J. S. (1977) *J. Am. Chem. Soc. 99*, 584.

38. Orme-Johnson, W. H. and Holm, R. H. (1978) in *Methods in Enzymology* pp 53-268.

39. Kent, T. A., Dreyer, J. L., and Kennedy, M. C. (1982) *Proc. Natl. Acad. Sci. USA 79*, 1096.

40. Kent, T. A. (1982) *J. Biol. Chem. 257*, 6259.

41. Beinert, H. and Thomson, A. J. (1983) *Arch. Biochem. Biophys. 222*, 333.

42. Martin, A. (1990) *Proc. Natl. Acad. Sci. USA 87*, 598.

43. Dickson, D. P. E., Johnson, C. E., Cammack, R., Evans, M. C. W., Hall, D. O., and Rao, K. K. (1978) *Biochem. J. 139*, 105.

44. Evans, M. C. W., Hall, D. O., and Johnson, C. E. (1970) *Biochem. J. 119*, 289.

45. Middleton, P., Dickson, D. P. E., Johnson, C. E., and Rush, J. D. (1980) *Eur. J. Biochem. 104*, 289-296.

46. Rafik, G. L. (2002) *In EPR in Biochemstry and Medicine*.

47. Berg, J. M. and Holm, R. H. (1982) pp 1-66, Wiley Interscience, New York.

48. Gütlick, P., Link, R., and Trautwein, A. (1978) in *Mössbauer Spectroscopy and Transition Metal Chemistry* Springer Verlag, Berlin.

49. Sands, R. H. and Dunham, N. R. (1975) *Q. Rev. Biophys. 7*, 443.

50. Beinert, H. (2000) *J. Biol. Inor. Chem 5*, 2-15.

51. Frey, M., Sieker, L. C., Payan, F., Haser, R., Brusci, M., Pepe, G., and Legall, I. J. (1987) *J. Mol. Biol. 197*, 525-541.

52. Adman, E. T., Sieker, L. C., and Jenson, L. H. (1990) *J. Mol. Biol. 217*, 337-352.

53. Ackrell, B. A. C., Johnson, M. K., Gunsalus, R. P., Cecchini, G., and Muller, F. (1992) in *Chemistry and Biochemistry of Flavoenzymes* (Muller, F., Ed.).

54. Nitschke, W., Joliot, P., Liebel, U., Rutherford, A. W., Hauska, G., Muller, A., and Riedel, A. (1995) *Biochim. Biophys. Acta 1102*, 266-268.

55. Shergill, J. K., Joannu, C. L., Mason, J. R., and Cammack, R. (1995) *Biochemistry 34*, 16533-16542.

56. Anemüller, S., Schmidt, C. L., Schäefer, G., Bill, E., Tratwein, A. X., and Teixeira, M. (1994) *Biochem. Biophys. Res. Comm. 202*, 252-257.

57. Link, T. A. and Iwata, S. (1996) *Biochim. Biophys. Acta. -Bioeng 1275*, 54-60.

58. Ackrell, B. A. C., Johnson, M. K., Gunsalus, R. P., Cecchini, G., and (Muller, F. e. (1992) in *Chemistry and Biochemistry of Flavoenzymes* (Muller, F., Ed.).

59. Thomson, A. J. (1985) *Metalloproteins: Metal proteins with Redox Roles* Weinheim, Florida.

60. Thomson, A. J. (1985) *Metalloproteins, Part 1, (Harrison, P. M., ed) Chapter 3,* Verlag Chemie, Deerfield Beach, Florida.

61. Hunsicker-Wang, L. M., Heine, A., Chen, Y., Luna, E. P., and Todaro, T. e. a. (2003) *Biochemistry 42*, 7303-7317.

62. Lanzilotta, W. N., Christiansen, J., Dean, D. R., and Seefeldt, L. C. (1998) *Biochemistry 37*, 11376-11384.

63. Beinert, H., Kennedy, M., and Stout, C. D. (1996) *Chemical Review 96*, 2335-2373.

64. Duin, E. C., Madadi-Kahkesh, S., and Johnson, M. K. (2002) *FEBS Letters 512*, 263-268.

65. Beinert, H., Reed, G. H., and Frey, P. A. (1998) *Biochemistry 37*, 2578-2585.

66. Duin, E. C., Lafferty, M. E., and Johnson, M. K. (1997) *Biochemistry 36*, 11811-11820.

67. Kulzer, R. and Pils, T. (1998) *J. Biol. Chem* 4897-4903.

68. Broderick, J. B., Duderstadst, R. E., and Johnson, M. K. (1997) *Journal of American Chemical Society 119*, 7396-7397.

69. Grandoni, J. A., Switzer, R. L., Makaroff, C. A., and Zalkin, H. (1989) *J. Biol. Chem 264*, 6058-6064.

70. Hidalgo, E., Ding, H., and Demple, B. (1997) *Trends Biochem. Sci. 22*, 207-210.

71. Demple, B., Ding, H., and Jorgensten, M. (2002) *Methods in Enzymology*.

72. Grandu, P. and Weiss, B. (1996) *Proc. Natl. Acad. Sci. USA 93*, 10094-10098.

73. Killey, P. J. and Beinert, H. (2003) *Curent Opini. Microbiol. 6*, 181-182.

74. Emptage, M. H., Kent, T. A., Huynh, B. H., Rawlings, J., Orme-Johnson, W. H., and Münck, E. (1990) *J. Biol. Chem 255*, 1795.

75. Glusker, J. P. (1971) *The Enzymes* Academic Press, New York.

76. Kennedy, C., Rauner, R., and Gawron, O. (1972) *Biochem. Biophys. Res. Comm. 47*, 740.

77. Kent, T. A., Dreyer, J.-L., Emptage, M. H., Moura, I., Moura, J. J., Xavier, A. V., Huynh, B. H., Legall, I. J., Beinert, H., Orme-Johnson, W. H., and Münck, E. (1982) pp 371-374, Elsevier, New York.

78. Kent, T. A., Dreyer, J.-L., Kennedy, M. C., Huynh, B. H., Emptage, M. H., Beinert, H., and Münck, E. (1982) *Proc. Natl. Acad. Sci. USA 79*, 1096.

79. Beinert, H. and Kenndy, M. C. (1989) *Eur. J. Biochem. 186*, 5.

80. Kennedy, M. C., Emptage, M. H., Dreyer, J. L., and Beinert, H. (1983) *J. Biol. Chem. 258*, 11098.

81. Kennedy, M. C., Emptage, M. H., Dreyer, J.-L., and Beinert, H. (1983) *J. Biol. Chem. 258*, 98.

82. Robins, A. H. and Stout, C. D. (1989) *Proc. Natl. Acad. Sci. USA 86*, 3639.

83. Beinert, H., Kennedy, D., and Stout, C. D. (1996) *Chemical Review 96*, 2335-2373.

84. Cleland, W. W. and Kreevoy, M. M. (1994) *Science 264*, 1887.

85. Schloss, J. V., Porter, D. J. T., Bright, H. J., and Cleland, W. W. (1980) *Biochemistry 19*, 2358.

86. Droux, M., Jacquot, J.-P., Miginac-Maslow, M., Gadal, P., Huet, J. C., Crawford, N. A., Yee, B. C., and Buchhanan, B. B. (1987) *Arch Biochem Biophys 252*, 426-439.

87. Staples, C. R., Ameyibor, E., Fu, W., Gardet-Salvi, L., Stritt-Etter, A.-L., Schünemann, V., and Knaff, D. B. (1996) *Biochemistry 35*, 11425-11434.

88. Staples, C. R., Gaymard, E., Stritt-Etter, A.-L., Telser, J., Hoffman, B., Schünemann, V., Knaff, D. B., and Johnson, M. K. (1998) *Biochemistry 37*, 4612-4620.

89. Williams, C. R. (1992) *Chemistry and Biochemistry of Flavoproteins* CRC Press, Boca Raton, FL.

90. Duin, E. C., Madadi-Kahkesh, S., Hedderich, R., Clay, M. D., and Johnson, M. K. (2002) *FEBS Letters 512*, 263-268.

91. Banerjee, R. (2003) *Chemical Review 103*, 2083-2094.

92. Cheek, J. and Broderick, J. B. (2001) *J. Biol. Inor. Chem 6*, 226.

93. Leuthner, B., Leutwein, C., Schulz, H., Hörth, P., Haehael, W., Schlitz.E., Schägger, H., and Helder, J. (1998) *Molecular Microbiology 28*, 615-628.

94. Ollagnier, S., Mülliez, E., Schmidt, P. P., Eliasson, R., Caillard, J., Deronzier, C., Bergman, T., Gräslund, A., Reichard, P., and Fontecave, M. (1997) *J. Biol. Chem. 272*, 24216-24223.

95. Frey, P. A. and Booker, S. J. (2001) *Adv. Protein Chem. 58*, 1-45.

96. Frey, P. A. (2003) *Chemical Review 103*, 2129-2148.

97. Jarett, J. T. (2003) *Curr. Opin. Chem. Biol. 7*, 174-182.

98. Layer, G., Moser, J., Heinz, D. W., and Schubert, W.-D. (2003) *EMBO J. 22*, 6214-6224.

99. Layer, G., Verfürth, K., Mahlitz, E., and Jahn, D. (2002) *J. Biol. Chem 277*, 34136-34142.

100. O'Brien, J. R., Raynaud, C., Croux, C., Gilbal, L., and Soucaille, P. (2004) *Biochemistry 43*, 4635-4645.

101. Külzer, R., Pits, T., Kappi, R., Hütterman, J., and Knappe, J. (1998) *J. Biol. Chem 273*, 4897-4903.

102. Tamarit, J., Gerezc, C., Meler, C., Mulliez, E., Trautwein, A., and Fontecave, M. (2000) *J. Biol. Chem 275*, 15669-15675.

103. Walsby, C. J., Hong, W., Broderick, W. E., Cheek, J., Ortillo, D., Broderick, J. B., and Hoffman, B. M. (2002) *J. Am. Chem. Soc. 124*, 3143-3151.

104. Walsby, C. J., Ortillo, D., Broderick, W. E., Broderick, J. B., and Hoffman, B. M. (2002) *J. Am. Chem. Soc. 124*, 11270-11271.

105. Liu, A. and Gräslund, A. (2000) *J. Biol. Chem. 275*, 12367-12373.

106. Ollagnier, S., Meler, C., Mulliez, E., Gaillard, J., Schünemann, V., Trautwein, A., Mattioli, T., Lutz, M., and Fontecave, M. (1999) *J. Am. Chem. Soc. 121*, 6344-6350.

107. Krebs, C., Henshaw, T. F., Cheek, J., Huynh, B. H., and Broderick, J. B. (2000) *J. Am. Chem. Soc. 122*, 12497-12506.

108. Broderick, J. B., Henshaw, T. F., Cheek, J., Wojtuszewski, K., Smith, S. R., Trojan, M. R., McGhan, R. M., Kopf, A., Kibbey, M., and Broderick, W. E. (2000) *Biochem Biophys Res Commun 269*, 451-456.

109. Wagner, A. F., Frey, M., Neugebauer, F. A., Schafer, W., and Knappe, J. (1992) *Proc. Natl. Acad. Sci. USA 89*, 996-1000.

110. Bianchi, V., Eliasson, R., Fontecave, M., Mulliez, E., Hoover, D. M., Matthews, R. G., and Reichard, P. (1993) *Biochem Biophys Res Commun 197*, 792-797.

111. Picclocchi, A., Douce, R., and Alban, C. (2003) *J. Biol. Chem. 278*, 24966-24975.

112. Chen, D. e. al. (2003) *J. Am. Chem. Soc. 124*, 14006-14007.

113. Cosper, M. M., Cosper, N. J., Hong, W., Shokes, J. E., Broderick, J. B., Broderick, W. E., Johnson, M. K., and Scott, R. A. (2003) *Protein Science 12*, 1573-1577.

114. Jarrett, J. T. (2003) *Curr. Opin. Chem. Biol. 7*, 174-182.

115. Berkovitch, F. and Nicolet, Y. (2004) *Science 303*, 76-79.

116. Bayley, P., Brown, S. B., Gans, P., Geddes, A. J., Jones, R., Penzer, G. R., and Wood, E. J. (1980) *An Introduction to Spectroscopy for Biochemists* Academic Press, New York.

117. Weil, J. A., Bolton, J. R., and Wertz, J. E. (1994) *Electron Paramagnetic Resonance: Elementary Thory and Practical Applications* John Wiley & Sons, New York.

118. Bell, J. E. (1982) *Spectroscopy in Biochemistry* CRC Press, Inc., Boca Racon, Florida.

119. Wright, J. R., Hendrickson, W. A., Osaki, S., and James, G. T. (1986) *Physical Methods for Inorganic Biochemistry* Plenum Press, New York.

120. Ingram, D. J. E. (1969) *Biological and Biochemical Applications of Electron Spin Resonance* Hilger, London.

121. Alger, R. (1968) in *EPR Techniques and Applications* Wiley Interscience, New York.

122. Poole, C. P. (1983) *"Electron Spin Resonance" in A comprehensive Treatise on Experimental Techniques". 2nd Edition* Wiley, New York.

123. Miller, A.-F. and Brudvig, G. W. (1991) *Biochim. Biophys. Acta 1056*, 1-5.

124. Beinert, H. and Orme-Johnson, W. H. (1967) in *Magnetic Resonance in Biological Systems* pp 221, Pergamon, Oxford.

125. Albracht, S. P. J. and Beinert, H. (1982) *Biochim. Biophys. Acta 683*, 245-277.

126. Aasa, R. and Vanngard, J. (1975) *J. Magn. Reson. 19*, 308.

127. Palmer, G. (2000) in *Physical Methods in Bioinorganic: Spectroscopy and Magnetism* (Que, L. Jr., Ed.) pp 132-133, University Science Books, California.

128. Sarifut-Denov, R. G. and Larina, L. I. (2001) *EPR in Biochemistry and Medicine* Kluwer, New York.

129. Hagen, W. R. (1992) *Adv. Inorganic Chem. 38*, 164-222.

130. Brudvig, G. W. (1995) *Methods in Enzymology* Academic Press, California.

131. Hagen, K. S., Walson, A. D., and Holm, R. H. (1983) *J. Am. Chem. Soc. 105*, 3905.

132. Hoffman, B. M. (1991) *Acc. Chem. Res. 24*, 164-170.

133. Abragam, A. and Bleaney, B. (1986) *Electron Paramagnetic Resonance of Transition Ions* Dover Publications, New York.

134. Fan, C., Gorst, C. M., and Hoffman, B. M. (1991) *Biochemistry 30*, 431-439.

135. True, A. E., Nelson, M. J., Hoffman, B., and Orme-Johnson, W. H. (1998) *J. Am. Chem. Soc. 110*, 1935.

136. Bollengir, J. M. J., Tong, W. H., Huynh, B. H., Ravi, W. H., Edmondson, D. E., and Stubbe, J. (1994) *J. Am. Chem. Soc. 116*, 8015-8023.

137. Burdi, D., Willems, J., Riggs-Gelasco, P., Antholine, W. E., Stubbe, J., and Hoffman, B. (1998) *J. Am. Chem. Soc. 120*, 12910-12919.

138. Hoffman, B., DeRose, V. J., Gubriel, R. J., Houseman, L. P., Doan, P. E., and elser, J. (1993) *In Biological Magnetic Resonance: EMR of Paramagnetic Molecules (Berliner, L. J., Reuben, J., Eds.)* Plenum Press, New York.

139. Gubriel, R. J., Batie, C. J., Hoffman, B. M., and Ballou, D. P. (1989) *Biochemistry 28*, 4861-4871.

140. Bennett, B., Gruel, M. J., Guest, J. R., and Thomson, A. J. (1998) *Eur. J. of Biochem. 239*, 317-326.

141. Nakamoto, N. K. (1986) *Infrared and Raman Spectra of Inorganic and Coordination Compounds* Wiley Intersscience, New York.

142. Long, D. A. (1977) *Raman Spectroscopy* McGraw-Hill, New York.

143. Tu, A. T. (1982) *Raman Spectroscopy in Biology: Principles and Applications* Wiley Interscience Publication.

144. Willard, H. H., Merritt, L. L., Dean, J. A., and Settle, F. A., Jr. (1988) *Instrumental Methods of Analysis (7th Ed.)*.

145. Spiro, T. G. and Czernuszewicz, R. S. (2000) in *Physical Methods in Bioinorganic Chemistry: Spectroscopy and Magnetism* (Que, L. Jr., Ed.) pp 59-91, University Science Books, Sausalito, California.

146. Maret, W. (1993) *Methods in Enzymology*.

147. Spiro, T. G. (1974) *Acct. Chem. Res. 7*, 339-344.

148. Tang, J. and Albrecht, A. C. (1970) *Raman Spectroscopy* Plenum, New York.

149. Spiro, T. G. and Czernuszewicz, R. S. (1995) *Methods in Enzymology*.

150. Altincicek, B., Duin, E. C., Reichenberg, A., Hedderich, R., Kollas, A. K., Hintz, M., Wagner, S., Wiesner, J., Beck, E., and Jomaa, H. (2002) *FEBS Letters 532*, 437-440.

151. Fish, W. W. (1988) in *Methods in Enzymology* pp 357-358, Academic Press, New York.

152. Lin, Y., Gerfen, G. J., Rousseau, D. L., and Yeh, S.-R. (2003) *Analytical Chemistry 75*, 5381-5386.

153. Kilpatrick, L. K., Kennedy, M. C., Beinert, H., Czernuszewicz, R. S., Qui, D., and Spiro, T. G. (1994) *J. Am. Chem. Soc. 116*, 4053-4061.

154. Antanaitis, B. C. and Moss, T. H. (1975) *Biochim. Biophys. Acta 405*, 262-279.

155. Dunham, W. R., Hagen, W. R., Fee, J. A., Sands, R. H., Dunbar, J. B., and Humblet, C. (1991) *Biochim. Biophys. Acta 1079*, 253-262.

156. Walters, E. M., Garcia-Serres, R., Jameson, G. N. L., Glauser, D. A., Bourquin, F., Manieri, W., Schürmann, P., Johnson, M. K., and Huynh, B. H. (2005) *J. Am. Chem. Soc. 127*, 9612-9624.

157. Jameson, G. N. L., Walters, E. M., Manieri, W., Schürmann, P., Johnson, M. K., and Huynh, B. H. (2003) *J. Am. Chem. Soc. 125*, 1146-1147.

158. Wolff, M., Seemann, M., Bui, T. S., Frapart, Y., Tritsch, D., Estrabot, A. G., Boronat, A., Marquet, A., and Rohmer, M. (2003) *FEBS Letters 341*, 115-120.

159. Seemann, M., Tse Sum Bui, B., Wolff, M., Tritsch, D., Campos, N., Boronat, A., Marquet, A., and Rohmer, M. (2002) *Angew. Chem. Int. Ed. 41*, 4337-4339.

160. Kollas, A. K., Duin, E. C., Eberl, M., and Altincicek, B. et. a. (2002) *FEBS Letters 532*, 432-436.

161. Hecht, S., Eisenreich, W., Adam, P., Amslinger, S., Kis, K., Bacher, A., Arigoni, D., and Rohdich, F. (2001) *Proc. Natl. Acad. Sci. USA 98*, 14837-14842.

162. Brandt, W., Dessoy, M. A., Fulhorst, M., Gao, W., Zenk, M. H., and Wessjohann, L. A. (2004) *ChemBio-Chem 5*, 311-323.

163. Rohdich, F., Zepeck, F., Adam, P., Hecht, S., Kaiser, J., Laupitz, R., Gräwert, T., Amslinger, S., Eisenreich, W., Bacher, A., and Arigoni, D. (2003) *Proc. Natl. Acad. Sci. USA 100*, 1586-1591.